

Accepted Manuscript

Preliminary research on 1-(4-bromo-2-nitroimidazol-1-yl)-3-[^{18}F]fluoropropan-2-ol as a novel brain hypoxia PET tracer in a rodent model of stroke

Elena Nieto, Mercedes Delgado, Mónica Sobrado, María L. de Ceballos, Ramón Alajarín, Luis García-García, James Kelly, Ignacio Lizasoain, Miguel A. Pozo, Julio Álvarez-Builla

PII: S0223-5234(15)30099-4

DOI: [10.1016/j.ejmech.2015.06.023](https://doi.org/10.1016/j.ejmech.2015.06.023)

Reference: EJMECH 7950

To appear in: *European Journal of Medicinal Chemistry*

Received Date: 18 December 2014

Revised Date: 10 April 2015

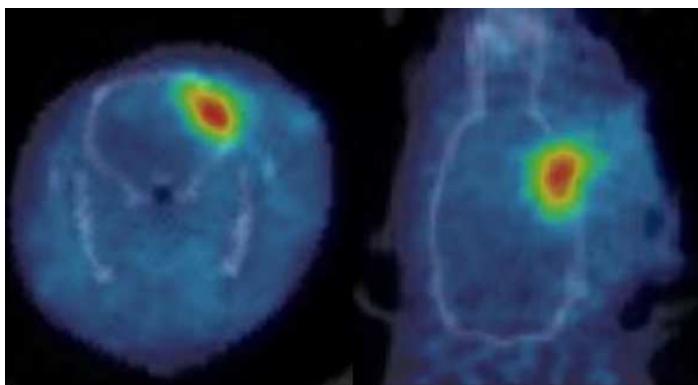
Accepted Date: 8 June 2015

Please cite this article as: E. Nieto, M. Delgado, M. Sobrado, M.L. de Ceballos, R. Alajarín, L. García-García, J. Kelly, I. Lizasoain, M.A. Pozo, J. Álvarez-Builla, Preliminary research on 1-(4-bromo-2-nitroimidazol-1-yl)-3-[^{18}F]fluoropropan-2-ol as a novel brain hypoxia PET tracer in a rodent model of stroke, *European Journal of Medicinal Chemistry* (2015), doi: 10.1016/j.ejmech.2015.06.023.

This is a PDF file of an unedited manuscript that has been accepted for publication. As a service to our customers we are providing this early version of the manuscript. The manuscript will undergo copyediting, typesetting, and review of the resulting proof before it is published in its final form. Please note that during the production process errors may be discovered which could affect the content, and all legal disclaimers that apply to the journal pertain.



Graphical abstract



Preliminary research on 1-(4-bromo-2-nitroimidazol-1-yl)-3-[¹⁸F]fluoropropan-2-ol as a novel brain hypoxia PET tracer in a rodent model of stroke

Elena Nieto,^a Mercedes Delgado,^b Mónica Sobrado,^{c,1} María L. de Ceballos,^d Ramón Alajarín,^a Luis García-García,^b James Kelly,^{e,2} Ignacio Lizasoain,^c Miguel A. Pozo,^{b,e,3} Julio Álvarez-Builla,^{a,3,}*

^a Departamento de Química Orgánica y Química Inorgánica, Universidad de Alcalá, 28871-Alcalá de Henares, Madrid, Spain

^b CAI Cartografía Cerebral, Instituto Pluridisciplinar UCM, Paseo Juan XXIII, 1, Madrid 28040, Spain

^c Unidad de Investigación Neurovascular, Departamento de Farmacología, Facultad de Medicina, Universidad Complutense, Avenida Complutense s/n, 28040 Madrid, Spain

^d Departamento de Neurobiología Molecular, Celular y del Desarrollo, Instituto Cajal, Avda. Doctor Arce, 37, Madrid 28002, Spain

^e Instituto Tecnológico PET, Calle Manuel Bartolomé Cossío, 10, Madrid 28040, Spain

ABSTRACT

The synthesis of the new radiotracer precursor 4-Br-NITTP and the radiolabeling of the new tracer 1-(4-bromo-2-nitroimidazol-1-yl)-3-[¹⁸F]fluoropropan-2-ol (4-Br-[¹⁸F]FMISO) is reported. The cyclic voltammetry behaviour, neuronal cell toxicity, transport through the brain endothelial cell monolayer, *in vivo* PET imaging and preliminary calculations of the tracer uptake for a rodent model of stroke were studied for the new compound and the results were compared to those obtained with [¹⁸F]FMISO, the current gold standard PET hypoxia tracer. The new PET brain hypoxia tracer is more easily reduced, has higher *CLogP* than [¹⁸F]FMISO and it diffuses more rapidly through brain endothelial cells. The new compound is non-toxic to neuronal cells and it allows the *in vivo* mapping of stroke in mice with higher sensitivity. 4-Br-[¹⁸F]FMISO is a good candidate for further development in ischemic stroke.

Keywords

1-(4-bromo-2-nitroimidazol-1-yl)-3-[¹⁸F]fluoropropan-2-ol, PET imaging, hypoxia, fluorine-18, stroke, nitroimidazole

Abbreviations

BBB, blood-brain barrier; CBF, cerebral blood flow; CT, computed tomography; DHP, 3,4-dihydro-2*H*-pyran; FDG, 2-fluoro-2-deoxy-D-glucose; FMISO, fluoromisonidazole, 1-fluoro-3-(2-nitroimidazol-1-yl)-propan-2-ol; FON, 1-(8-fluorooctyl)-2-nitro-1*H*-imidazole; FPN, 1-(3-fluoropropyl)-2-nitro-1*H*-imidazole; LDH, lactate dehydrogenase; MRI, magnetic resonance imaging; MTT, 3-(4,5-dimethylthiazol-2-yl)-2,5-diphenyltetrazolium bromide; NBPh, *N*-bromophthalimide; NBS, *N*-bromosuccinimide; NITTP, 3-(2-nitroimidazol-1-yl)-2-(tetrahydropyran-2-yloxy)-prop-1-yl tosylate; 4-Br-NITTP, 3-(4-bromo-2-nitroimidazol-1-

yl)-2-(tetrahydropyran-2-yloxy)-prop-1-yl tosylate; OD, optical density; PET, positron emission tomography; pMCAO, permanent occlusion of the right middle cerebral artery; PPTS, pyridinium *p*-toluenesulfonate; SPECT, single photon emission computed tomography; TBABF₄, tetrabutylammonium tetrafluoroborate; THP, tetrahydropyranyl.

* *Corresponding author:* J.A.-B., Tel. +341918854606. Fax, +341918854686. E-mail, julio.alvarez@uah.es; *Present addresses:* ¹ M.S., Servicio de Neurología, Instituto de Investigación Sanitaria, Hospital Universitario La Princesa, Calle Diego de León, 62, 28006 Madrid, Spain; ² J.K., Weill Cornell Medical College, Belfer Research Building, 413 E 69th St, New York, NY 10021. *Author contributions:* ³ J.A.-B. and M.A.P contributed equally to this work. J.A.-B., M.A.P and I.L. conceived the project, E.N. performed the synthesis of precursors and cold tracers, M.D. and L.G.-G. carried out micro-PET experiments, M.S. prepared the pMCAO model and tested compounds on LDH and MTT assays, M.L.C. performed BBB-permeability assay, R.A. designed chemical experiments, J.K. performed the radiosynthesis, E.N., M.D., M.S., M.L.C., R.A., L.G.-G. and J.K. wrote the manuscript. All authors edited and approved the final version of the manuscript.

1. Introduction

Stroke is an increasing common disease both in first-world and emergent countries as a consequence of factors such as old age, high blood pressure, previous stroke, transient ischemic attack, diabetes, high cholesterol, tobacco smoking and atrial fibrillation. As a medical emergency, acute stroke requires quick diagnosis and treatment, i.e., within the first minutes to hours after the stroke event. A rapid response is critical in order to initiate therapy before the ischemic but still viable tissue becomes necrotic. One goal in the clinical treatment

of stroke is to identify the presence and to map the extent, by neuroimaging techniques, of hypoxic but still viable tissue – ischemic penumbra – that can be recovered through suitable cerebral revascularization therapy. This possibility would facilitate the selection of patients who may benefit from revascularization treatments, excluding those for whom the risk of complications is very high or the brain damage by infarct is irreversible [1,2].

The identification and mapping of ischemic penumbra is the target for the current diagnostic techniques used for the imaging of brain hypoxia, such as X-ray computed tomography (CT), magnetic resonance imaging (MRI), positron emission tomography (PET) and single photon emission computed tomography (SPECT) [3]. In the context of improving the sensitivity and accessibility of current neuroimaging techniques, hypoxia radiotracers based on the nitroimidazole core have received particular attention due to their ability to accumulate in hypoxic but viable tissue and these may be good candidates for imaging in ischemic stroke [4]. Once the radiotracer crosses the cell membrane, in the first step, the nitro group is reduced by intracellular reductases to its radical nitro anion which is rapidly reoxidized in normoxic cells and the tracer returns to blood flow. In hypoxic cells, the radical nitro anion is then reduced in further stages to species that bond to cell components and the modified tracer is unable to diffuse out from the cell, thus allowing the imaging of hypoxic cells [5-9].

Fig.1. (2-column size)

[¹⁸F]Fluoromisonidazole ([¹⁸F]FMISO, [¹⁸F]**1**) is currently the gold standard for PET imaging in oncology [10]. In acute stroke the use of this tracer is limited by poor brain penetration, slow accumulation in the penumbral area and slow clearance from normoxic

regions. As a consequence, long acquisition times are required late after the stroke event and this compromises the early start of the therapy and the lifespan of recoverable tissue [4]. Researchers have focused on new hypoxia radiotracers with better pharmacokinetic properties. [^{18}F]FMISO ([^{18}F]1) is a low lipophilicity compound ($\text{Log}P_{\text{octanol/water}}$: -0.40) [11] and more lipophilic analogs have been prepared (Figure 1). The concentration of 4- [^{82}Br]bromomisonidazole (4- [^{82}Br]BrMISO, [^{18}F]2) increased in the hypoxic portion of EMT-6/UW tumor at 2 hours, but high blood levels contributed to excessive background [12,13]. The initial uptake of 4-Br- [^{18}F]FPN (4-bromo-1-(3- [^{18}F]fluoropropyl)-2-nitro-1*H*-imidazole, [^{18}F]3) into rat brain was significantly higher than that for [^{18}F]FMISO ([^{18}F]1) and this was followed by a rapid washout from the brain. The uptake in mice muscle tumor was somewhat enhanced compared to the levels obtained with [^{18}F]FMISO ([^{18}F]1) and [^{18}F]FPN ([^{18}F]4), but with lower tumor localization than [^{18}F]FMISO ([^{18}F]1) [14]. [^{18}F]FON (1-(8- [^{18}F]fluorooctyl)-2-nitro-1*H*-imidazole, [^{18}F]5) and [^{18}F]FPN ([^{18}F]4) had increased initial uptake in normal rat brain relative to [^{18}F]FMISO ([^{18}F]1), and this was followed by a rapid washout from brain. Both [^{18}F]4 and [^{18}F]5 had significantly lower tumor uptake and lower tumor-to-blood ratios than [^{18}F]FMISO ([^{18}F]1), a finding that suggests a poor trapping mechanism within the tumor tissue. Neither [^{18}F]4 nor [^{18}F]5 offered improved biological properties over [^{18}F]FMISO ([^{18}F]1) [11,14].

On the other hand, a newer generation of hypoxia radiotracers (Figure 1) includes 2-(2-nitro-1*H*-imidazol-1-yl)-*N*-(2,2,3,3,3- [^{18}F]pentafluoropropyl)-acetamide ([^{18}F]EF5, [^{18}F]6) [15], [^{18}F]fluoroazomycin arabinoside ([^{18}F]FAZA, [^{18}F]7) [16,17], 3- [^{18}F]fluoro-2-(4-((2-nitro-1*H*-imidazol-1-yl)methyl)-1*H*-1,2,3,-triazol-1-yl)-propan-1-ol ([^{18}F]HX4, [^{18}F]8) [18,19] and Cu-labeled bis(thiosemicarbazone) complexes such as ^{62}Cu -diacetyl-bis(N^4 -methylthio-semicarbazone) (^{62}Cu -ATSM, [^{18}F]9) [20] and ^{64}Cu -diacetyl-bis(N^4 -ethylthiosemicarbazone) (^{64}Cu -ATSE, [^{18}F]10) [21], all of which have been studied for tumor

hypoxia imaging without consensus on the best radiotracer [18,22]. It has been suggested that tracer [^{18}F]**10** is a more sensitive marker of neurological hypoxia than analog [^{18}F]**9** as the former is reduced at higher tissue oxygen concentrations [21]. To the best of our knowledge, there is only one report in which compounds [^{18}F]**7**, [^{18}F]**9** and [^{18}F]**10** have been compared as PET tracers for brain hypoxia mapping in a rodent model of stroke. Unfortunately, none of the examples surpassed or even equaled [^{18}F]FMISO ([^{18}F]**1**) for the early detection of acute focal brain hypoxia and further development of these compounds in ischemic stroke is not warranted [23].

In the field of stroke imaging there is still a need to find suitable tracers that can be developed into radiopharmaceuticals for general use in acute stroke events in an effort to allow patients to overcome the event with the lowest level of brain alteration. Important issues that require improvement include: the amount of tracer that reaches the hypoxic cell through cerebral blood flow (CBF) and blood flow across the blood-brain barrier (BBB), the fraction that is further reduced from the radical nitro anion, the washout from normoxic cells, the rate of trapping in hypoxic tissue which in turn yields better or worse imaging contrast and the presence of cytosolic biomolecules that bind to the tracer.

We hypothesized, as it was also suggested before [12], that the modification of [^{18}F]FMISO ([^{18}F]**1**) by the addition of bromo-substituents on the imidazole ring could have a positive effect on the pharmacological properties of the radiotracer, such as redox potential and BBB permeation. Thus, the tracer would provide better PET imaging at shorter times after injection because of an easier reduction and higher lipophilicity. A nitroimidazole-based tracer that bears a bromine on the imidazole ring (4-[^{82}Br]BrMISO, [^{18}F]**2**) was reported to have increased concentration in the hypoxic portion of tumors at 2 hours while [^{18}F]FMISO ([^{18}F]**1**) showed to be useful at 4 hours. However, high blood levels of [^{18}F]**2** contributed to

high background, incompatible with imaging [12]. Although [^{18}F]**2** could be prone to lose the radiolabel since a bromine on the imidazole ring is less stable than a fluorine at the end of an alkyl chain [12], the label remains on the imidazole ring, and [^{18}F]**2** is stable and appears to retain its label *in vivo* [13]. Furthermore, the major metabolite corresponds to the desmethyl derivative [12,24] Herein, we report the synthesis of 1-(4-bromo-2-nitroimidazol-1-yl)-3-fluoropropan-2-ol (4-Br-FMISO) and 1-(4,5-dibromo-2-nitroimidazol-1-yl)-3-fluoropropan-2-ol, and the pharmacological study and radiolabeling of (4-Br- ^{18}F]FMISO). The imaging of ischemic penumbra in an experimental model of stroke in mouse is also reported in order to evaluate 4-Br- ^{18}F]FMISO as a more lipophilic and easier to reduce nitroimidazole-based brain hypoxia PET tracer.

2. Results and discussion

2.1. Chemistry

The synthesis of precursors started from diol **11**, which was prepared as reported in a synthesis of NITTP (**12**) (Scheme 1) [25]. Bromination of **11** with *N*-bromophthalimide (NBPhT) using 1.4 and 4.0 equivalents in DMF provided **13** (79%) and **14** (36%), respectively. Subsequent selective tosylation yielded **15** (72%) and **16** (51%) as single regioisomers [26]. Finally, the protection of the hydroxyl group as a tetrahydropyranyl (THP) ketal provided the precursors **17** (4-Br-NITTP, 68%) and **18** (69%) as 1:1 and 44:56 mixtures of diastereomers, respectively, for radiolabeling. Precursor **17** (69%) was also prepared as a 67:33 diastereomeric mixture by bromination of **12** using *N*-bromosuccinimide (NBS). Compounds **12**, **17** and **18** were used for radiolabeling. Compounds **19** (69%) and **20** (31%) were prepared as 45:55 diastereomeric mixtures by fluoride nucleophilic displacement of tosylate, using CsF in *tert*-amyl alcohol [27]. Subsequent removal of the THP protecting

group by treatment with AcOH gave **21** (4-Br-FMISO, 65%) and **22** (69%). FMISO (**1**) was also prepared by fluorination of **12** to give **23** (82%) as a 66:34 mixture of diastereomers followed by hydrolysis of the ketal (55%). The diastereomeric ratios were measured by ^1H NMR. They were calculated by integration of the corresponding signals to the proton on the ketal carbon at the THP ring. For **12**, **17**, **19** and **23** the signals for the protons on the imidazole ring were also used.

Scheme 1. (2-column size)

Compounds **17** and **18** could not be prepared by reaction of 4(5)-bromoimidazole (**24**) or 4,5-dibromoimidazole (**25**) with ditosylate **26** using the reported procedure for NITTP (**12**) (Scheme 2) [28]. Firstly, the stoichiometric bromination of 2-nitroimidazole (**27**) has been reported to give a mixture of **25** and **27** and only a trace amount of **24**, while **25** (97%) was prepared quantitatively when 2 equivalents of NBS were used [29]. Furthermore, the reactions of **25** and **26** only gave trace amounts of **18** even under harsh conditions, probably due to the low nucleophilicity of imidazololate anion **28**.

Scheme 2. (1-column size)

2.2. Radiosynthesis

The radiosynthesis of [^{18}F]**1** was performed as reported [28]. The labeling of the protected tosyl precursor **17** with [^{18}F]fluoride was carried out on an automated radiosynthesis platform (Scheme 3). In the synthesis of [^{18}F]**21**, the [^{18}F]fluoride was separated from the bulk H_2^{18}O

solution by anion exchange chromatography following retention in a quaternary ammonium cartridge and elution with K_2CO_3 in an $H_2O/MeCN$ solution containing kryptofix. [^{18}F]Fluoride was dried at 100 °C under reduced pressure and a solution of precursor **17** (9 ± 3 mg in 2.5 mL MeCN) was added. Labeling was performed at 130 °C over 5 minutes and the reaction vessel was then cooled to 100 °C for hydrolysis of the THP ketal with 1N HCl.

The reaction mixture was transferred to a semi-preparative HPLC column for purification and approximately 80% of the total activity was transferred. Free [^{18}F]fluoride eluted after 3 minutes and a number of minor radiolabeled impurities were observed. A major impurity eluted after 21 minutes and the major product eluted after 33 minutes. Both impurity and product were collected and analyzed by HPLC and compared with the cold standard **21**. The peak for the product with a retention time of 33 minutes corresponded to the peak of the cold standard. The impurity could not be identified by comparison with any known standard. The total synthesis time was 55 minutes and [^{18}F]**21** (4-Br- ^{18}F FMISO) was synthesized in 18% yield (decay corrected) with a specific activity of 150 ± 15 GBq/ μ mol (at the end of radiosynthesis).

Radiosynthesis conditions were also applied to **18** but unfortunately evidence for [^{18}F]**22** was not observed. This result can be understood by considering the good leaving group character of the very weakly basic imidazolate anion **28** and the presence of excess K_2CO_3 under radiolabeling conditions, which could give rise to substitution or elimination reactions involving the base. Further studies were only carried out with **1**, [^{18}F]FMISO ([^{18}F]**1**), **21** and 4-Br- ^{18}F FMISO ([^{18}F]**21**).

Scheme 3. (1-column size)

2.3. Cyclic voltammetry

The *in vivo* reduction of nitroimidazole compounds is performed by cytosolic nitroreductases through an initial single electron transfer to the nitro group to give the radical nitro anion (Eq. 1), which under anaerobic conditions can be reduced to the nitroso, hydroxylamino and amino compounds (Eq. 2–4) [30-32]. However, in aprotic media, such as DMF, the radical nitro anion is reduced to the nitro dianion under a more negative potential (Eq. 5) [33,34].



In order to ascertain the influence that the 4-bromo-substituent on the nitroimidazole ring has on the redox potential, compounds **21** and **1** were studied by cyclic voltammetry in aprotic media ($\text{Bu}_4\text{NBF}_4/\text{DMF}$) and under anaerobic conditions (Table 1, Figure 2). A first reversible peak (Ia) was observed for the reduction of the nitro group to the radical nitro anion (Eq. 1; **1**: -1.04 V; **21**: -0.89 V), and a peak (Ib) was also observed for the oxidation of the radical nitro anion to the nitro group (Eq. 1 reverse). A second irreversible peak (II) for the reduction of the radical nitro anion to the nitro dianion (Eq. 5; **1**: -1.97 V; **21**: -1.64 V)

was also observed. Compound **21** is more easily reduced than **1** to both the radical anion and dianion, thus making **21** a better hypoxia probe.

Table 1.

Fig.2. (1-column size)

2.4. Toxicity

Before carrying out animal experimentation in order to study **21** as *in vivo* tracer, its toxicity was evaluated by viability/mortality *in vitro* assays performed in parallel with the cold tracer **1** as reference (Figure 3). Assays were carried out on primary cultures of rat cortical cells, both neuronal (see supplementary data) and mixed. Toxicity was determined by LDH (lactate dehydrogenase) and MTT (3-(4,5-dimethylthiazol-2-yl)-2,5-diphenyltetrazolium bromide) assays. Compound **21** showed a toxicity profile similar to that of **1** at the concentrations assayed. It did not show toxicity when compared to vehicle (0 μM) – even at the highest concentration assayed (100 μM) – and did not show higher cell mortality ($P>0.05$; one-way ANOVA and pos hoc Tukey's test; Figure 4).

Fig. 3. (1.5-column size)

Fig. 4. (1-column size)

2.5. Lipophilicity

The ability to cross the BBB and reach the therapeutic target is the major challenge for CNS drug candidates and it has been estimated that 98% fail to reach the target [35]. Important concepts in brain penetration such as unbound drug concentration, unbound brain-to-plasma ratio, total brain-to-plasma ratio, fraction unbound, BBB passive permeability and efflux ratio have to be considered together. A screening paradigm for the key brain penetration properties has recently been developed to guide CNS compound optimization [36]. Lipophilicity, measured as $\text{Log}P$, is a parameter that is intimately related with BBB passive transport and a mean $\text{CLog}P$ value of 2.5 for the marketed CNS drugs has been reported [37]. The $\text{Log}P_{\text{oct/water}}$ and $\text{CLog}P$ values for previously reported tracers **1–10** and compounds **21** and **22** are shown in Table 2. Compound **21** has a $\text{CLog}P$ higher than most of the nitroimidazole radiotracers in Figure 1, but specially higher than FMISO. Further *in vitro* and *in vivo* experiments (see sections 2.6 and 2.7) showed that **21** crosses BBB.

Table 2.

Compound **21** showed a better reduction potential and higher $\text{CLog}P$ than **1**, it had a comparable toxicity, and it was possible to radiolabel this compound. [^{18}F]**21** was therefore a good candidate for further PET imaging in a rodent model of stroke.

2.6. Blood-brain barrier permeability

As shown in Figure 5, FMISO (**1**) diffused across the bEnd-5 cell monolayer. More than 50% of the drug was present in the lower compartment at 15 min after the addition of the

drug. Similar amounts of transported **1** were observed at 30 and 45 minutes and the level increased slightly at 60 minutes. The diffusion of the bromo-derivative **21** was also rapid and it tended to be higher compared to **1** at 15 min, although the difference did not reach statistical significance. However, at longer times (30–60 minutes) compound **21** attained significantly higher transport in comparison to **1** and almost all of it was present in the lower compartment (99.4%).

The rapid initial diffusion of both compounds is compatible with a rapid access to the brain. The limited permeability of **1** may be related to its lower $\text{Log}P$ value, but the possibility that the compound is retained in the cells and/or is metabolized cannot be ruled out. In contrast, compound **21** completely diffused over time and its higher permeability is consistent with its higher $\text{CLog}P$ compared to FMISO.

Fig. 5. (1-column size)

2.7. [^{18}F]**21** PET imaging of the hypoxic area

In order to evaluate 4-Br- ^{18}F FMISO (^{18}F **21**) as an in vivo tracer, this compound, and FMISO (**1**) as control, were assessed in an experimental model of brain ischemia by permanent occlusion of middle cerebral artery (pMCAO) in male Fischer rats. The image analysis revealed that 3 hours after pMCAO, the radiotracers ^{18}F **21** and ^{18}F FMISO (^{18}F **1**) were accumulated in the frontoparietal cortical area corresponding to middle cerebral artery occlusion. The retention of both hypoxia tracers corresponds to the hypoxic region, as revealed by ^{18}F fluorodeoxyglucose (^{18}F FDG)-PET neuroimaging performed 24 hours after the ischemic onset. The degree of lesion estimated as the reduction of glucose brain

metabolism 24 hours after pMCAO was in the range 17–41% from the non-affected contralateral area of [^{18}F]FDG uptake. Representative [^{18}F]21 and [^{18}F]FDG-PET images are shown in Figure 6.

Fig. 6. (1-column size)

To compare the labeling capability of [^{18}F]21 and [^{18}F]FMISO ([^{18}F]1) to the hypoxic area, accumulation in the injured region for both tracers were calculated. The uptake (see Experimental section for a detailed description of how this parameter was obtained) for [^{18}F]21 corrected for lesion severity was 54% higher than that of the standard [^{18}F]FMISO ([^{18}F]1) (Table 3). Therefore, this result shows that [^{18}F]21 yields an improved sensibility compared to [^{18}F]FMISO ([^{18}F]1). This would allow an earlier and more sensitive detection of the eventual brain damage generated by ischemia than [^{18}F]FMISO ([^{18}F]1), thus enabling an earlier pharmacological treatment for preventing or minimizing the potential stroke-induced consequences.

Table 3.

PET-CT rat brain coronal images of [^{18}F]FMISO ([^{18}F]1) and [^{18}F]21, for which the uptake at the hypoxic tissue 3 hours after pMCAO can be compared, are shown in Figure 7. As observed, the areas visualized by both hypoxia tracers are fairly similar.

Fig. 7. (1-column size)

In order to study the ability of the tracer to follow up the progression of the ischemic lesion, [^{18}F]**21** was injected at 3 different time points after the onset of the pMCAO. This tracer enabled the evolution of hypoxia to be evaluated. At 3 hours after ischemia onset, the hypoxic area was clearly visualized (Figure 8, left panel). When evaluated at 9 hours, the [^{18}F]**21** uptake was spread out to the neighbouring area (Figure 8, central panel), suggesting that the penumbra area showed hypoxia signs. After 15 hours, a sharply reduced [^{18}F]**21** uptake in the center of the injury was detected, probably as a consequence of neuronal death located at the level of the core. On the other hand, the surrounding penumbra area still showed clear signs of hypoxia (Figure 8, right panel).

Fig. 8. (1-column size)

3. Conclusions

The radiotracer 4-Br- ^{18}F FMISO (^{18}F]**21**) is an interesting probe with medicinal chemical properties as a potential radiopharmaceutical for the imaging of stroke. In comparison with the gold standard PET hypoxia tracer [^{18}F]**1**, compound **21** shows comparable *in vitro* low toxicity on neuronal cells, better reduction potential, higher *Clog P* and faster and total permeability through an *in vitro* model of the BBB. The *in vivo* PET molecular imaging of [^{18}F]**21** in a rodent model of stroke shows a relative accumulation that is 54% higher than that obtained with the reference [^{18}F]**1**. In short, [^{18}F]**21** is a new radiotracer with improved properties with respect to [^{18}F]**1** for the *in vivo* mapping of the brain ischemic area developed after an experimental stroke event in rodents. This radiotracer could be a good candidate for further development in the study of

ischemic stroke. The ongoing research is focusing on pharmacokinetic and imaging data and results will be published elsewhere.

4. Experimental section

4.1. Chemistry

Solvents (HPLC quality, Scharlau) were dried in a Solvent Purification System (MBraun) by passing through a pre-activated alumina column or were purchased as anhydrous quality. Reagents were purchased from Sigma-Aldrich and were used as received. The reactions in which moisture-sensitive compounds were handled were performed under an atmosphere of dry argon. The reactions were monitored by thin-layer chromatography (TLC) on silica-coated aluminum sheets (Alugram silica gel 60 F₂₅₄). The compounds were visualized by UV light (254 nm). Column chromatography was carried out with Merck silica gel (0.030–0.075 mm) and the solvents were used as received (Scharlau). Infrared spectra (IR, NaCl windows) were recorded on a Perkin-Elmer FTIR 1725X instrument. The frequencies (ν) of the more intense bands are given in cm^{-1} . Nuclear magnetic resonance spectra (^1H and ^{13}C NMR) were recorded using a Varian Gemini 200 (200 and 50 MHz, respectively), a Varian Mercury-VX-300 MHz (300 and 75 MHz, respectively) and a Varian-UNITY^{PLUS}-500 (500 and 125 MHz, respectively) instrument. Chemical shifts (δ) are given in ppm and are referenced to the residual signal of the non-deuterated solvent. Coupling constants (J) are given in Hz. Elemental analyses (C, H, N) were determined on a LECO CHNSO-932 elemental analyzer and were within $\pm 0.4\%$ of the theoretical values. All compounds were analyzed by tandem HPLC-MS. HPLC was performed on a C18, 3 μm column (Luna, Phenomenex, 3 \times 100 mm)

using a gradient of MeOH/water/4% formic acid at a flow rate of 1.0 mL min⁻¹. Products were detected at $\lambda = 254$ nm. Compounds were $\geq 95\%$ pure. Mass spectra were recorded on a Hewlett-Packard 5988A mass spectrometer. High-resolution mass spectra were recorded on an Agilent 6210 LC/MS TOF mass spectrometer.

4.2. General procedure for bromination of **11**

A solution of diol **11** and *N*-bromophthalimide in anhydrous DMF was stirred under an argon atmosphere. The solvent was removed under reduced pressure. Cold MeOH (20 mL) was added and the phthalimide was filtered off. The solvent was removed under reduced pressure and the residue was chromatographed on silica gel using hexane/AcOEt 2:1 as eluent.

4.2.1. 3-(4-Bromo-2-nitroimidazol-1-yl)propane-1,2-diol (**13**)

A mixture of diol **11** (2.25 g, 12.03 mmol) and *N*-bromophthalimide (3.80 g, 16.84 mmol) in DMF (12 mL) was stirred at rt for 3 h. Compound **13** (2.51 g) was obtained as a yellowish oil. Yield: 79%; $R_{f(\text{hex}/\text{AcOEt } 2:1)}$: 0.32; ¹H NMR (300 MHz, CD₃OD) δ 7.56 (s, 1H, H_{5-Im}), 4.75 (dd, 1H, $J = 13.8$ Hz, $J = 3.3$ Hz, CH₂-Im), 4.37 (dd, 1H, $J = 13.8$ Hz, $J = 8.5$ Hz, CH₂-Im), 4.00–3.93 (m, 1H, CH-OH), 3.60 (m, 2H, CH₂-OH) ppm; ¹³C NMR (75 MHz, CD₃OD) δ 145.3 (C₂Im), 128.6 (C₅Im), 114.4 (C₄Im), 71.3 (CH-OH), 64.6 (CH₂-OH), 54.0 (CH₂-Im) ppm; IR (ν_{max} , KBr): 3369 (OH), 15943 (C=N), 1469 (NO₂), 1369 (NO₂) cm⁻¹; HRMS (TOF-APCI-POS) m/z calcd for C₆H₉BrN₃O₄ [M]⁺ 265.9776, found 265.9777.

4.2.2. 3-(4,5-Dibromo-2-nitroimidazol-1-yl)propane-1,2-diol (**14**)

A mixture of diol **11** (1.56 g, 8.38 mmol) and *N*-bromophthalimide (7.57 g, 33.53 mmol) in DMF (5 mL) were stirred at 10 °C for 18 h. Compound **14** (1.03 g) was obtained as a yellow solid. Yield: 36%; mp: 98–100 °C; R_f (_{hex/AcOEt 2:1}): 0.26; $^1\text{H NMR}$ (300 MHz, CD_3OD) δ 4.70 (d, 2H, $J = 5.9$ Hz, $\text{CH}_2\text{-Im}$), 3.95 (q, 1H, $J = 5.9$ Hz, CH-OH), 3.62 (dd, 2H, $J = 5.9$ Hz, $J = 3.9$ Hz, $\text{CH}_2\text{-OH}$) ppm; $^{13}\text{C NMR}$ (75 MHz, CD_3OD) δ 117.5 (C5_{Im}), 114.5 (C4_{Im}), 71.3 (CH-OH), 65.1 ($\text{CH}_2\text{-OH}$), 53.8 ($\text{CH}_2\text{-Im}$); (ν_{max} , KBr): 3392 (OH), 2933; 1543 (C=N), 1478 (NO_2), 1363 (NO_2) cm^{-1} ; HRMS (TOF-APCI-POS) m/z calcd for $\text{C}_6\text{H}_8\text{Br}_2\text{N}_3\text{O}_4$ [M] $^+$ 343.8876, found 343.8847.

4.3. General procedure for regioselective tosylation

A solution of diol **13** or **14**, tosyl chloride, triethylamine and dibutyltin oxide in anhydrous CH_3CN was stirred under an argon atmosphere at rt. The solvent was removed under reduced pressure and the residue was treated as indicated below.

4.3.1. Toluene-4-sulfonic acid 3-(4-bromo-2-nitroimidazol-1-yl)-2-hydroxypropyl ester (**15**)

A mixture of diol **13** (50.0 mg, 0.267 mmol), tosyl chloride (50.0 mg, 0.267 mmol), triethylamine (0.037 mg, 0.267 mmol) and dibutyltin oxide (1.3 mg, 0.053 mmol) in CH_3CN (4 mL) was stirred for 5 h. The residue was chromatographed on silica gel using AcOEt/hexane 8:2. Compound **15** (76.0 mg) was obtained as a yellow solid. Yield: 83%; mp: 140.9–143.5 °C; R_f (_{AcOEt/hex 8:2}): 0.45; $^1\text{H NMR}$ (300 MHz, CD_3OD) δ 7.85 (d, 2H, $J = 8.2$ Hz, $\text{H}_{\text{o-Ts}}$), 7.49 (d, 2H, $J = 8.2$ Hz, $\text{H}_{\text{m-Ts}}$), 7.41 (s, 1H, $\text{H}_{5\text{-Im}}$), 7.13 (s, 1H, $\text{H}_{4\text{-Im}}$), 4.66 (dd, 1H, $J = 13.8$ Hz, $J = 3.3$ Hz, $\text{CH}_2\text{-Im}$), 4.36 (dd, 1H, $J = 13.8$ Hz, $J = 8.2$ Hz, $\text{CH}_2\text{-Im}$), 4.12–4.05 (m, 3H, CH , $\text{CH}_2\text{-OTs}$), 2.50 (s, 3H, CH_3) ppm; $^{13}\text{C NMR}$ (50 MHz, DMSO-d_6) δ 144.6 (C4_{Ts}), 144.38 (C2_{Im}), 131.4 (C1_{Ts}), 129.7 (2C, C3_{Ts}), 127.9 (C5_{Im}), 127.2 (2C, C2_{Ts}), 126.8 (C4_{Im}), 71.0 (CH-OH), 66.2 ($\text{CH}_2\text{-OTs}$), 50.7 ($\text{CH}_2\text{-Im}$), 20.6 (CH_3) ppm; IR (ν_{max} , KBr):

3204 (OH), 1539 (C= N), 1492 (NO₂), 1365 (SO₂), 1171 (SO₂) cm⁻¹; HRMS (TOF-APCI-POS) *m/z* calcd for C₁₃H₁₆N₃SO₆ [M]⁺ 342.0706, found 342,0624; Anal. (C₁₃H₁₅N₃O₆S) theoretical: C, 45.74; H, 4.42; N, 12.31; S, 9.39. Found: C, 45.58; H, 4.42; N, 12.11; S, 9.61.

4.3.2. Toluene-4-sulfonic acid 3-(4,5-dibromo-2-nitroimidazol-1-yl)-2-hydroxypropyl ester (**16**)

A mixture of diol **14** (0.905 g, 2.64 mmol), tosyl chloride (0.503 g, 2.64 mmol), triethylamine (0.268 g, 2.64 mmol) and dibutyltin oxide (0.013 g, 0.052 mmol) in CH₃CN (40 mL) was stirred for 24 h. The residue was dissolved in CH₂Cl₂ (20 mL), filtered and washed with brine (2 × 10 mL). The aqueous phase was extracted with CH₂Cl₂ (3 × 10 mL) and the combined organic extracts were dried over anhydrous Na₂SO₄, filtered, and evaporated to dryness. Finally, the residue was chromatographed on silica gel using a gradient of hexane/AcOEt from 8:2 to 6:4. Compound **16** (0.67 g) was obtained as a yellow solid. Yield: 51%; mp: 44–46 °C; R_f(Hex/AcOEt 6:4): 0.50; ¹H NMR (300 MHz, CDCl₃) δ 7.84 (d, 2H, *J* = 8.0 Hz, H_{o-Ts}), 7.48 (d, 2H, *J* = 8.0 Hz, H_{m-Ts}), 4.62 (m, 2H, CH₂-Im), 4.11 (s_{ap}, 3H, CH-OH, CH₂-OTs), 2.50 (s, 3H, CH₃) ppm; ¹³C NMR (75 MHz, CD₃OD) δ 146.8 (C_{4-Ts}), 133.9 (C_{1-Ts}); 131.1 (2C, C_{3-Ts}), 129.1 (2C, C_{2-Ts}), 117.6 (C_{5-Im}), 114.6 (C_{4-Im}), 72.1 (CH-OH), 68.3 (CH₂-OTs), 52.8 (CH₂-Im), 21.6 (CH₃) ppm; IR (ν_{max}, KBr): 3413 (OH), 1597 (C=N), 1474 (NO₂), 1362 (NO₂), 1175 (SO₂) cm⁻¹; HRMS (TOF-APCI-POS) *m/z* calcd for C₁₃H₁₄Br₂N₃O₆S [M]⁺ 497.8965, found 497.8991; Anal. (C₁₃H₁₃Br₂N₃O₆S) theoretical: C, 31.28; H, 2.65; N, 8.42; S 6.42. Found: C, 31.39; H, 2.67; N, 8.61; S, 6.49).

4.4. General procedure for tetrahydropyranyl ketal formation

A solution of **15** or **16**, DHP and PPTS in anhydrous CH₂Cl₂ was stirred at 0 °C under an argon atmosphere. The solvent was removed at rt under reduced pressure. The residue was chromatographed on silica gel using AcOEt/hexane 6:4 as eluent.

4.4.1. *Toluene-4-sulfonic acid 3-(4-bromo-2-nitroimidazol-1-yl)-2-(tetrahydropyran-2-yloxy)propyl ester (17)*

A mixture of alcohol **15** (1.2 g, 2.85 mmol), DHP (0.74 g, 8.83 mmol) and PPTS (0.89 g, 3.54 mmol) in CH₂Cl₂ (78 mL) was stirred for 22 h. Compound **17** (1.0 g) was obtained as a yellow solid. Yield: 68%; mp: 120.0–122.3 °C; R_f(Hex/AcOEt 6:4): 0.44; ¹H NMR (500 MHz, CDCl₃) δ 7.79 (d, 2H, *J* = 8.1 Hz, H_{o-Ts}, dias. A), 7.78 (d, 2H, *J* = 8.1 Hz, H_{o-Ts}, dias. B), 7.36 (d, 2H, *J* = 8.1 Hz, H_{m-Ts}, dias. A+B), 7.09 (s, 1H, H_{5-Im}, dias. B), 7.01 (s, 1H, H_{5-Im}, dias. A), 4.79 (dd, 1H, *J* = 14.0 Hz, *J* = 3.3 Hz, CH₂-Im, dias. A), 4.68 (dd, 1H, *J* = 14.0 Hz, *J* = 3.3 Hz, CH₂-Im, dias. B), 4.44 (m, 1H, H_{2-THP}, dias. B), 4.34 (m, 2H, CH₂-Im dias. A+B), 4.27 (m, 1H, H_{2-THP}, dias. A), 4.21 (m, 2H, CH-OTHP, dias. B + CH₂-OTs, dias. A), 4.11 (dd, 1H, *J* = 11.2 Hz, *J* = 4.5 Hz, CH₂-OTs, dias. B), 4.05–3.98 (m, 3H, CH-OTHP, dias. B + CH₂-OTs, dias. A+B), 2.45 (s, 3H, CH₃, dias. A+B), 1.67–1.38 (m, 6H, H_{3,4,5-THP}, dias. A+B) ppm; ¹³C NMR (75 MHz, CDCl₃) δ 145.8, 132.5, 130.1 (2C), 128.0 (2C), 126.3, 115.3, 100.9, 97.8, 74.1, 70.3, 68.5, 67.0, 63.2, 51.1, 50.5, 30.3, 30.1, 24.9, 24.8, 21.7, 19.7, 19.3 ppm; IR (ν_{max}, KBr): 3449 (OH), 1535 (C=N), 1499 (NO₂), 1350 (SO₂), 1168 (SO₂) cm⁻¹; HRMS (TOF-APCI-POS) *m/z* calcd for C₁₈H₂₃BrN₃O₇S [M]⁺ 504.0440, found 504.0400; Anal (C₁₈H₂₂BrN₃O₇S) theoretical: C, 42.86; H, 4.39; N, 8.33; S, 6.35. Found: C, 42.60; H, 4.46; N, 8.24; S, 6.36.

4.4.2. *Toluene-4-sulfonic acid 3-(4,5-bromo-2-nitroimidazol-1-yl)-2-(tetrahydropyran-2-yloxy)propyl ester (18)*

A mixture of alcohol **16** (0.62 g, 1.25 mmol), DHP (0.34 g, 3.75 mmol) and PPTS (0.38 g, 1.5 mmol) in CH₂Cl₂ (35 mL) was stirred for 4 h. Compound **18** (0.5 g) was obtained as an oil which was treated with Et₂O to give a yellow solid. Yield: 69%; mp: 51.0–53.0 °C; R_f(Hex/AcOEt 6:4): 0.54; ¹H NMR (300 MHz, CDCl₃) δ 7.78 (d, 2H, *J* = 8.3 Hz, H_{o-Ts}, dias.

A+B), 7.36 (d, 2H, $J = 8.3$ Hz, H_{m-Ts}, dias. A+B), 4.66 (m, 2H, H_{2-THP}, CH₂-Im, dias. A+B), 4.36–3.95 (m, 4H, CH₂-Im + CH-OTHP + CH₂-OTs dias. A+B), 3.67–3.27 (m, 1H, H_{6-THP}, dias. A+B), 3.13 (m, 1H, H_{6-THP}, dias. A+B), 2.45 (s, 3H, CH₃, dias. A+B), 1.54–1.18 (m, 6H, H_{3,4,5-THP}, dias. A+B) ppm; ¹³C NMR (75 MHz, CDCl₃) δ 145.8, 145.4, 132.4, 132.2, 131.8, 130.0 (2C), 127.9 (2C), 101.3, 97.5, 74.7, 70.6, 67.9, 63.9, 62.9, 51.5, 50.5, 30.3, 24.7, 21.7, 20.2, 19.2 ppm; IR (ν_{\max} , KBr): 3435 (OH), 2945, 1597 (C=N), 1545, 1474 (NO₂), 1363 (NO₂), 1176 (SO₂) cm⁻¹; HRMS (TOF-APCI-POS) m/z calcd for C₁₈H₂₂Br₂N₃O₇S (M)⁺ 581.9540, found 581.9545; Anal (C₁₈H₂₁Br₂N₃O₇S) theoretical: C, 37.06; H, 3.62; N, 7.20; S, 5.49. Found: C, 37.13; H, 3.63; N, 7.25; S, 5.67.

4.5. General procedure for fluorination

A solution of sulfonate **17** (0.99 mmol) or **18** (0.35 mmol) and CsF (3 equiv) in *tert*-amyl alcohol (3.3 mL per mmol of sulfonate) was heated at 120 °C for 3 h. The solvent was removed under reduced pressure and the residue was chromatographed on silica gel.

4.5.1. 4-Bromo-1-[3-fluoro-2-(oxiran-2-yloxy)-propyl]-1H-2-nitroimidazole (**19**)

Compound **17** (0.50 g) gave **19** (0.24 g) as a yellowish oil after chromatography using AcOEt/hexane 6:4 as eluent. Yield: 69%; R_f(AcOEt/Hex 6:4): 0.42; ¹H NMR (300 MHz, CDCl₃) δ 7.17 (s, 1H, H_{5-Im}, dias. B), 7.11 (s, 1H, H_{5-Im}, dias. A), 4.81 (dd, 1H, $J = 14.1$ Hz, $J = 3.6$ Hz, CH₂-Im, dias. A), 4.73 (dd, 1H, $J = 14.1$ Hz, $J = 3.6$ Hz, CH₂-Im, dias. B), 4.65–4.30 (m, 4H, H_{2-THP}+CH₂-Im+CH₂-F, dias. A+B), 4.28–4.16 (m, 1H, CH-OTHP, dias. A), 4.11–4.01 (m, 1H, CH-OTHP, dias. B), 3.81–3.74 (m, 1H, H_{6-THP}, dias. A), 3.45–3.38 (m, 1H, H_{6-THP}, dias. A), 3.25–3.21 (m, 2H, H_{6-THP}, dias. A+B), 1.70–1.37 (m, 6H, H_{3,4,5-THP}, dias. A+B) ppm; IR (ν_{\max} , KBr): 3420 (OH), 1595 (C=N), 1462 (NO₂), 1354 (NO₂), 1358 (SO₂), 1178 (SO₂) cm⁻¹; HRMS (TOF-APCI-POS) m/z calcd for C₁₁H₁₆BrFN₃O₄ [M]⁺ 352.0303, found 352.0315.

4.5.2. 4,5-Dibromo-1-[3-fluoro-2-(oxiran-2-yloxy)propyl]-1H-2-nitroimidazole (**20**)

Compound **18** (0.20 g) gave **20** (0.045 g) as a yellowish oil after chromatography using AcOEt/hexane 7:3 as eluent. Yield: 31%; $R_{f(\text{AcOEt/Hex } 7:3)}$: 0.48; $^1\text{H NMR}$ (300 MHz, CDCl_3) δ 4.81–4.40 (m, 5H, $\text{H}_{2\text{-THP}}+\text{CH}_2\text{-Im}+\text{CH}_2\text{-F}$, dias. A+B), 4.24–4.16 (m, 2H, CH-OTHP, dias. A+B), 3.80 (m, 1H, $\text{H}_{6\text{-THP}}$, dias. A), 3.46 (m, 1H, $\text{H}_{6\text{-THP}}$, dias. A), 3.20 (m, 2H, $\text{H}_{6\text{-THP}}$, dias. B), 1.64–1.22 (m, 6H, $\text{H}_{3,4,5\text{-THP}}$, dias. A+B) ppm; HRMS (TOF-APCI-POS) m/z calcd for $\text{C}_{11}\text{H}_{15}\text{Br}_2\text{FN}_3\text{O}_4$ $[\text{M}]^+$ 429.9408, found 429.9404.

4.6. General procedure for tetrahydropyranyl ketal deprotection

The THP ketal **19** (0.59 mmol) or **20** (0.10 mmol) was dissolved in AcOH (4.1 mL per mmol), THF (2.2 mL per mmol) and H_2O (1.1 mL per mmol) and the mixture was heated at 65 °C. The solvent was removed under reduced pressure and the residue was chromatographed on silica gel using hexane/AcOEt. The resulting thick oil was treated with Et_2O to give a pale-yellow solid which was filtered off and dried.

4.6.1. 1-(4-Bromo-1H-2-nitroimidazol-1-yl)-3-fluoropropan-2-ol (**21**)

Compound **19** (0.209 g) was heated for 6 h to give **21** (0.103 g) after chromatography using AcOEt/hexane 4:6 as eluent. Yield: 65%; mp: 104–105 °C; $R_{f(\text{AcOEt/Hex } 4:6)}$: 0.44; $^1\text{H NMR}$ (500 MHz, CD_3OD): δ 7.57 (s, 1H, $\text{H}_{5\text{-Im}}$), 4.75 (dd, 1H, $J = 13.8$ Hz, $J = 3.3$ Hz, $\text{CH}_2\text{-Im}$), 4.47 (dd, 2H, $^1J_{\text{H-F}} = 47.1$ Hz, $J = 4.3$ Hz, $\text{CH}_2\text{-F}$), 4.44 (dd, 1H, $J = 13.8$ Hz, $J = 8.9$ Hz, $\text{CH}_2\text{-Im}$), 4.18 (dq, 1H, $^2J_{\text{H-F}} = 19.8$ Hz, $J = 4.0$ Hz, CH-OH) ppm; $^{13}\text{C NMR}$ (75 MHz, CD_3OD) δ 146.0 ($\text{C}_{2\text{Im}}$), 128.7 ($\text{C}_{5\text{Im}}$), 114.6 ($\text{C}_{4\text{Im}}$), 85.3 (d, 1C, $^1J_{\text{C-F}} = 171.2$ Hz, $\text{CH}_2\text{-F}$), 69.5 (d, 1C, $^2J_{\text{C-F}} = 19.8$ Hz, CH-OH), 53.1 (d, 1C, $^3J_{\text{C-F}} = 7.4$ Hz, $\text{CH}_2\text{-Im}$) ppm; IR (ν_{max} , KBr): 3398, 3103, 1541, 1510, 1470, 1400, 1377, 1261, 1012, 959, 845 cm^{-1} ; HRMS (TOF-

APCI-POS) m/z calcd for $C_6H_8BrFN_3O_3$ $[M]^+$ 267.9733, found 267.9719; Anal ($C_6H_7BrFN_3O_3$) theoretical: C, 26.89; H, 2.63; N, 15.68. Found: C, 26.67; H, 2.82; N, 15.91.

4.6.2. 1-(4,5-Dibromo-1H-2-nitroimidazol-1-yl)-3-fluoropropan-2-ol (**22**)

Compound **20** (0.045 g) was heated for 3 h to give **22** (0.025 g) as a yellowish oil after chromatography using AcOEt/hexane 4:6 as eluent. Yield: 69%; $R_{f(AcOEt/Hex\ 4:6)}$: 0.44; 1H NMR (300 MHz, CD_3OD) δ 4.75 (dd, 2H, $J = 6.6$ Hz, $J = 0.6$ Hz, CH_2-Im), 4.50 (dd, 2H, $^1J_{H-F} = 47.1$ Hz, $J = 4.4$ Hz, CH_2-F), 4.24–4.12 (m, 1H, CH-OH) ppm; ^{13}C NMR (125 MHz, CD_3OD): δ 146.3 ($C2_{Im}$), 117.7 ($C5_{Im}$), 114.7 ($C4_{Im}$), 85.3 (d, 1C, $^1J_{C-F} = 170.7$ Hz, CH_2-F), 69.3 (d, 1C, $^2J_{C-F} = 20.0$ Hz, CH-OH), 52.5 (d, 1C, $^3J_{C-F} = 7.6$ Hz, CH_2-Im) ppm; IR (ν_{max} , KBr): 3404, 1547, 1473, 1361, 1248 cm^{-1} ; HRMS (TOF-APCI-POS) m/z calcd for $C_6H_7Br_2FN_3O_3$ $[M]^+$ 345.8833, found 345.8879.

4.7. Cyclic voltammetry

Compounds were dissolved in 0.1 M Bu_4NBF_4 in DMF as SSE (solvent support electrolyte) to a concentration of 4×10^{-3} M. Cyclic voltammetry was carried out in a VoltaLab PGZ100 potentiostat at 25 ± 1 °C under an argon atmosphere using glassy carbon electrode, platinum as auxiliary electrode and Ag/satd Ag^+ as reference electrode at a scan speed of 100 mV/s. In the procedure, SSE (20 mL) was added to the cuvette, electrodes were submerged into the solution, solvent was deoxygenated using a flow of argon for 15 min and a scan of SSE was carried out. The compound (**21** or **1**) was added and the solvent was again deoxygenated for 15 min. Finally, scans were performed using cycles from 0 to -2.5 V and from -2.5 to 0 V recording cyclic voltammograms for each compound.

4.8. bEnd5 cell line cultures

Murine brain endothelial cells (b.End5), which are recognized as having brain endothelium-like properties, were obtained from the European Collection of Cell Cultures (UK). This cell model is an appropriate choice to study blood-brain barrier function [38,39]. The cells were grown in Dulbeccos's Modified Eagle's Medium, with high glucose content (4.5 g/L; Lonza), supplemented with 10% heat inactivated fetal bovine serum (FBS, Gibco) and gentamicin (40 $\mu\text{g}/\text{mL}$), and samples were maintained under standard cell culture conditions at 37 °C and 5% CO_2 in a humid atmosphere. The cells were trypsinized (Trypsin 0.5 mg/mL/EDTA 0.2 mg/mL, in Hank's balanced salt solution, Sigma) and 50,000 cells in 100 μL of medium were seeded in inserts (culture treated polycarbonate membrane, pore size 0.4 μm ; 9 mm diameter; Costar). 700 μL of medium was added to the lower compartment. Cultures were incubated for 24 h and the medium was changed to the same medium but without phenol red and FBS prior to the assessment of drug transport. Sister cultures in P96 plates were used to assess confluency. The drugs at the concentrations used did not alter the viability of the cells at 24 h after the addition (not shown; MTT assay).

4.9. Transport across an endothelial cell monolayer

The transport of the compounds under study was assessed in an *in vitro* system consisting of a confluent endothelial cell monolayer on an insert (upper compartment), which was placed onto a P24 well plate (lower compartment). Inserts placed in P24 transwell plates consisted in 6.5 mm diameter inserts, with tissue culture treated polycarbonate membrane and 0.4 μm pore size (Costar, Corning Inc., NY, USA). The compounds were added to the upper compartment and the medium in the lower compartment was collected (600 μL) at 15 min intervals up to 60 min after its addition. Duplicate cultures were used for each drug and for each time. The media samples were freeze-dried and were stored at 4 °C prior to

quantification by HPLC analysis. Transport was expressed as percentage of the actual amount used each day, which was also measured by HPLC.

4.10. Primary cultures and assessment of neuronal injury

Primary mixed cultures were prepared from the cerebral cortex of 18-day-old Wistar rat embryos and were grown in minimum essential medium (Invitrogen-Life Technologies, Carlsbad, CA, USA) as described previously [40]. Where indicated, primary cultures were also grown in neurobasal medium (Invitrogen-Life Technologies) with serum-free B-27 supplement. Stock solutions (20 mM) in DMSO were prepared for **1** and **21**. From these solutions, new stock solutions (2 mM) in DMSO were made for each compound. The same was carried out from the former solutions to prepare new stock solutions (0.2 mM) for both compounds. Aliquots (10 μ L) were taken from the 20, 2 and 0.2 mM solutions to prepare 100, 10 and 1 μ M solutions in DMEM medium (2 mL), respectively. The final concentration of DMSO in these solutions was 0.5 %. Cultures were then treated with different concentrations (0, 1, 10, 100 μ M) of compounds **1** and **2** at 7–9 days of *in vitro* culture. The MTT and LDH reduction assays were used to measure cell viability after 24 h of incubation with compounds. MTT (Aldrich, M2128) (0.5 mg/mL) was added to the medium and, after 2 h at 37 °C, the resulting formazan salts were dissolved in DMSO and were spectrophotometrically quantified (OD, optical density) at 540 nm (Thermomax, Molecular Devices). Viability percentage was calculated as % Viability = (OD treated cells / OD control cells) \times 100. Extracellular and intracellular LDH activities were spectrophotometrically measured by following tetrazolium reduction at an absorbance wavelength of 490 nm (Boehringer Mannheim kit). Total LDH activity was defined as the sum of intracellular and extracellular LDH activity. Released LDH was defined as the percentage of extracellular compared to total LDH activity.

4.11. Radiosynthesis

4.11.1. Generation of $^{18}\text{F}^-$

$^{18}\text{F}^-$ was produced by an $^{18}\text{O}(\text{p},\text{n})^{18}\text{F}$ reaction in an IBA cyclotron following bombardment of enriched H_2^{18}O (ROTEM Industries). When the theoretical activity was in the range 100 mCi to 3000 mCi (3.7 GBq to 111.0 GBq) the material was transferred in solution with H_2O^{18} to the synthesizer.

4.11.2. Radiolabeling of [^{18}F]21

The radiosynthesis was undertaken on a Synthera® (IBA Molecular) automated synthesizer using an Integrated Fluidic Processor (ABX). Reagents, including cryptand solution, HCl, MeCN and citrate buffer were purchased from ABX. Cartridges for solid phase purification were purchased from the Waters Corporation. The $^{18}\text{F}^-$ was trapped on a pre-conditioned Waters Sep-Pak QMA Light (quaternary methyl ammonium) anion exchange cartridge (46 mg, ABX) and washed with H_2O before it was eluted with cryptand solution (2.2 mg kryptofix-222 and 7 mg K_2CO_3 in 600 μL of a 1:1 mixture of H_2O and MeCN). The eluate was dried under reduced pressure and the reactor was heated to 130 °C over 5 minutes. Following addition of the precursor solution (6–12 mg dissolved in 2.5 mL MeCN), the reactor was sealed and the mixture was heated for 5 min. The reaction mixture was cooled to 100 °C over 3 minutes before a solution of HCl (1M, 1 mL) was added to effect hydrolysis, which was carried out at 100 °C over 5 minutes. The reaction mixture was buffered (pH = 5.8) with a solution (4.5 mL, Synthera® [^{18}F]FLT reagent sets buffer solution, ABX) containing 1M AcONa (0.5 mL), 1M NaOH (0.45 mL), EtOH (0.25 mL) and water (3.3 mL), mixed, and transferred automatically to the HPLC system.

4.11.3. Purification

The crude reaction mixture was purified by automated injection onto a semi-preparative C18 HPLC column (250 mm × 10 mm, 100 Å, Phenomenex) in a Synthera® HPLC system (ABX Molecular). Separated compounds were eluted with 95:5 H₂O/EtOH and a flow rate of 4 mL/min, and fractions were collected using the peak collection tool of the operating software. Under these conditions the retention time of [¹⁸F]21 was 33 minutes and a major radiochemical impurity eluted after 21 minutes. The total synthesis time was 55 minutes and the radiochemical yield was 18% (decay corrected) with a specific activity of 150 ± 15 GBq/μmol (at the end of radiosynthesis).

4.11.4. Formulation

Fractions were prepared for injection by dilution with a 0.9% saline solution in order to reach the desired activity concentration (mCi/mL).

4.11.5. Quality Control

Radiochemical purity was determined by analytical HPLC (Agilent 1200 series, Zorbax Eclipse Plus C18 Column, 5 μm, 4.6 × 100 mm; H₂O:EtOH = 95:5, flow rate = 1 mL/min) and was greater than 99%. The identity of the compound was confirmed by comparison of the radiolabeled peak with the UV peak contributed by the reference standard. Radionuclide identity was confirmed by GENIE multichannel analysis, with the area of the peak at 511 keV in excess of 97%. In addition, the half-life of the sample was determined by taking twenty-one activity measurements over a 20 minute interval and the use of the decay equation. The half-life was calculated to be 108 minutes. The pH of the sample was measured with colored pH strips and was found to be 6.9.

4.12. Permanent middle cerebral artery occlusion (pMCAO)

Male Fischer rats (250–300 g body weight; Harlan; Barcelona, Spain) (n = 7) were used in the study. All experimental protocols adhered to the guidelines of the Animal Welfare Committee of the Universidad Complutense (following EU directives 86/609/CEE and 2003/65/CE). Animals were housed individually under standard conditions of temperature and humidity and a 12 hours light/dark cycle (lights on at 08:00) with free access to food and water. Rats were anesthetized (isoflurane 1.5–2% in 100% oxygen) and underwent analgesia (metamizole 100 mg/kg ip). Body temperature was maintained at physiological levels with a heating pad during the surgical procedure and anesthesia recovery. The permanent cerebral ischemia model consisted of right pMCAO and of both common carotid artery occlusion [40]; after 75 min, the contralateral common carotid artery was de-occluded to reduce animal death rate. In this model, the characteristic changes of ischemic necrosis are limited to the parietal and sensory-motor cortex and large infarcts are reproducibly generated in the right MCA territory after 24 h of surgery. The injured area – seen at 3 h after surgery – showed a variable staining throughout the MCA territory combining: 1) areas with loss of cytoplasmic Nissl staining and rounded with swollen neuronal cells and 2) areas showing a triangular morphology with a reduced size of cell body and processes, indicating cellular damage, as reported previously [40]. After the surgery, animals were returned to their cages to recover from anaesthesia. The animals were then subjected to PET imaging study.

4.13. Positron emission tomography

For *in vivo* comparison of the hypoxia-imaging compounds, brain PET scans were performed in a dedicated small animal PET-CT hybrid tomograph (Albira ARS, Oncovision, Valencia, Spain). Briefly, [¹⁸F]FMISO ([¹⁸F]**1**) or [¹⁸F]**21** (55.5 MBq in approx. 0.2mL 0.9% NaCl, i.v.) were injected into animals 30 minutes after surgery. After an uptake period of 150 min, the rats were anesthetized with isoflurane (4.5% for induction and 1.5% for

maintenance) and placed on the bed of the scanner with the head centered in the field of view in a spread prone position to perform a static acquisition of 20 minutes. PET acquisition was immediately followed by a CT scan. After the acquisitions, tomographic images were reconstructed using 3D OSEM algorithm for PET and filtered back projection for the CT images. Corrections for decay, death-time, scatter, and random coincidences were applied during the PET reconstruction process. In order to estimate the degree of the ischemic lesion, a [^{18}F]FDG-PET was performed 24 hours after the pMCAO, as reported previously [40].

4.14. Image analysis and calculation of the uptake properties of the [^{18}F]21

For imaging analysis, the [^{18}F]FMISO ([^{18}F]1) or [^{18}F]21 scans were co-registered with the FDG scan of the same animal. For this purpose the CT image of the skull from [^{18}F]1 scan was co-registered to the CT image of [^{18}F]FDG scan. After the CT images were co-registered, the spatial mathematical transformation was saved and then applied to its own fused PET image as described previously [41]. This process allowed the correct matching between the two PET brain images. Due to the unavoidable variability of the damage generated by the ischemic surgical process, the simple calculation of [^{18}F]FMISO ([^{18}F]1) or [^{18}F]21 uptake in the brain damage area did not provide a reliable index of the radiotracer ability to bind to the hypoxic area. To overcome this drawback, this parameter was calculated as the ratio of the specific accumulation of tracer to hypoxic area 3 hours after the ischemic onset and the level of metabolic dysfunction in the same area obtained 24 hours later by using [^{18}F]FDG as a brain metabolism tracer. To this end, a 4.5 mm³ spherical VOI was placed in the center of the hypoxic area and it was mirrored to the non-affected contralateral brain hemisphere. These two VOIs were transposed to the [^{18}F]FDG PET images. The standardized uptake values (SUV) of the hypoxia tracers and [^{18}F]FDG in both two areas were then obtained. This allowed us to calculate the specific accumulation of the hypoxia tracers and the level of

hypometabolism. Afterwards, for each tracer the ratio of both parameters was obtained (i.e., the binding of the tracer in relation to hypometabolism). This ratio can be considered to be a valid estimative quantifier of [^{18}F]1 and [^{18}F]21 to specifically accumulate in the hypoxia area. All of these processes of visualization, co-registration, and quantification were performed using the PMOD 3.1 software (PMOD Technologies, Zurich, Switzerland). In order to check if [^{18}F]21 was able to follow up the evolution of the hypoxic area, additional PET scans with this tracer were performed at 9 and 15 hours after ischemic onset.

Notes

The authors declare no competing financial interest.

Acknowledgements

The authors acknowledge the Instituto Tecnológico PET (CENIT-20081013 CDTI UAH-17/2009), Comunidad de Madrid (Projects S-BIO-0170-2006 and S2011/BMD-2349), Ministerio de Economía y Competitividad (Projects CTQ-2008/05027/BQU and SAF2009-09020) and Universidad de Alcalá (Projects UAH2011/EXP-034 and UAH GC2012/001) for financial support. E.N. thanks University of Alcalá for a fellowship. We also thank Dr. Belén Batanero (University of Alcalá) for her kind guidance to carry out cyclic voltammetry experiments.

Animal experiments

All experimental protocols adhered to the guidelines of the Animal Welfare Committee of the Universidad Complutense (following EU directives 86/609/CEE and 2003/65/CE).

Apendix A. Supplementary data

Experimental procedures for the synthesis and full characterization of compounds **1** and **23**. ^1H and ^{13}C NMR, IR and HRMS spectra of compounds **1**, **13–19**, **21–23**. Graph for toxicity of FMISO (**1**) and **21** in rat embryo cortical neuron cell culture. Semi-preparative radio-HPLC of crude [^{18}F]**21** showing fractioning. Analytical radio-HPLC of purified [^{18}F]**21**. This material is available free of charge via the Internet at <http://>

References

- [1] Campbell, B.C.V., Oxley, T.J., Chapot, R. Acute ischemic stroke. Time, penumbra, and reperfusion. *Stroke* 45 (2014) 640-644.
- [2] Burton, K.R., Perlis, N., Aviv, R.I., Moody, A.R., Kapral, M.K., Krahn, M.D., Laupacis, A. Systematic review, critical appraisal, and analysis of the quality of economic evaluations in stroke imaging. *Stroke* 45 (2014) 807-814.
- [3] Muir, K.W., Buchan, A., von Kummer, R., Rother, J., Baron, J.C. Imaging of acute stroke, *Lancet Neurol.* 5 (2006) 755-768.
- [4] Takasawa, M., Moustafa, R.R., Baron, J.-C. Applications of nitroimidazole in vivo hypoxia imaging in ischemic stroke. *Stroke* 39 (2008) 1629-1637.
- [5] Nunn, A., Linder, K., Strauss, H.W. Nitroimidazoles and imaging hypoxia. *Eur. J. Nucl. Med.* 22 (1995) 265-280.
- [6] McClelland, R.A., Panicucci, R., Rauth, M. Products of reductions of 2-nitroimidazoles. *J. Am. Chem. Soc.* 109 (1987) 4308-4314.
- [7] Bolton, J.L., McClelland, R.A. Kinetics and mechanism of the decomposition in aqueous solutions of 2-(hydroxylamino)imidazoles. *J. Am. Chem. Soc.* 111 (1989) 8172-8181.
- [8] Brezden, C.B., McClelland, R.A., Rauth, M. Mechanism of the selective hypoxic cytotoxicity of 1-methyl-2-nitroimidazole. *Biochem. Pharmacol.* 48 (1994) 361-370.

- [9] Brezden, C.B., Horn, L., McClelland, R.A., Rauth, M. Mechanism of the selective hypoxic cytotoxicity of 1-methyl-2-nitroimidazole. *Biochem. Pharmacol.* 56 (1989) 335-344.
- [10] Lee, S.T., Scott, A.M. Hypoxia positron emission tomography imaging with ^{18}F -fluoromisonidazole. *Semin. Nucl. Med.* 37 (2007) 451-461.
- [11] Yamamoto, F., Oka, H., Antoku, S., Ichiya, Y.-I., Masuda, K., Maeda, M. Synthesis and characterization of lipophilic 1- ^{18}F fluoroalkyl-2-nitroimidazoles for imaging hypoxia. *Biol. Pharm. Bull.* 22 (1999) 590-597.
- [12] Grunbaum, Z., Freauff, S.J., Krohn, K.A., Wilbur, D.S., Magee, S., Rasey, J.S. Synthesis and characterization of congeners of misonidazole for imaging hypoxia. *J. Nucl. Med.* 28 (1987) 68-75.
- [13] Rasey, J.S., Krohn, K.A., Freauff, S.J. Bromomisonidazole, synthesis and characterization of a new radiosensitizer. *Radiat. Res.* 91 (1982) 542-554.
- [14] Yamamoto, F., Aoki, M., Furusawa, Y., Ando, K., Kuwabara, Y., Masuda, K., Sasaki, S., Maeda, M. Synthesis and evaluation of 4-bromo-1-(3- ^{18}F fluoropropyl)-2-nitroimidazole with a low energy LUMO orbital designed as brain hypoxia-targeting imaging agent. *Biol. Pharm. Bull.* 25 (2002) 616-621.
- [15] Ziemer, L.S., Evans, S.M., Kachur, A.V., Shuman, A.L., Cardi, C.A., Jenkis, W.T., Karp, J.S., Alavi, A., Dolbier, W.R., Koch, C.J. Noninvasive imaging of tumor hypoxia in rats using the 2-nitroimidazole ^{18}F -EF5. *Eur. J. Nucl. Med. Mol. Imaging* 30 (2003) 259-266.
- [16] Piert, M., Machulla, H.J., Picchio, M., Reischl, G., Ziegler, S., Kumar, P., Wester, H.-J., Beck, R., McEwan, A.J.B., Wiede, L.I., Schwaiger, L. Hypoxia-specific tumor imaging with ^{18}F -fluoroazomycin arabinoside. *J. Nucl. Med.* 46 (2005) 106-113.

- [17] Postema E.J., McEwan, A.J.B., Riauka, T.A., Kumar, P., Richmond, D.A., Abrams, D.N., Wiede, L.I. Initial results of hypoxia imaging using 1- α -D-(5-deoxy-5-[18 F]-fluoroarabinofuranosyl)-2-nitroimidazole (18 F-FAZA). *Eur. J. Nucl. Med. Mol. Imaging* 36 (2009) 1565-1573.
- [18] Peeters, S.G.J.A.; Zegers, C.M.L.; Lieuwes, N.G.; van Elmpt, W.; Eriksson, J.; van Dongen, G.A.M.S.; Dubois, L.; Lambin, P. A Comparative Study of the Hypoxia PET Tracers [18 F]HX4, [18 F]FAZA, and [18 F]FMISO in a Preclinical Tumor Model, *Int. J. Radiat. Oncol., Biol., Physics* 91 (2015) 351-359.
- [19] Zegers, C.M.L.; van Elmpt, W.; Reymen, B.; Even, A.J.G.; Troost, E.G.C.; Oellers, M.C.; Hoebbers, F.J.P.; Houben, R.M.A.; Eriksson, J.; Windhorst, A.D.; Mottaghy, F.M.; De Ruyscher, D.; Lambin, P. In Vivo Quantification of Hypoxic and Metabolic Status of NSCLC Tumors Using [18 F]HX4 and [18 F]FDG-PET/CT Imaging, *Clin. Cancer Res.* 20 (2014) 6389-6397.
- [20] Fujibayashi, Y., Taniuchi, H., Yonekura, Y., Ohtani, H., Konishi, J., Yokohama, A. Copper-62-ATSM: a new hypoxia imaging agent with high membrane permeability and low redox potential. *J. Nucl. Med.* 38 (1997) 1155-1160.
- [21] McQuade, P., Martin, K.E., Castle, T.C., Went, M.J., Blower, P.J., Welch, M.J., Lewis, J.S. Investigation into 64 Cu-labeled Bis(selenosemicarbazone) and Bis(thiosemicarbazone) complexes as hypoxia imaging agents. *Nucl. Med. Biol.* 32 (2005) 147-156.
- [22] Chitnemi, S.K., Palmer, G.M., Zalutsky, M.R., Dewhirst, M.W. Molecular imaging of hypoxia. *J. Nucl. Med.* 52 (2011) 165-168.
- [23] Williamson, D.J., Ejaz, S., Sitnikov, S., Fryer, T.D., Sawiak, S.J., Burke, P., Baron, J.-C., Aigbirhio, F.I. A comparison of four PET tracers for brain hypoxia mapping in a rodent model of stroke. *Nucl. Med. Biol.* 40 (2013) 338-334.

- [24] Jette, D.C.; Wiebe, L.I.; Chapman, J.D. Synthesis and in vitro studies of the radiosensitizer 4-^[82Br]bromomisonidazole. *Int. J. Nucl. Med.* 10 (1983) 205-210.
- [25] Nieto, E., Alajarín, R., Álvarez-Builla, J., Larrañaga, I., Gorospe, E., Pozo, M.A. A new and improved synthesis of the precursor of the hypoxia marker [^{18F}]-FMISO. *Synthesis* (2010) 3700-3704.
- [26] Martinelli, M.J., Vaidyanathan, R., Pawlak, J.M., Nayyar, N.K., Dhokte, U.P., Doecke, C.W., Zollars, L.M.H., Moher, E.D., Khau, V.V., Košmrlj, B. Catalytic regioselective sulfonylation of α -chelatable alcohols: Scope and mechanistic insight. *J. Am. Chem. Soc.* 124 (2002) 3578.
- [27] Kim, D.W., Ahn, D.-S., Oh, Y.-H., Lee, S., Kil, H.S., Oh, S.J., Lee, S.J., Kim, J.S., Ryu, J.S., Moon, D.H., Chi, D.Y. A new class of SN2 reaction catalyzed by protic solvents: Facile fluorination for isotopic labeling of diagnostic molecules. *J. Am. Chem. Soc.* 128 (2006) 16394-16397.
- [28] Oh, S.J., Chi, D.Y., Mosdzianowski, C., Kim, J.Y., Gil, H.S., Kang, S.H., Ryu, J.S., Moon, D.H. Fully automated synthesis of [^{18F}]fluoromisonidazole using a conventional [^{18F}]FDG module. *Nucl. Med. Biol.* 32 (2005) 899-905.
- [29] Palmer, B.D., Denny, W.A. Synthesis and reactions of brominated 2-nitroimidazoles. *J. Chem. Soc. Perkin Trans. I* (1989) 95-99.
- [30] Pacheco-Torres, J., Perez-Mayoral, E., Soriano, E., López-Larrubia, P., Ouari, O., González-Cortés, A., Cerdán, S., Ballesteros, P. A convenient and efficient synthesis of the first (nitroimidazolyl)succinic esters and their diacids. *Synthesis* (2006) 3859-3864.
- [31] Carbajo, J., Bollo, S., Núñez-Vergara, L.J., Campero, A., Squella, J.A. Cyclic voltammetric study of the disproportionation reaction of the nitro radical anion from 4-nitroimidazole in protic media. *J. Electroanal. Chem.* 531 (2002) 187-194.

- [32] Cavalcanti, J.C.M., Oliveira, N.V., de Moura M.A.B.F., Fruttero, R., Bertinaria, M., Goulart, M.O.F. Evidence of self-protonation on the electrodic reduction mechanism of an anti-*Helicobacter pylori* metronidazole isostere. *J. Electroanal. Chem.* 571 (2004) 177-182.
- [33] Jensen, B.S., Parker, V.K. Reversible anion radical-dianion redox equilibriums involving ions of simple aromatic compounds. *J. Chem. Soc. Chem. Commun.* (1974) 367-368.
- [34] Arguelho, M.L.P.M., Silva, G.M., Stradiotto, N.R. Electroreduction of benznidazole in dimethyl sulfoxide. *J. Electrochem. Soc.* 148 (2001) D1-D3.
- [35] Pardridge, W.M. Crossing the blood-brain barrier: are we getting right? *Drug Discovery Today* 6 (2001) 1-2.
- [36] Di, L., Rong, H., Feng, B. Demystifying brain penetration in central nervous system drug discovery. *J. Med. Chem.* 56 (2013) 2-12.
- [37] Pajouhesh, H.; Lenz, G.R. Medicinal chemical properties of successful central nervous system drugs, *NeuroRx* 2 (2005) 541-553.
- [38] Yang, T., Roder, K.E., Abbruscato, T.J. Evaluation of bEnd5 cell line as an in vitro model for the blood-brain barrier under normal and hypoxic/aglycemic conditions. *J. Pharm. Sci.* 96, (2007) 3196-3213.
- [39] Steiner, O., Coisne, C., Engelhardt, B., Lyck, R. Comparison of immortalized bEnd5 and primary mouse brain microvascular endothelial cells as in vitro blood-brain barrier models for the study of T cell extravasation. *J. Cereb. Blood Flow Metab.* 31 (2011) 315-327.
- [40] Sobrado, M., Delgado, M., Fernández-Valle, E., García-García, L., Torres, M., Sánchez-Prieto, J., Vivancos, J., Manzanares, R., Moro, M.A., Pozo, M.A, Lizasoain, I.

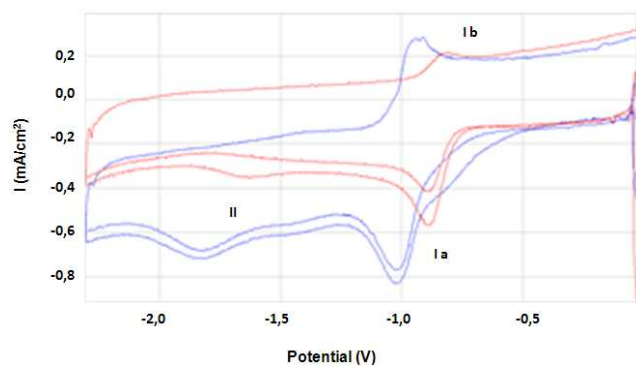


Fig. 2. Cyclic voltammetry of **1** (blue line) and **21** (red line) (4 mM) in 0.1M $\text{Bu}_4\text{NBF}_4/\text{DMF}$. Scan speed 100 mV/s. Glassy carbon/platinum electrodes.

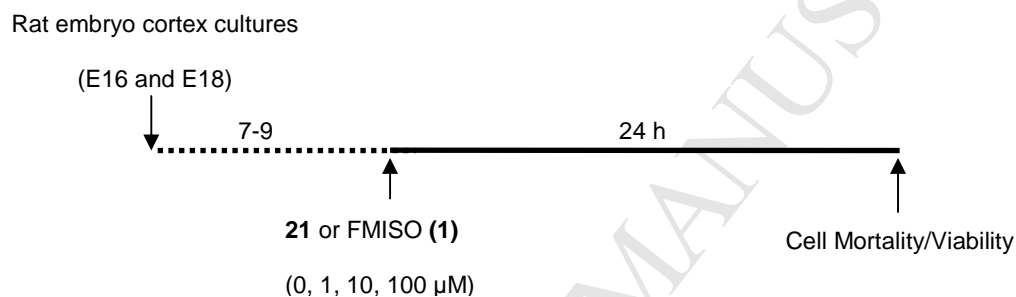


Fig. 3. Scheme for cell toxicity assays in primary cultures of rat cerebral cortical cells.

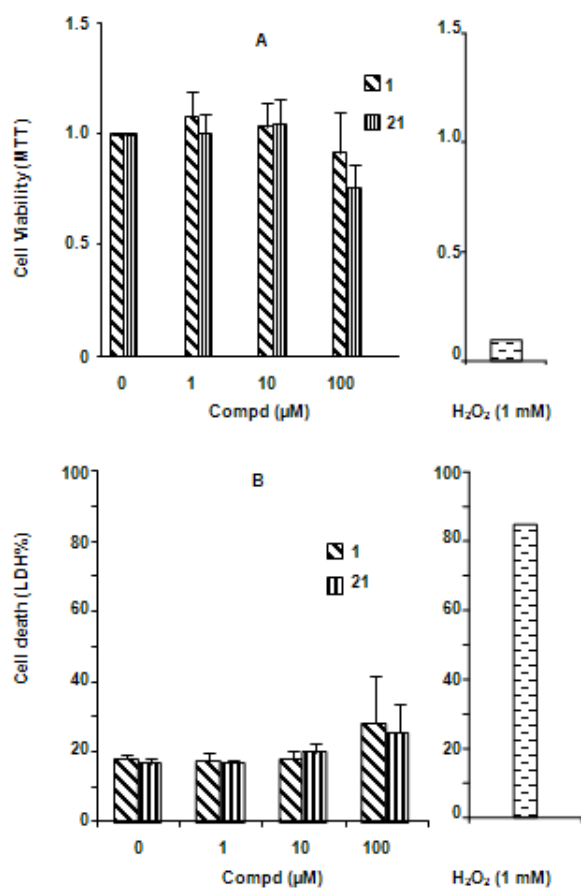


Fig. 4. Dose-response histograms for **1** and **21** in a rat cortical mixed neuronal culture. A: Cell viability measured by MTT assay 24 h after incubation with the compounds. B: Cell death measured as $(LDHe/LDHe+LDHi)*100$, 24 h after incubation with the compounds. 0 μ M corresponds to vehicle (0.5% DMSO). H₂O₂ was used as a control for toxicity under our conditions. Data represent means \pm SD and correspond to N = 3 mixed neuronal culture, with six different wells used for each condition. (LDHe: extracellular LDH; LDHi: intracellular LDH).

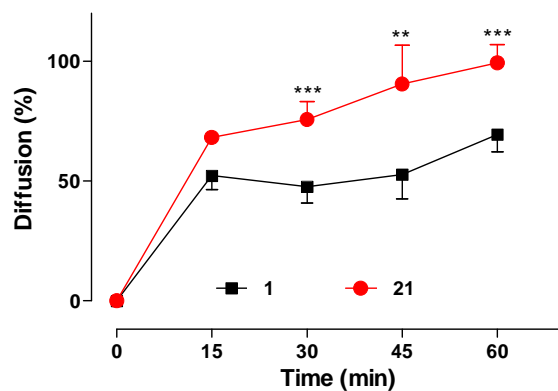


Fig. 5. Evolution over the time of the diffusion of **1** and **21** in cultured bEnd-5 cells. Cells were seeded in the upper compartment and the compounds were added (10 μ g), followed by collection of the medium from the lower compartment at different time points. Results are expressed as percentage of the compound added (100%) and are mean \pm SEM (n = 3–4 independent cultures in duplicate). **p<0.01; ***p<0.001 vs **1** (two-way ANOVA, followed by Student's t test).

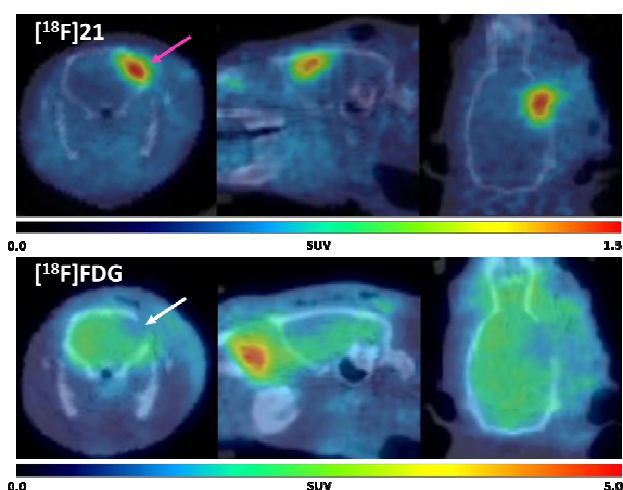


Fig. 6. PET/CT fused images (in coronal, sagittal and trans-axial views) of the same rat showing the hypoxic area as visualized by [^{18}F]21 PET (pink arrow; upper row) 3 h after PMCAO onset and the reduction of the glucose brain metabolism as detected by [^{18}F]FDG PET (white arrow; bottom row), 24 h after the ischemic procedure. As this figure shows, there is a good agreement between the hypoxic and hypometabolic areas as detected by [^{18}F]21 and [^{18}F]FDG, respectively.

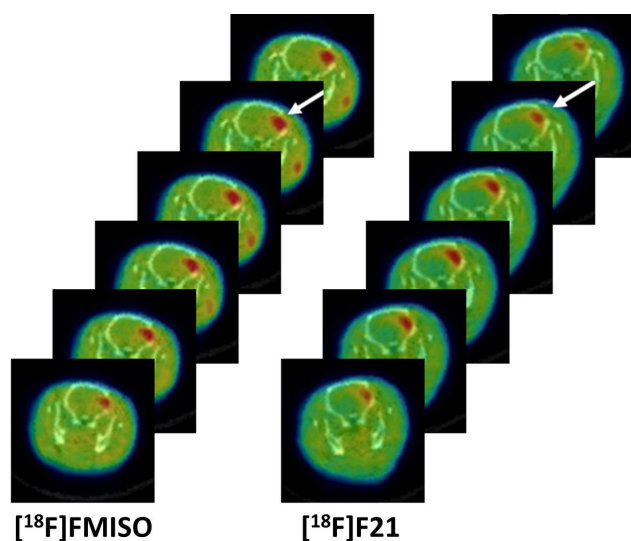


Fig. 7. Six consecutive PET/CT rat brain coronal sections of pMCAO injured rats, injected with [^{18}F]FMISO (1) (left) and [^{18}F]21 (right) obtained 3 h after the ischemic onset, showing the accumulation of the hypoxia tracers at the level of the damaged brain areas (marked with white arrows).

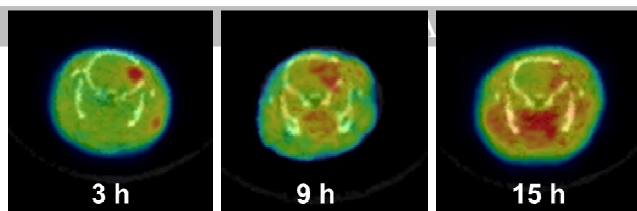
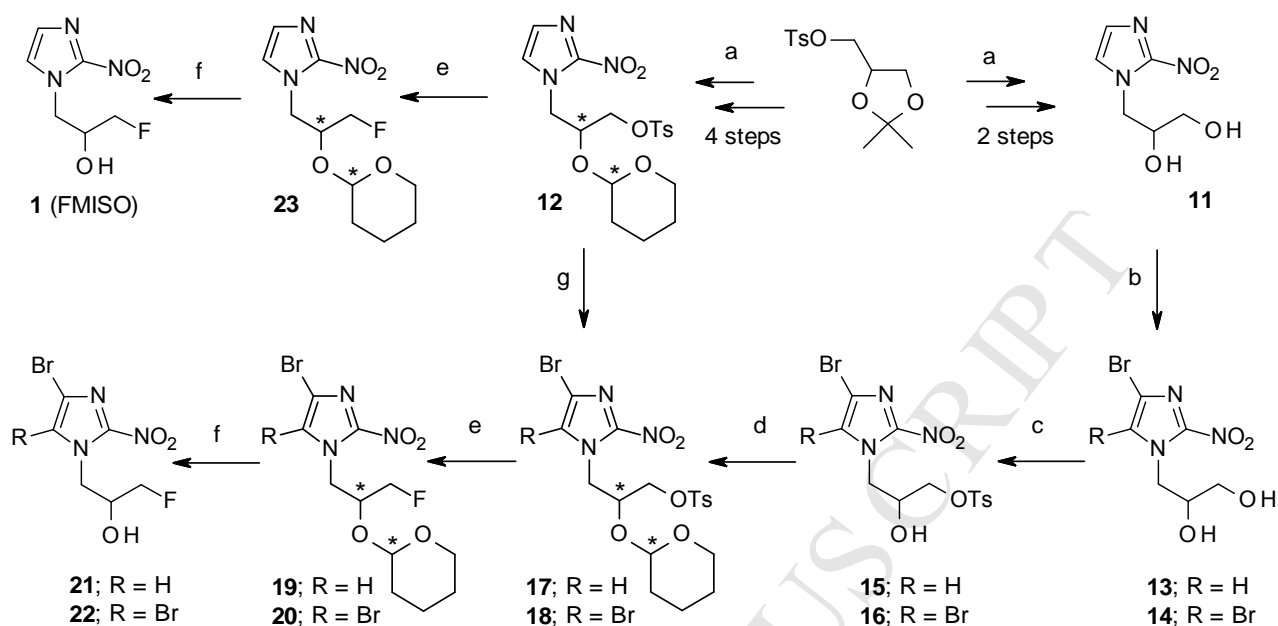
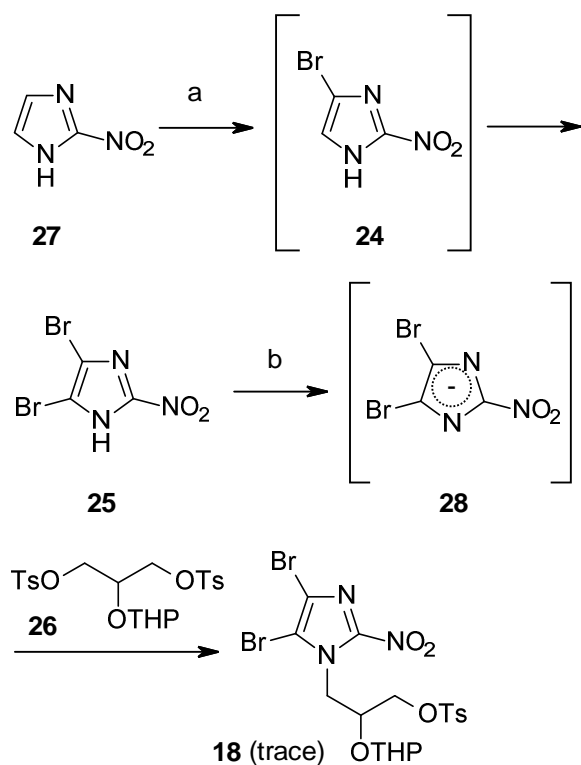


Fig. 8. [^{18}F]21 PET-CT coronal images obtained 3, 9 and 15 h after the ischemic onset. The progress of the hypoxic area can be observed. In all cases, the tracer [^{18}F]21 was injected 150 min before each PET acquisition.

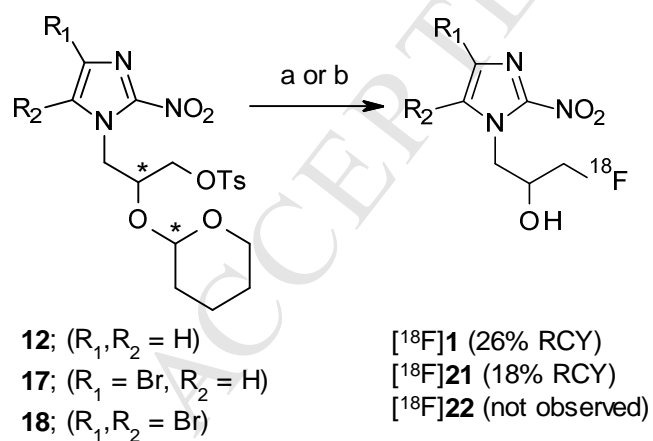


Scheme 1. Synthesis of precursors **17** and **18** and cold tracers **21**, **22**, and FMISO (**1**).

Reagents and conditions: (a) See ref. 25; (b) NBPh₄, DMF, rt, 3 h (**13**) or 10 °C, 18 h (**14**); (c) TsCl, Et₃N, Bu₂SnO, CH₃CN, rt, 5 h (**15**) or 24 h (**16**); (d) DHP, PPTS, CH₂Cl₂, 0 °C, 22 h (**17**) or 4 h (**18**); (e) CsF, *tert*-amyl alcohol, 120 °C, 3 h; (f) AcOH, THF, H₂O, 65 °C, 6 h (**21**), 3 h (**22**) or 4 h (**1**); (g) NBS, DMF, 0 °C, 17 h (**17**).



Scheme 2. Unsuccessful synthesis of precursor **18**. *Reagents and conditions:* (a) NBS, DMF, rt, 45 min; (b) CsCO₃, DMF, 60 °C, 24 h then 100 °C, 24 h.



Scheme 3. Radiosynthesis of [¹⁸F]FMISO ([¹⁸F]1) and 4-Br-[¹⁸F]FMISO ([¹⁸F]21). *Reagents and conditions:* (a) **12**, see ref. 28; (b) **17** or **18**, [kryptofix 2.2.2 ⊂ K⁺][¹⁸F⁻], MeCN, 130 °C, 5 min; then 1N HCl, 100 °C, 3 min.

Tables

Table 1

Peak potential of **1** and **21** (4 mM) vs Ag/Ag⁺ in DMF/TBABF₄

Compd	E _{pc1} (V) ^a	E _{pc2} (V) ^b	E _{pa1} (V) ^c
1	-1.04	-1.97	-0.97
21	-0.89	-1.64	-0.82

^aE_{pc1}: cathodic potential at peak 1.^bE_{pc2}: cathodic potential at peak 2.^cE_{pa1}: anodic potential at peak 1.

Table 2

Log*P*_{oct/water} and CLog*P* values for tracers **1–10** and compounds **21** and **22**

Compd	1 ^a	2 ^b	3 ^c	4 ^a	5 ^a	6	7	8	9	10	21	22
Log <i>P</i>	-0.40	2.87	1.09	0.28	2.72	-	-	-	-	-	-	-
(CLog <i>P</i>) ^d	0.27	1.00	1.94	0.96	3.26	1.25	-0.19	0.13	2.26	3.52	1.25	1.79

^aRef. 11.^bRef. 12.^cRef. 14.^dCalculated using licensed Marvin software from ChemAxon.

Table 3

Relative binding affinities of [^{18}F]21 (n = 2) and [^{18}F]FMISO (1) (n = 3).

	[^{18}F]21	[^{18}F]FDG	[^{18}F]21
	SUV ^a	SUV ^a	Binding affinity ^b
Ipsilateral	1.03 ± 0.250	1.37 ± 0.096	
Contralateral	0.42 ± 0.001	1.96 ± 0.189	9.16 ± 1.70
Ratio	2.47 ± 0.580	0.29 ± 0.120	
	[^{18}F]FMISO (1)	[^{18}F]FDG	[^{18}F]FMISO (1)
	SUV ^a	SUV ^a	Binding affinity ^b
Ipsilateral	0.62 ± 0.019	1.56 ± 0.117	
Contralateral	0.44 ± 0.249	2.10 ± 0.249	5.94 ± 0.63
Ratio	1.40 ± 0.060	0.25 ± 0.020	

^a Mean ± SEM. SUV was assessed at 3 h after the onset of pMCAO for [^{18}F]21 and [^{18}F]1, and at 24 h for [^{18}F]FDG.

^b See experimental section for details of the calculation

Highlights

4-Br-[¹⁸F]FMISO and its precursor 4-Br-NITTP were synthesised

Cyclic voltammetry and neuronal toxicity were studied for 4-Br-FMISO

It is more easily reduced than FMISO and it shows similar neuronal toxicity

It crosses more rapidly than FMISO through brain endothelial cells

4-Br-[¹⁸F]FMISO accumulates 54% more than [¹⁸F]FMISO in ischemic tissue

Preliminary research on 1-(4-bromo-2-nitroimidazol-1-yl)-3-[¹⁸F]fluoropropan-2-ol as a novel brain hypoxia PET tracer in a rodent model of stroke

Elena Nieto, Mercedes Delgado, Mónica Sobrado, María L. de Ceballos, Ramón Alajarín, Luis García-García, James Kelly, Ignacio Lizasoain, Miguel A. Pozo, Julio Álvarez-Builla

Appendix A. Supplementary data

Contents

Fig. SD.1. Toxicity of 1 and 21 in rat embryo cortical neuronal culture	2
Fig. SD.2. Semi-preparative radio-HPLC chromatogram for crude [¹⁸ F] 21	3
Fig. SD.3. Analytical radio-HPLC chromatogram for puree [¹⁸ F] 21	3
Synthesis of 23	4
Synthesis of 1	4
¹ H, ¹³ C NMR, IR and HRMS spectra of bromoderivatives 13 , 15 , 17 , 19 and 21	6-23
¹ H, ¹³ C NMR, IR and HRMS spectra of dibromoderivatives 14 , 16 , 18 and 22	24-39
¹ H, ¹³ C NMR and IR spectra of 23 and 1	40-44

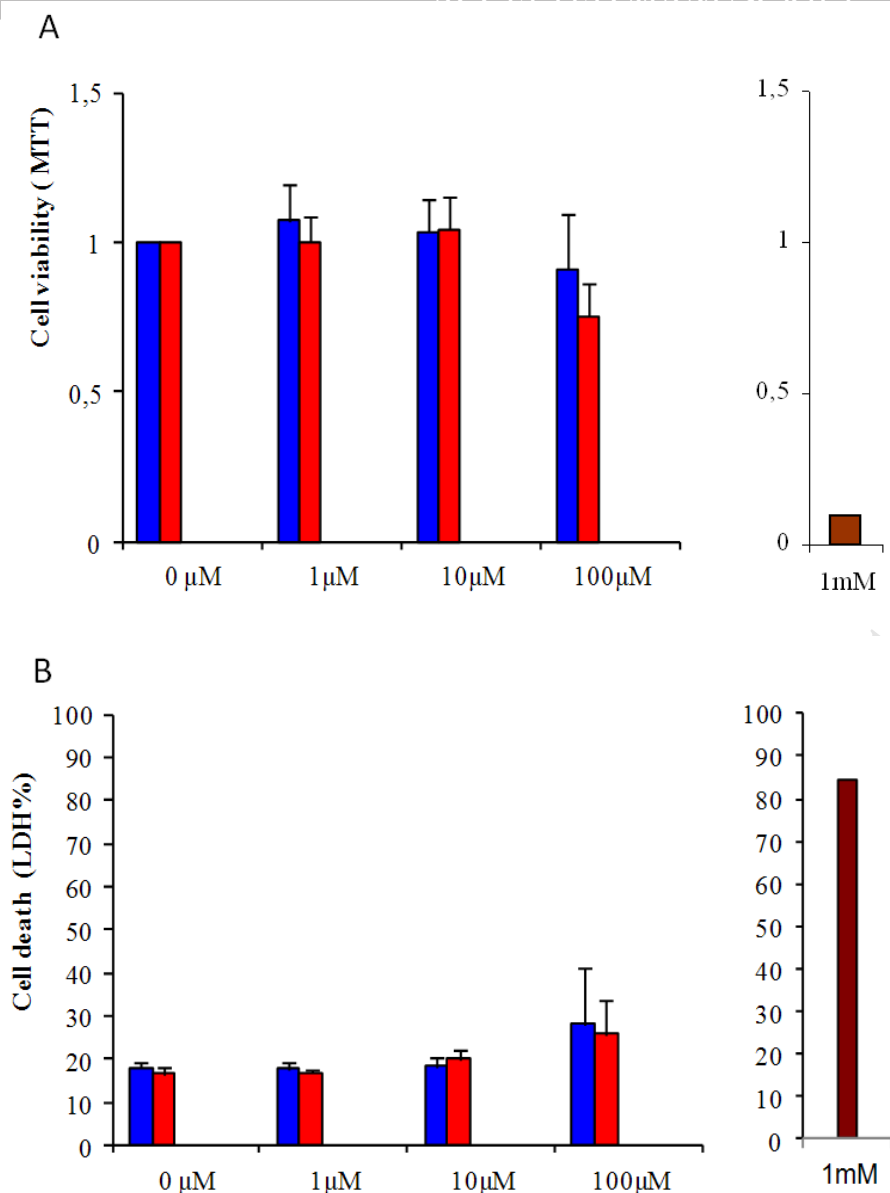


Fig. SD.1. Dose-response curves testing **1** (blue) and **21** (red) in rat embryo cortical neuronal culture. A: Cell viability measured by MTT assay 24 h after incubation of molecules. B: Cell death measured as $(LDHe/LDHe+LDHi)*100$, 24 h after incubation of molecules. 0 μ M corresponds to vehicle (1% DMSO). H₂O₂ (brown) was used as control of toxicity in our conditions. Data represent means \pm SD and correspond to N=3 rat embryo cortical neuron culture, with six different wells used for each condition. (LDHe: extracellular LDH; LDHi: intracellular LDH).

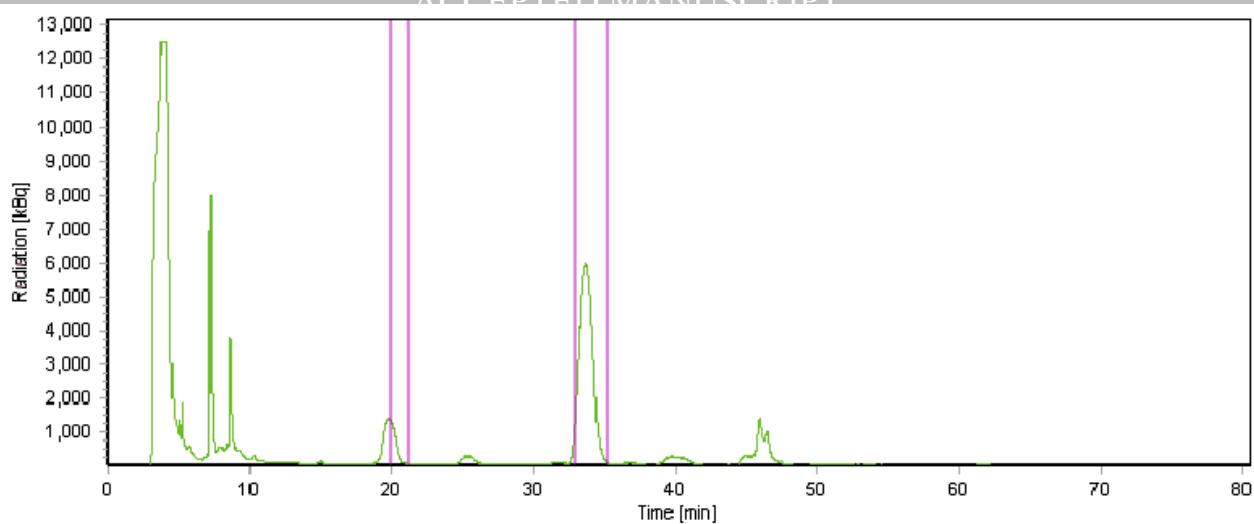


Fig. SD.2. Semi-preparative radio-HPLC chromatogram of crude mixture during the purification of $[^{18}\text{F}]\mathbf{21}$ (33 min).

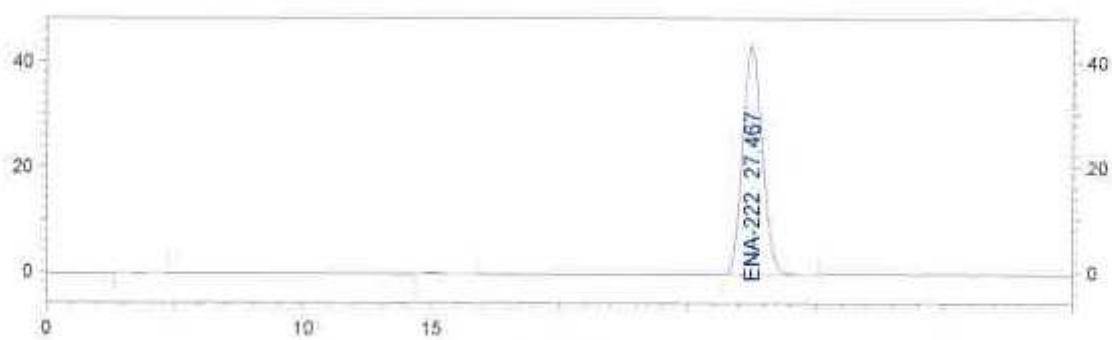
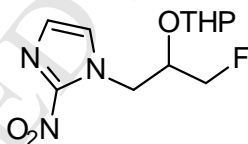


Fig. SD.3. Analytical radio-HPLC chromatogram of $[^{18}\text{F}]\mathbf{21}$ (27.47 min) after purification.

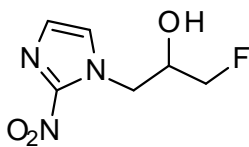
Synthesis of 1-[3-fluoro-2-(oxiran-2-yloxy)-propyl]-1H-2-nitroimidazole (23)

A solution of NITTP (**12**) (0.4 g, 0.94 mmol) and CsF (0.428 g, 2.82 mmol) in *tert*-amyl alcohol (3.13 mL) was heated at 120 °C for 3 h. Then the solvent was removed under reduced pressure and the residue was chromatographed on silica gel using ethyl acetate/hexane as eluent to give **23** (0.21 g) as a yellowish oil. Yield: 82%; $R_{f(\text{AcOEt/Hex } 6:4)}$: 0.49; $^1\text{H NMR}$ (300 MHz, CDCl_3) δ 7.18 (s, 1H, $\text{H}_{5\text{-Im}}$, dias. B), 7.13 (s, 2H, $\text{H}_{5\text{-Im}}$, dias. A $\text{H}_{4\text{-Im}}$, dias. B), 7.12 (s, 1H, $\text{H}_{4\text{-Im}}$, dias. A), 4.85 (dd, 1H, $J = 14.1$ Hz, $J = 3.6$ Hz, $\text{CH}_2\text{-Im}$, dias. A+B), 4.75 (dd, 1H, $J = 14.1$ Hz, $J = 3.6$ Hz, $\text{CH}_2\text{-Im}$, dias. A+B), 4.66–4.22 (m, 5H, $\text{H}_{2\text{-TPH}} + \text{CH}_2\text{-Im} + \text{CH}_2\text{-F}$, dias. A+B, CH-OTHP, dias. B), 4.15–4.04 (m, 1H, CH-OTHP, dias. A), 3.81 (m, 1H, $\text{H}_{6\text{-THP}}$, dias. A), 3.45 (m, 1H, $\text{H}_{6\text{-THP}}$, dias. A), 3.28–3.15 (m, 2H, $\text{H}_{6\text{-THP}}$, dias. B), 1.71–1.46 (m, 6H, $\text{H}_{3,4,5\text{-THP}}$, dias. A+B) ppm; $^{13}\text{C NMR}$ (75 MHz, CD_3OD) δ 144.8 ($\text{C}_{2\text{Im}}$), 127.9 ($\text{C}_{5\text{Im}}$), 127.7 ($\text{C}_{4\text{Im}}$), 100.6 ($\text{C}_{2\text{THP}}$ dias A), 96.9 ($\text{C}_{2\text{THP}}$, dias B), 82.6 (d, 1C, $^1J_{\text{C-F}} = 172.6$ Hz, $\text{CH}_2\text{-F}$, dias A), 81.2 (d, 1C, $^1J_{\text{C-F}} = 172.6$ Hz, $\text{CH}_2\text{-F}$, dias B), 75.2 (d, 1C, $^2J_{\text{C-F}} = 20.7$ Hz, CH-OH, dias. A), 71.4 (d, 1C, $^2J_{\text{C-F}} = 19.1$ Hz, CH-OH, dias. B), 63.0 ($\text{C}_{6\text{THP}}$, dias A), 62.6 ($\text{C}_{6\text{THP}}$, dias B), 50.5 (d, 1C, $^3J_{\text{C-F}} = 7.6$ Hz, $\text{CH}_2\text{-Im}$ dias. A+B), 30.5 ($\text{C}_{3\text{THP}}$, dias. A), 30.2 ($\text{C}_{3\text{THP}}$, dias. B), 24.9 ($\text{C}_{5\text{THP}}$, dias. A), 24.8 ($\text{C}_{5\text{THP}}$, dias. B), 19.4 ($\text{C}_{4\text{THP}}$, dias. A), 19.3 ($\text{C}_{4\text{THP}}$, dias. B) ppm; IR (ν_{max} , KBr): 3419 (OH), 1596 (C=N), 1465 (NO_2), 1364 (NO_2), 1365 (SO_2), 1177 (SO_2) cm^{-1} ; HRMS (TOF-APCI-POS): m/z calcd for $\text{C}_{11}\text{H}_{17}\text{FN}_3\text{O}_4$ [M] $^+$ 274.1203, found 274.1228.

**23****Synthesis of 1-(1H-2-nitro-imidazol-1-yl)-3-fluoro-propan-2-ol (1, FMISO)**

A mixture of **23** (0.185 g, 0.67 mmol), AcOH (2.8 mL), THF (1.45 mL) and H_2O (0.73 mL) was heated at 65 °C for 4 h. The solvent was removed under reduced pressure and the residue was chromatographed on silica gel using AcOEt. The resulting thick oil was treated with Et_2O to give a solid which was filtered and dried. Compound **1** (0.07 g) was obtained as a pale-yellow solid. Yield: 55%; mp: 108–109 °C; $R_{f(\text{AcOEt})}$: 0.52; $^1\text{H NMR}$ (500 MHz, CD_3OD) δ 7.48 (s, 1H, $\text{H}_{5\text{-Im}}$), 7.17 (s, 1H, $\text{H}_{4\text{-Im}}$), 4.76 (dd, 1H, $J = 14.2$ Hz, $J = 3.6$ Hz, $\text{CH}_2\text{-Im}$), 4.47 (dd, 2H, $^1J_{\text{H-F}} = 47.4$ Hz, $J = 4.6$ Hz, $\text{CH}_2\text{-F}$), 4.47 (dd, 1H, $J = 14.2$ Hz, $J = 8.6$ Hz, $\text{CH}_2\text{-Im}$), 4.23–4.12 (dq, 1H, $^2J_{\text{H-F}} = 19.6$ Hz, $J = 4.4$ Hz, CH-OH) ppm; $^{13}\text{C NMR}$ (75 MHz, CD_3OD) δ 146.2 ($\text{C}_{2\text{Im}}$), 128.9 ($\text{C}_{5\text{Im}}$), 127.8 ($\text{C}_{4\text{Im}}$), 85.1 (d, 1C, $^1J_{\text{C-F}} = 171.5$ Hz, $\text{CH}_2\text{-F}$), 69.4 (d, 1C, $^2J_{\text{C-F}} = 19.9$ Hz, CH-OH), 52.3 (d, 1C, $^3J_{\text{C-F}} = 7.5$ Hz, $\text{CH}_2\text{-Im}$) ppm; IR (ν_{max} , KBr): 3255, 2951, 2420, 1537, 1490, 1509, 1366 cm^{-1} ; HRMS

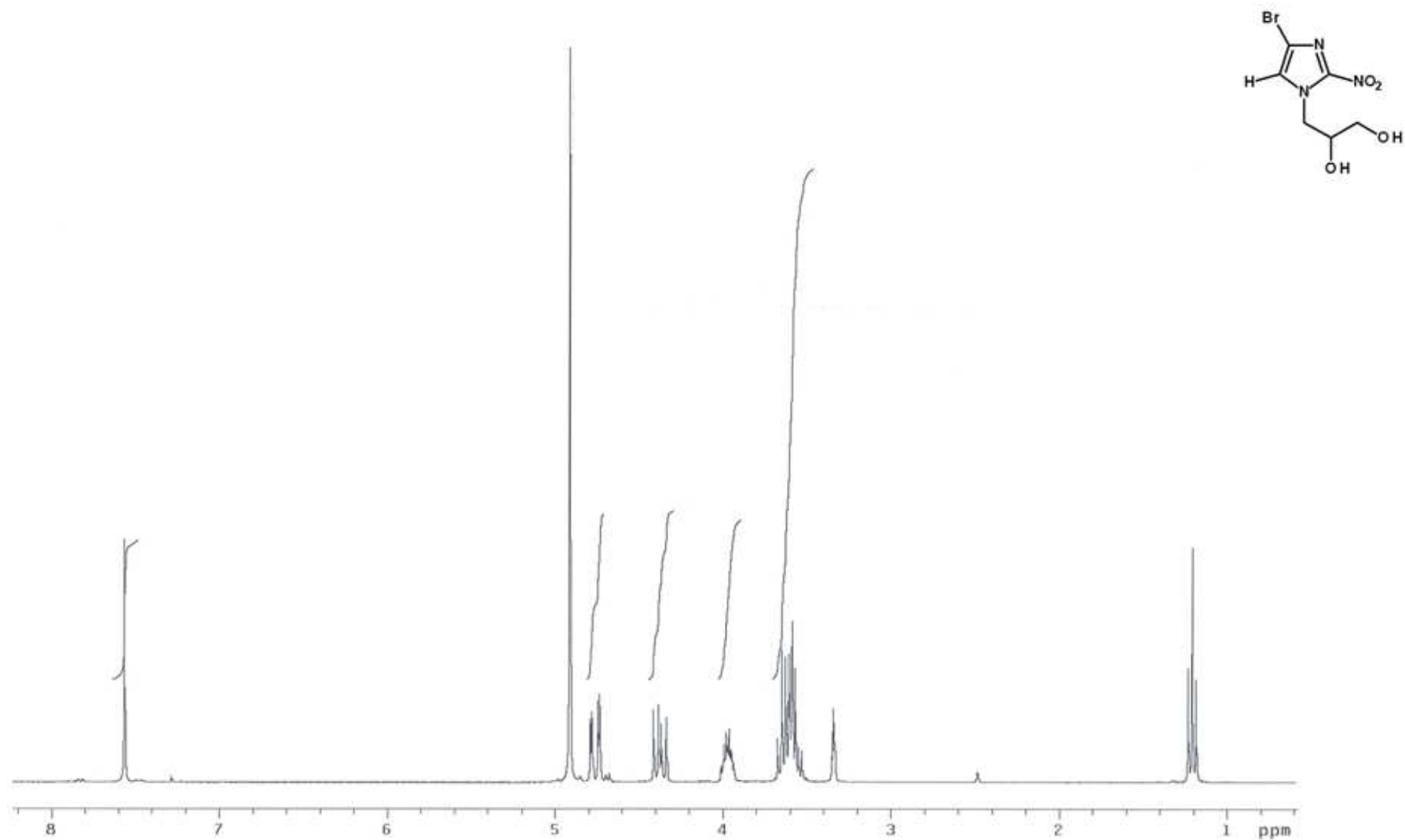
(TOF-APCI-POS): m/z calcd for $C_6H_9FN_3O_3$ $[M]^+$ 190.0628, found 190.0615; Anal ($C_6H_8FN_3O_3$) theoretical: C, 38.10; H, 4.16; N, 22.22. Found: C, 38.34; H, 4.38; N, 22.03.



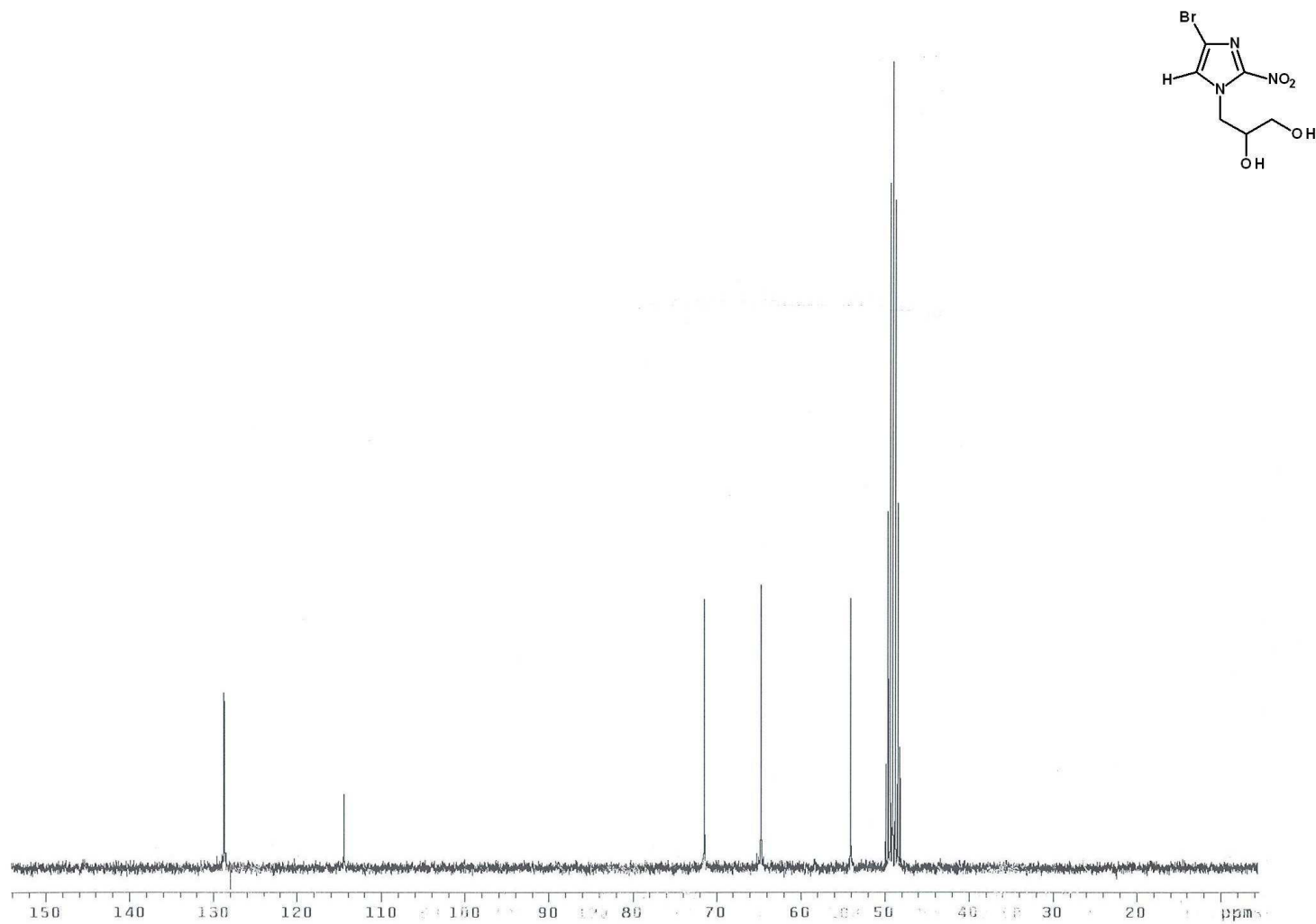
1

ACCEPTED MANUSCRIPT

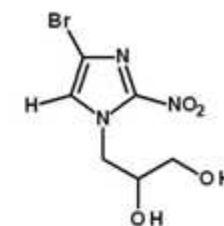
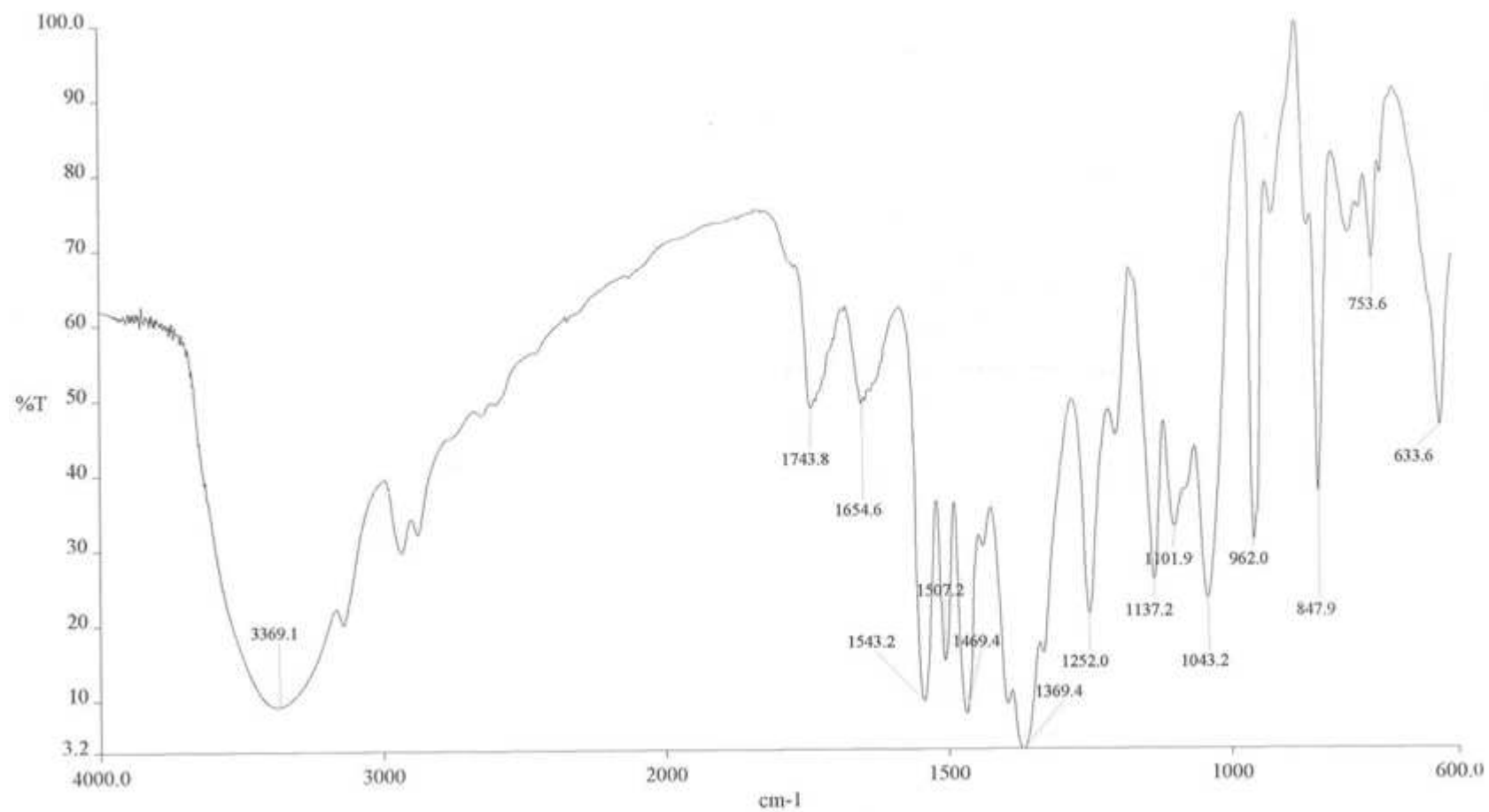
^1H NMR (300 MHz, CD_3OD) compound **13**

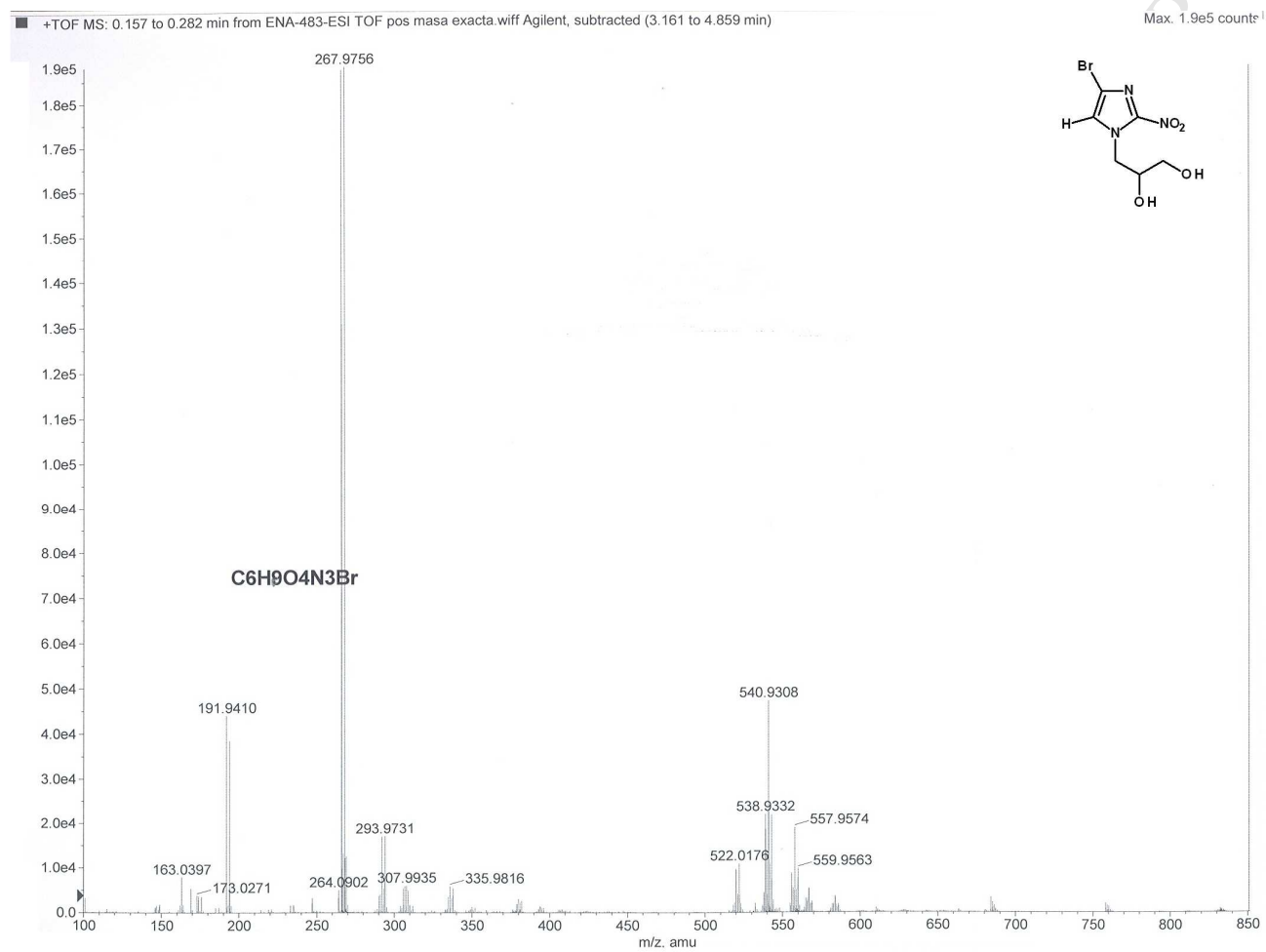


^{13}C -RMN (125 MHz, CDCl_3) compound **13**

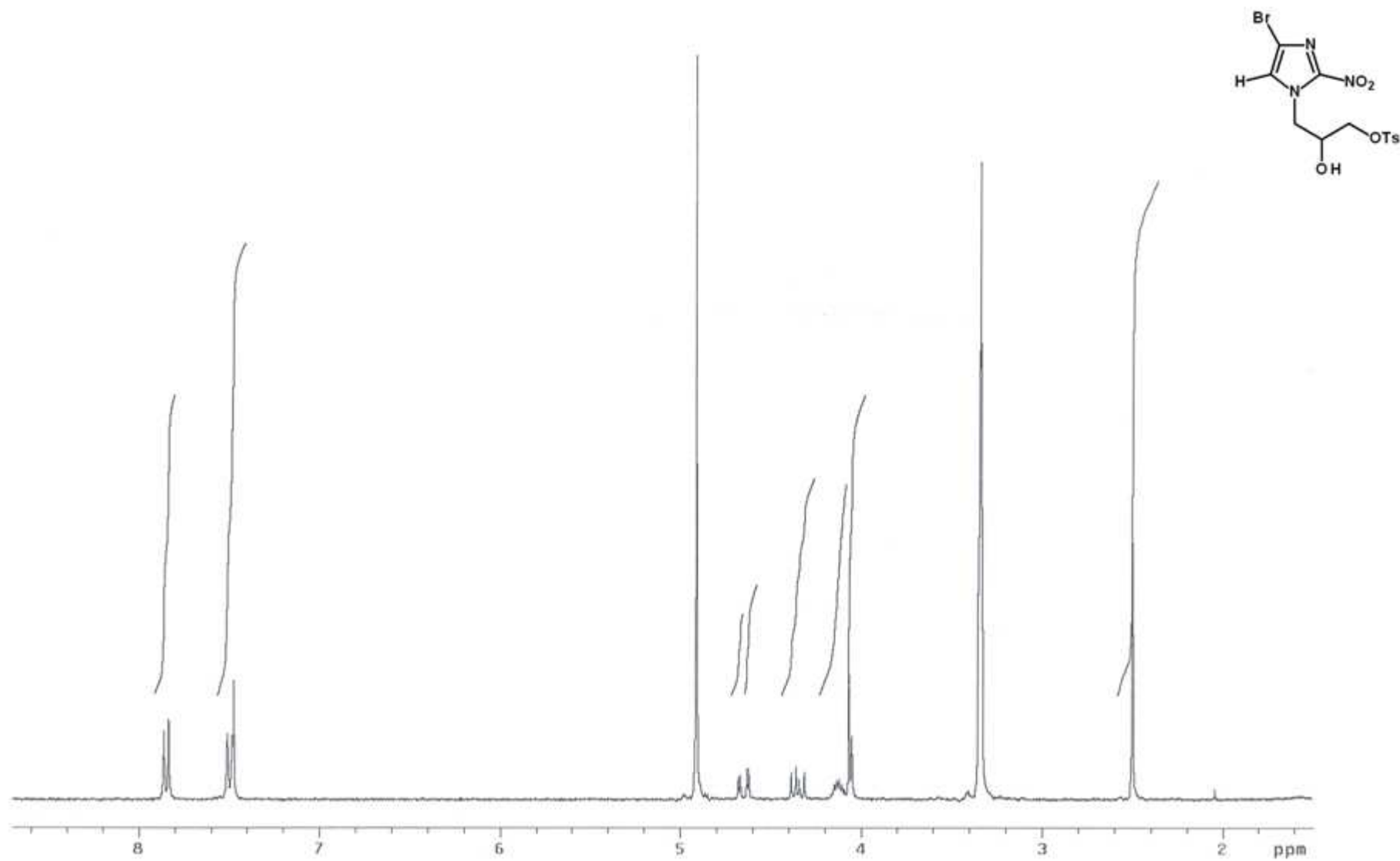


IR (KBr) compound 13

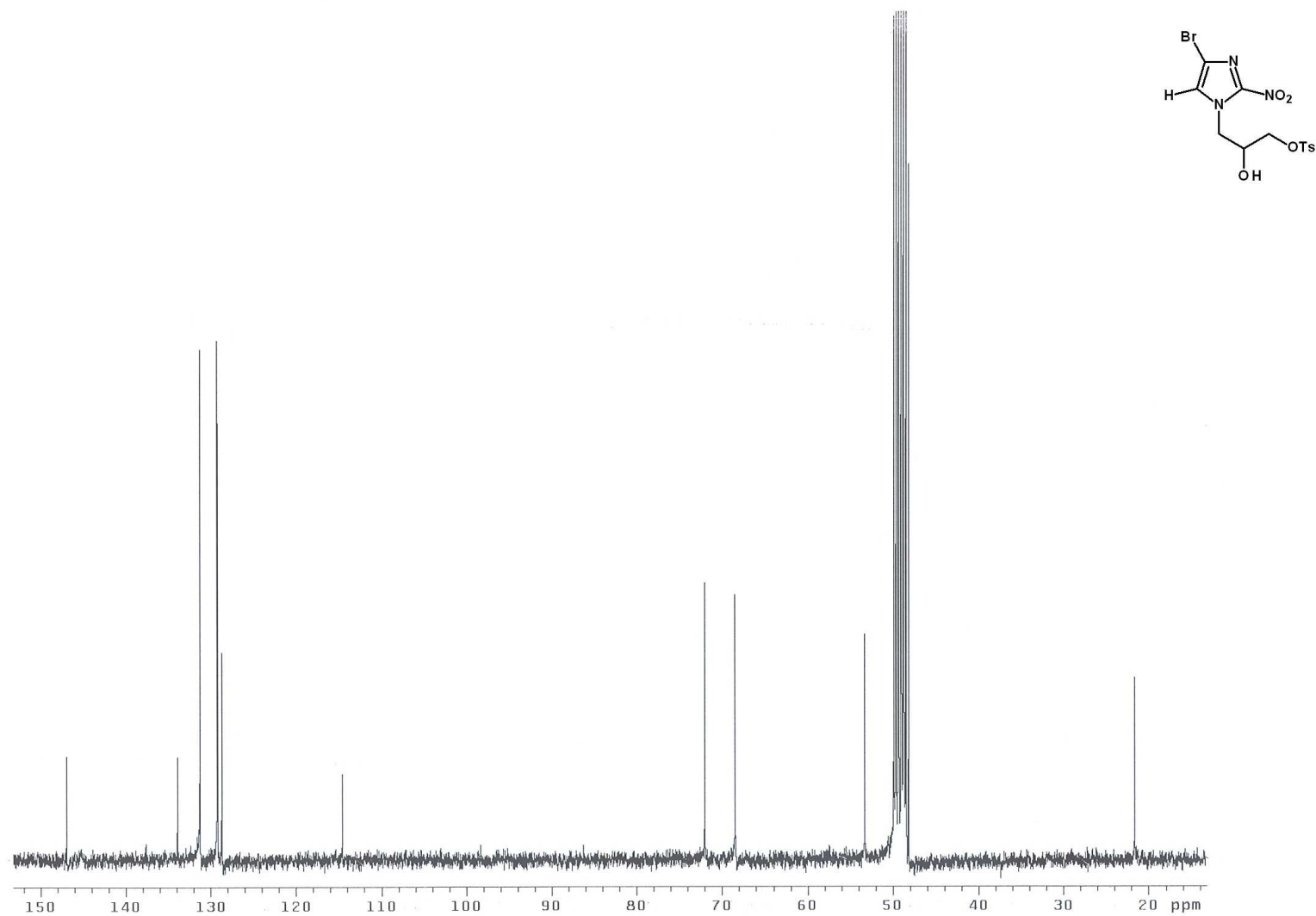


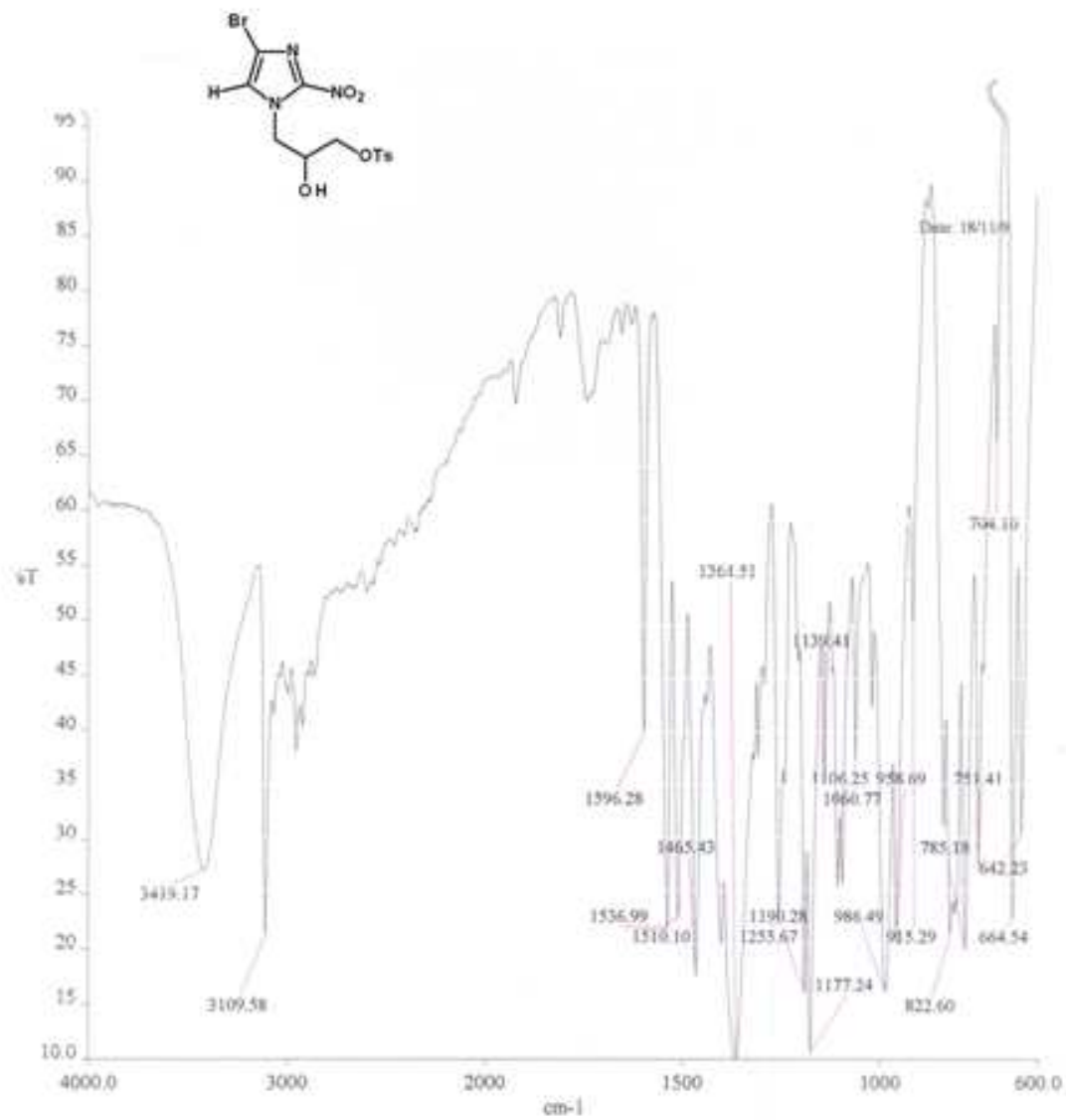
HRMS (TOF-ESI-POS) compound **13**

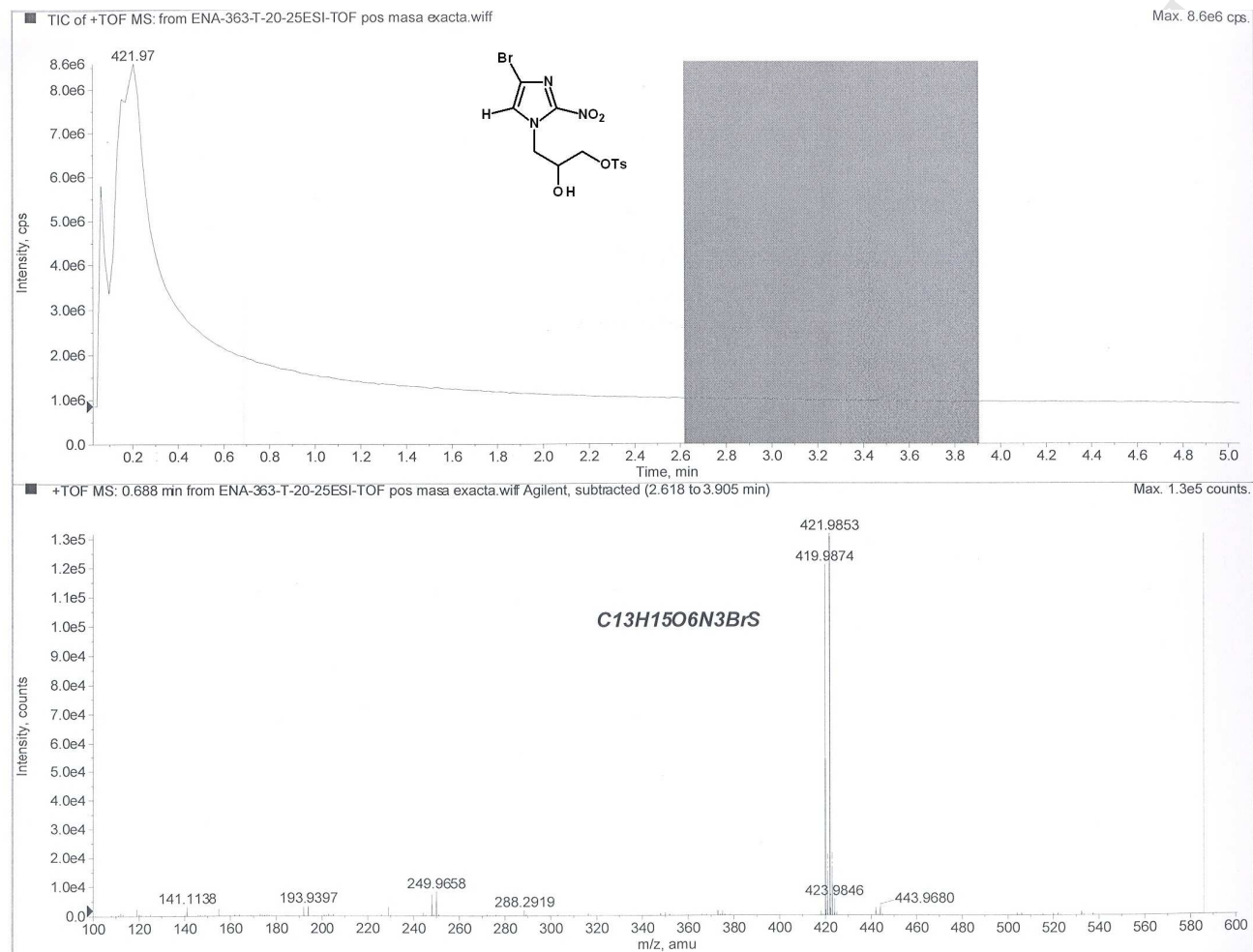
^1H -RMN (300 MHz, CD_3OD) compound **15**



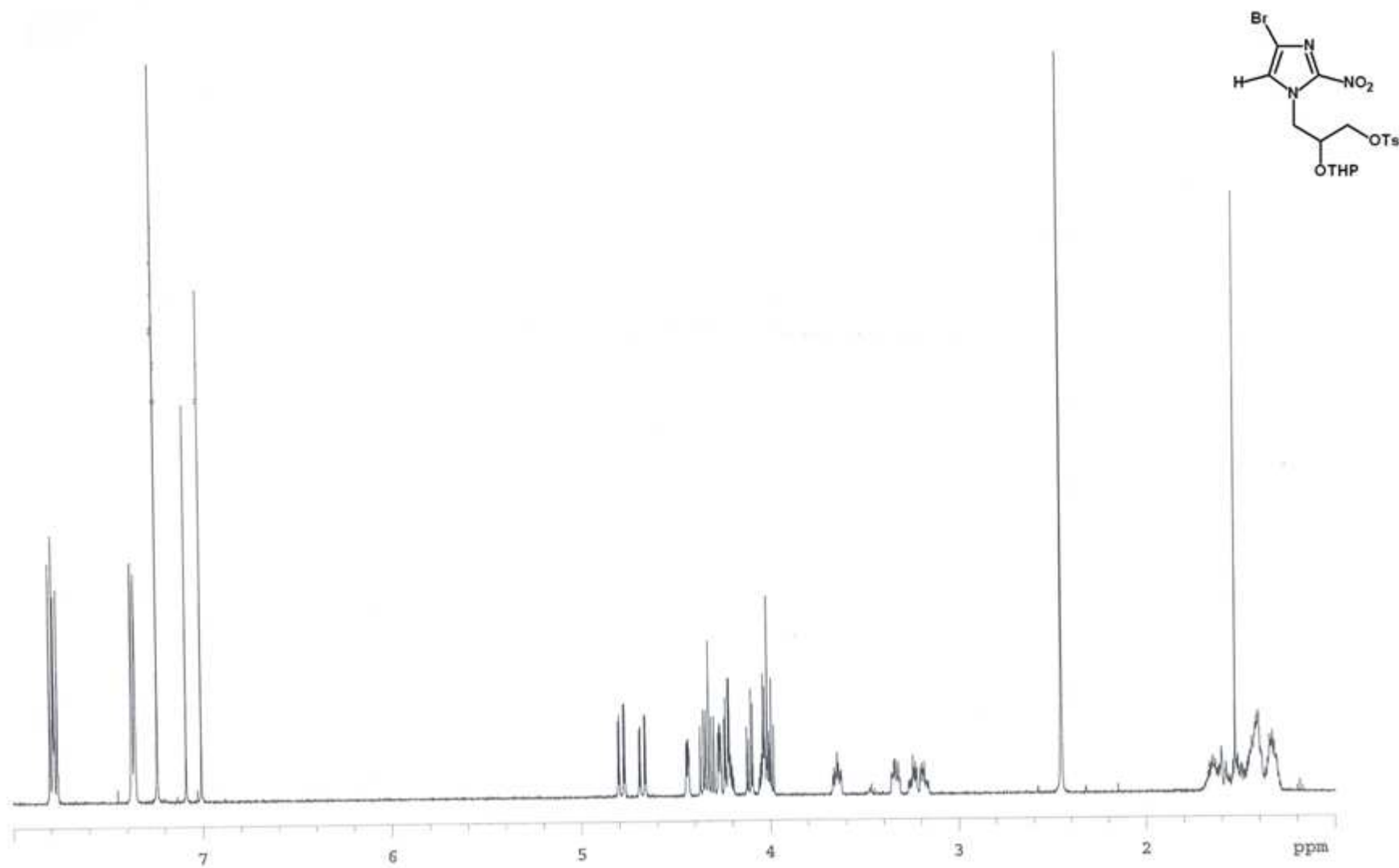
^{13}C -RMN (125 MHz, CDCl_3) compound **15**



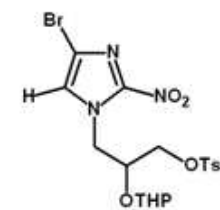
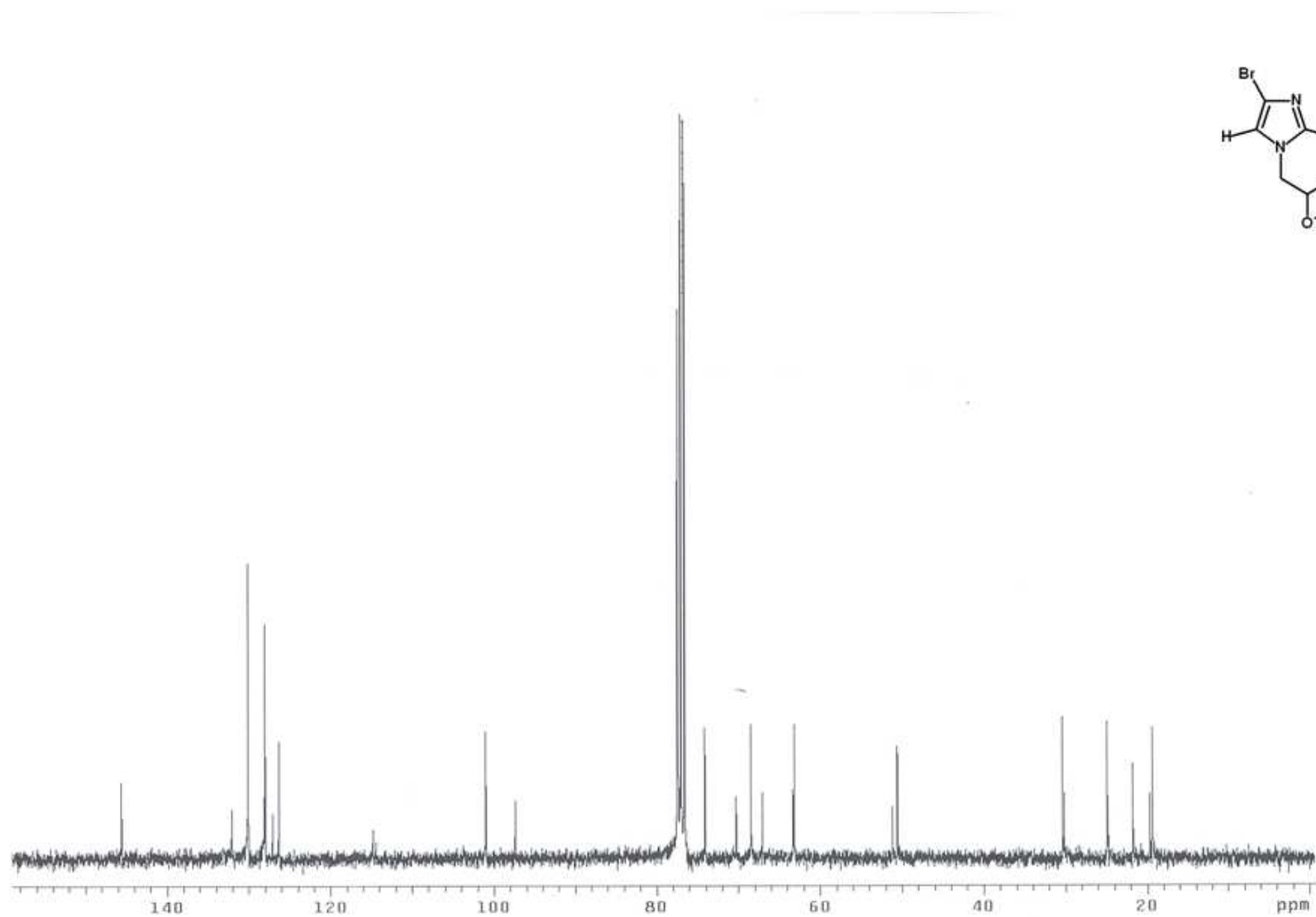
IR (KBr) compound **15**

HRMS (TOF-ESI-POS) compound **15**

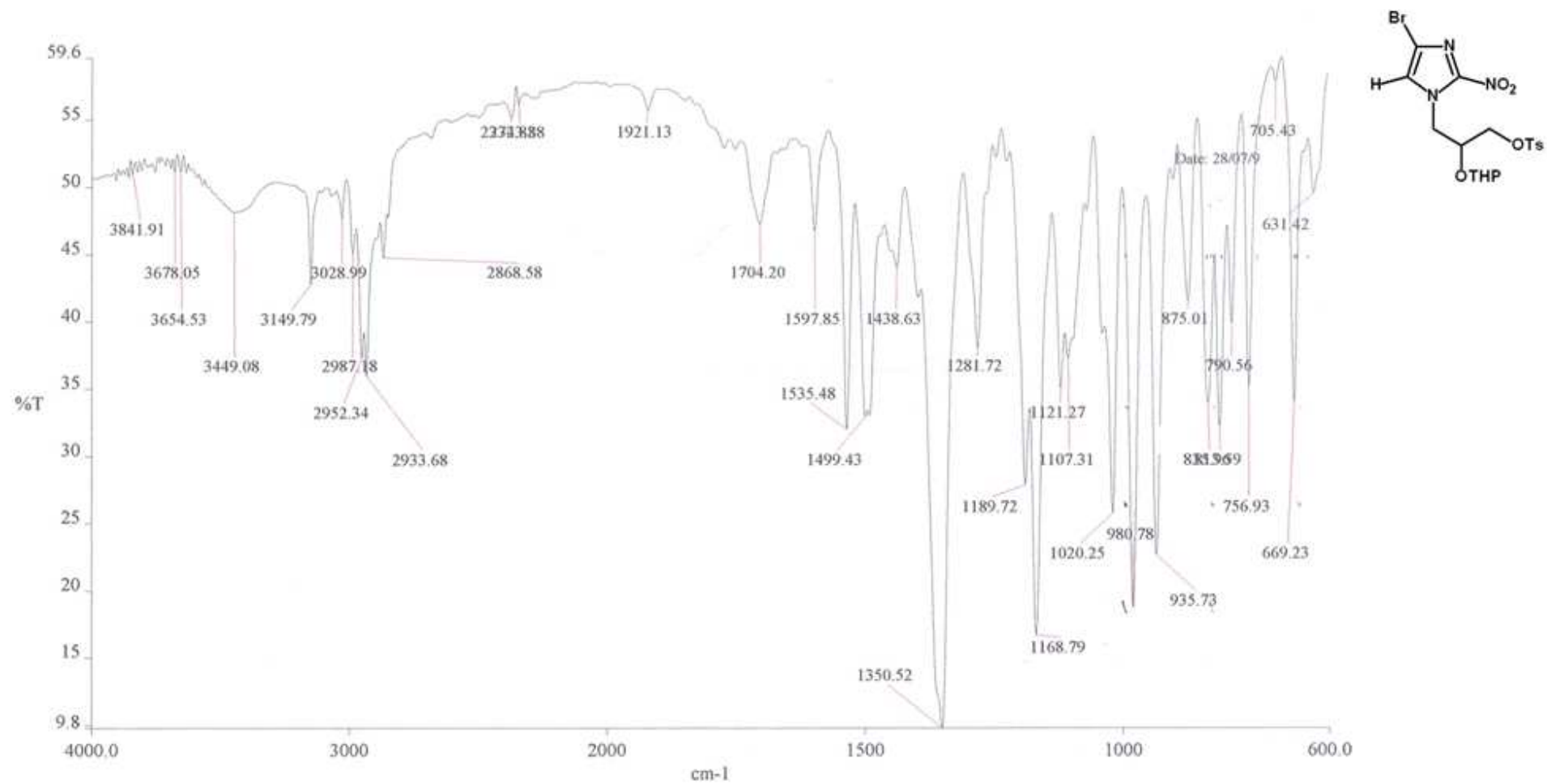
^1H -RMN (300 MHz, CD_3OD) compound **17**



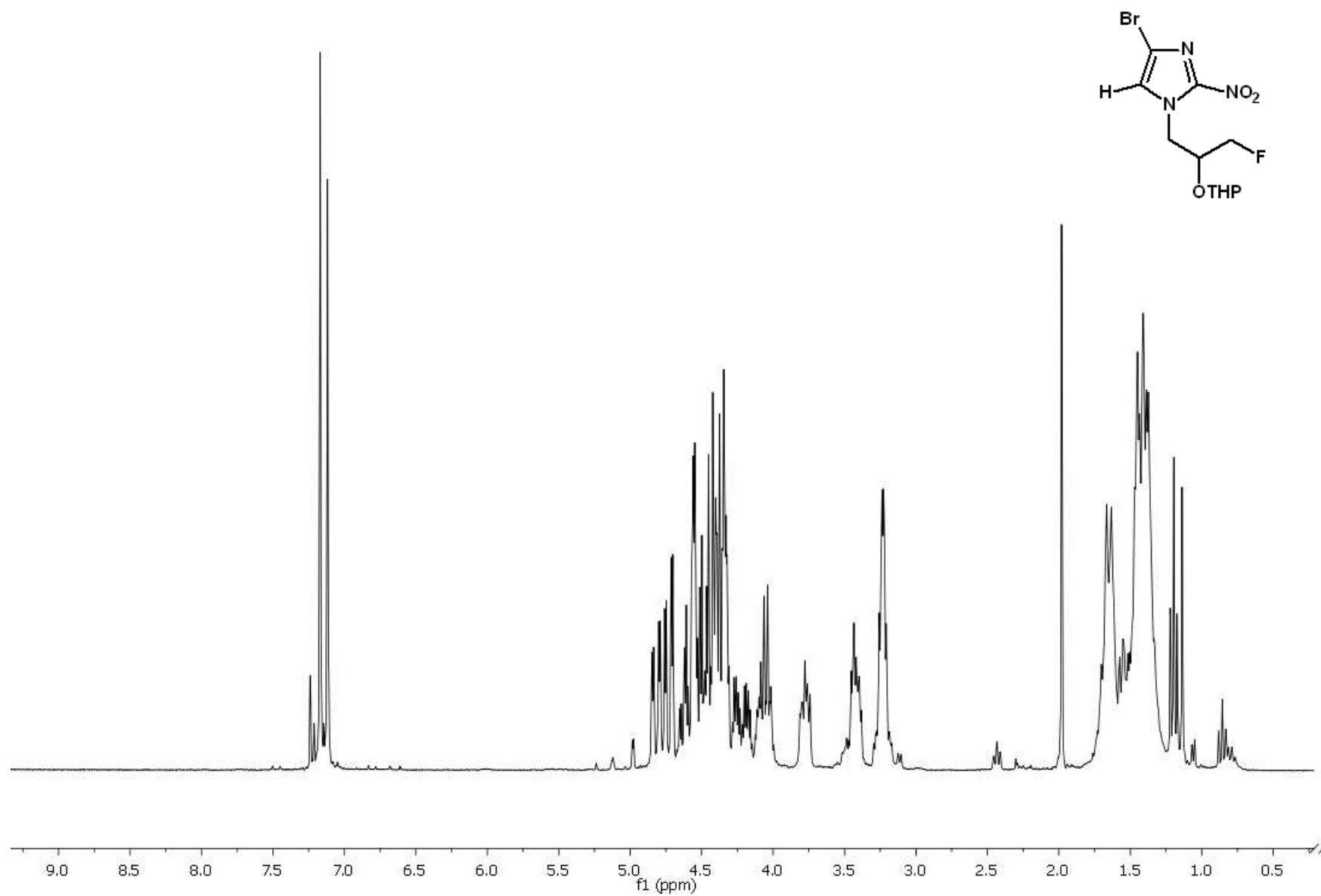
^{13}C -RMN (125 MHz, CDCl_3) compound **17**



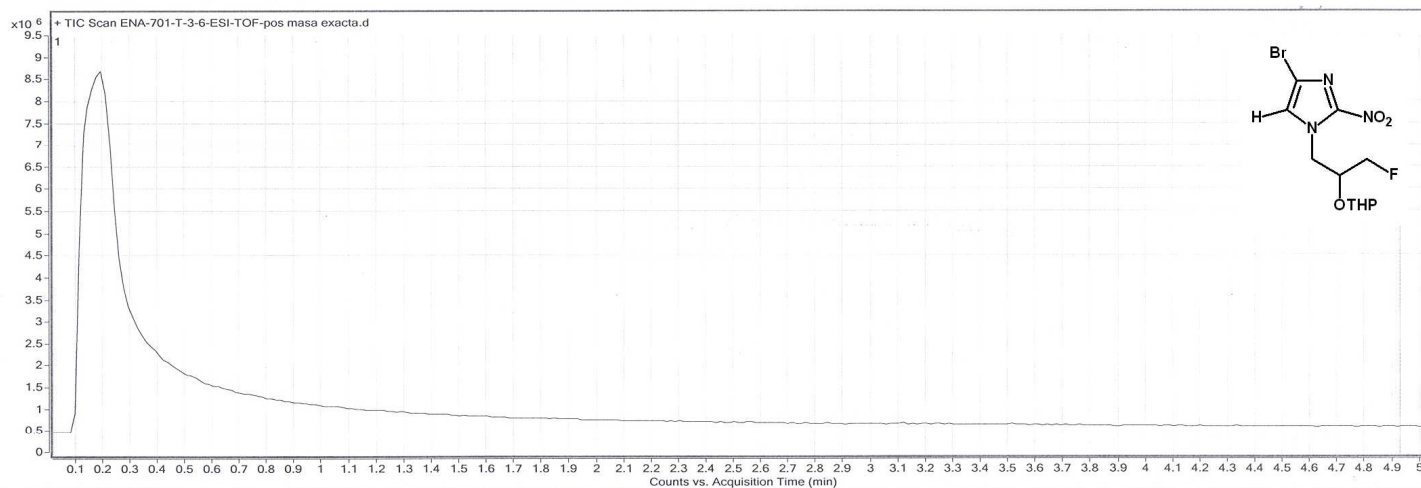
IR (KBr) compound 17



^1H -RMN (300 MHz, CD_3OD) compound **19**

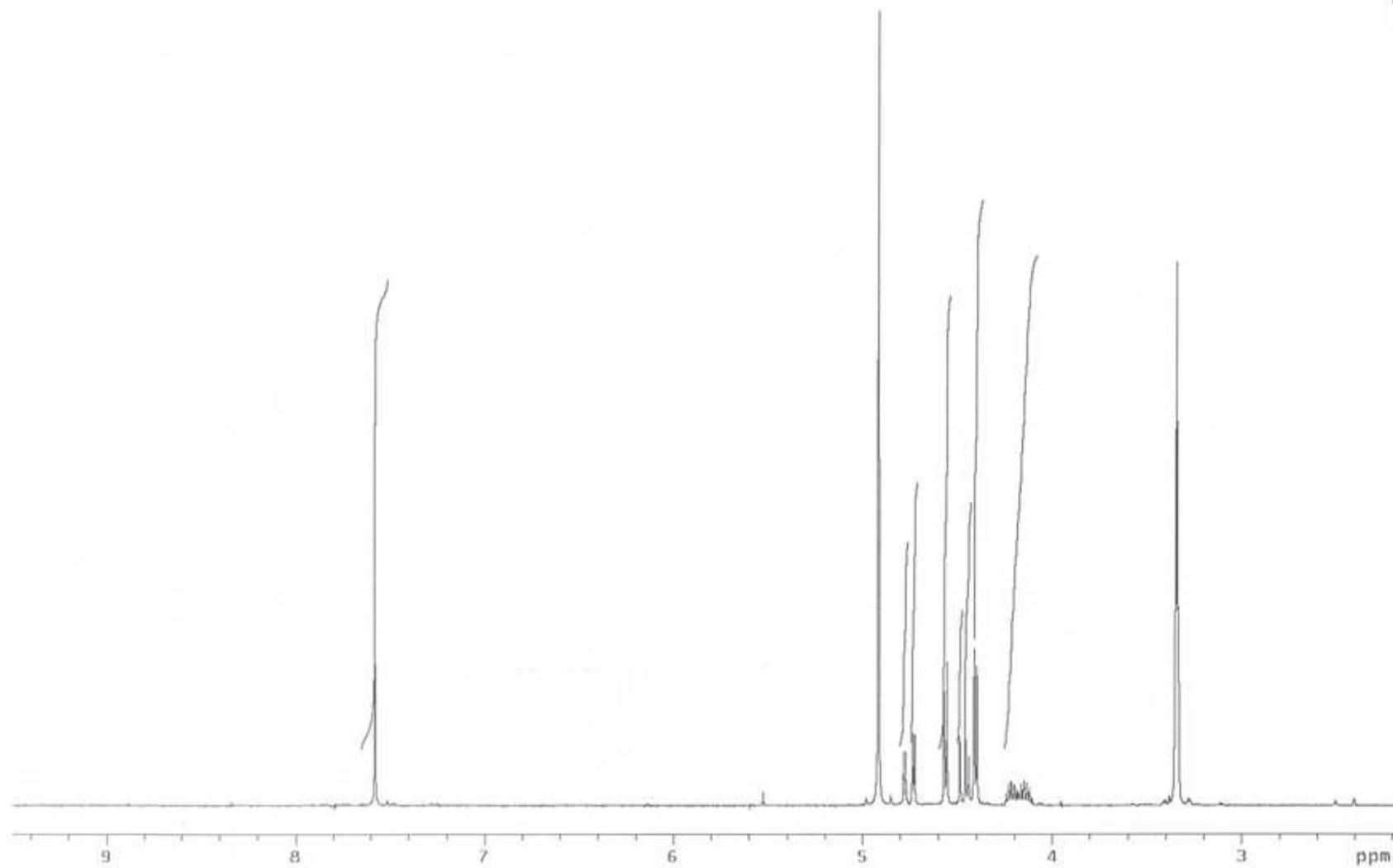
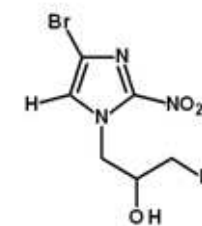


HRMS (TOF-ESI-POS) compound 19

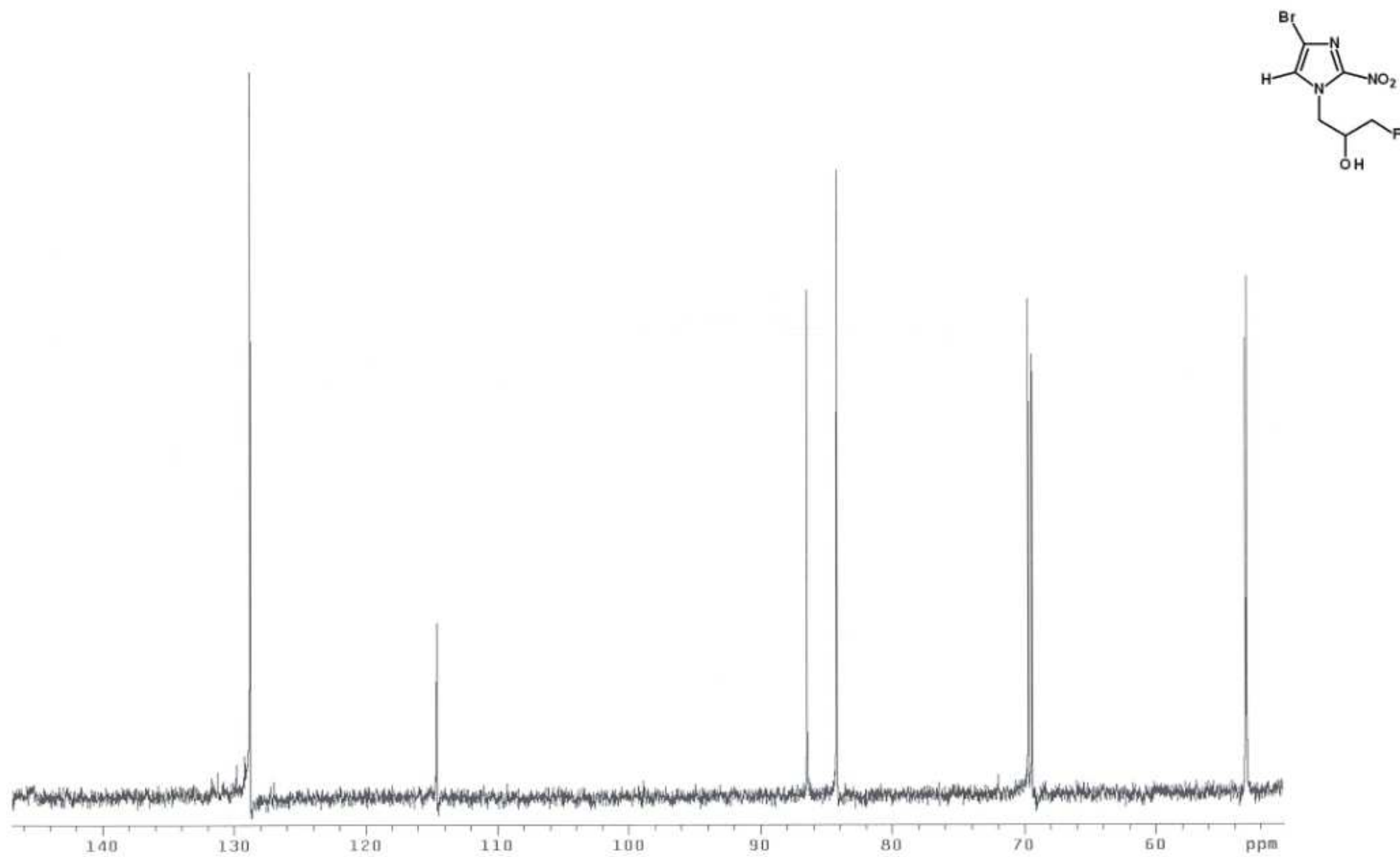


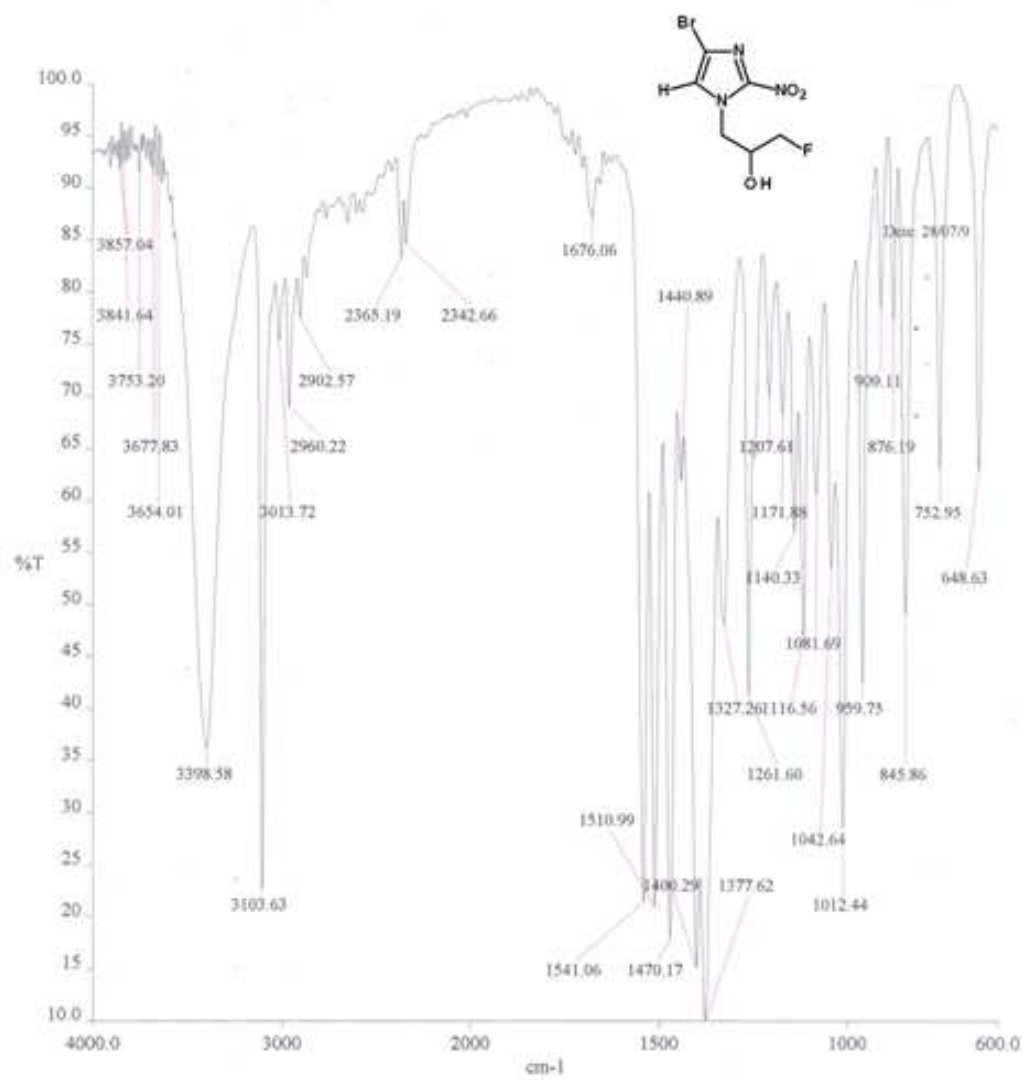
Best	Name	Formula	Score	Mass	Mass (Tgt)	Mass (DB)	Mass (MFG)	Diff (ppm)	Diff (abs. ppm)	
		C ₁₁ H ₁₅ BrFN ₃ O ₄	95.73	351.0241			351.023	-3.25	3.25	
	Ion Formula	m/z	Height	Score (MFG)	Score (MFG, MS)	Score (MFG, MS/M)	Score (MFG, mass)	Score (MFG, abund)	Score (MFG, iso. spa)	
	C ₁₁ H ₁₆ BrFN ₃ O ₄	352.0303	26496.3	95.73	95.73		92.08	98.94	99.17	
	m/z (Calc)	Δ m/z	Diff (ppm)	Diff (mDa)	Height (Calc)	Height Sum% (Calc)	Height % (Calc)	Height	Height %	Height Sum %
	352.0303	352.0315	-3.56	-1.3	28496.6	44	100	28860.8	100	44.6
	353.0332	353.0348	-4.6	-1.6	3798.5	5.9	13.3	3688.2	12.8	5.7
	354.0283	354.0294	-2.88	-1	28189.3	43.6	98.9	28410	98.4	43.9
	355.0312	355.0332	-5.57	2	3735.1	5.8	13.1	3305	11.5	5.1
	356.0333	356.0345	-3.39	-1.2	458.6	0.7	1.6	399	1.4	0.6
	357.0357	357.0298	16.4	5.9	39.1	0.1	0.1	54.1	0.2	0.1

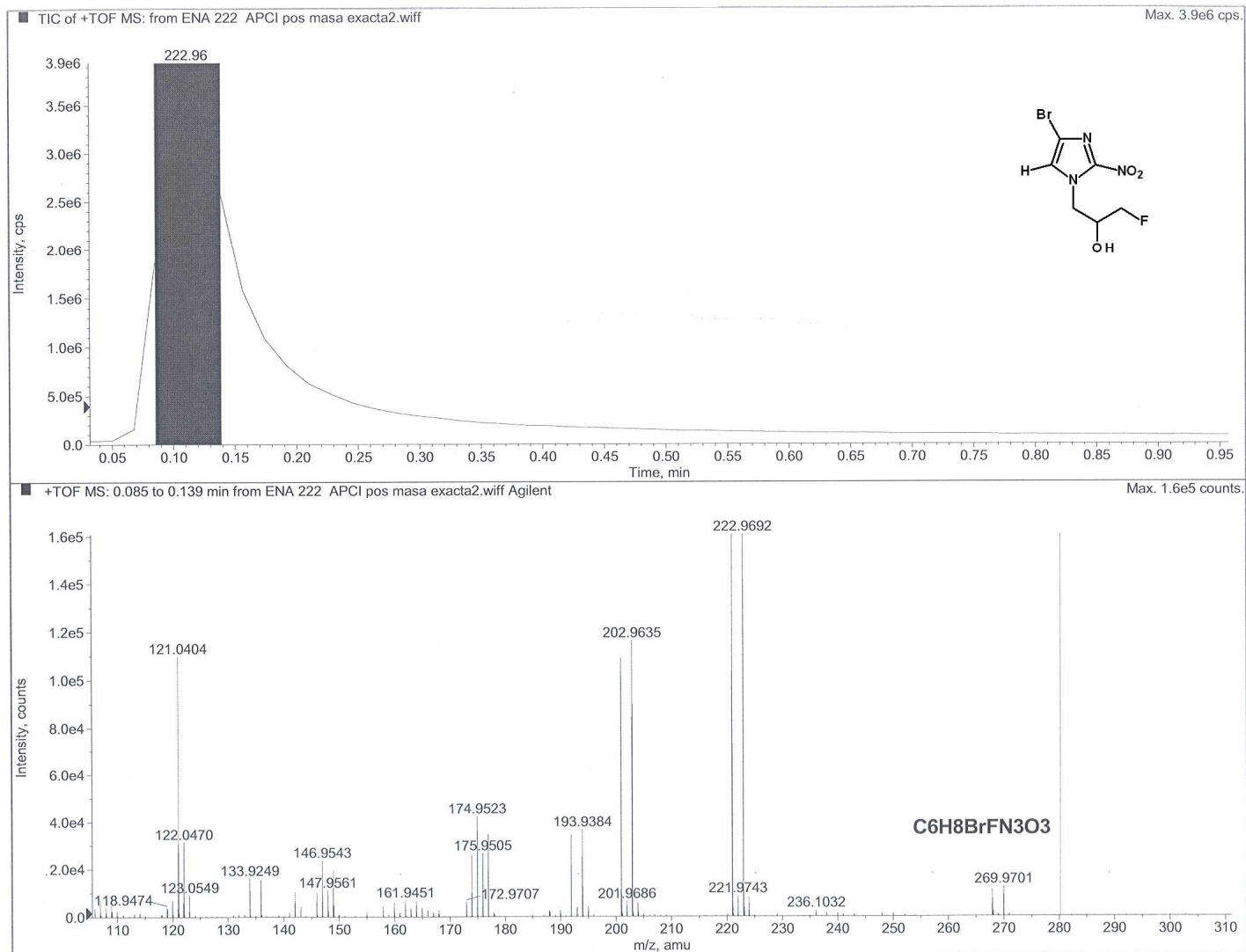
^1H -RMN (300 MHz, CD_3OD) compound **21**



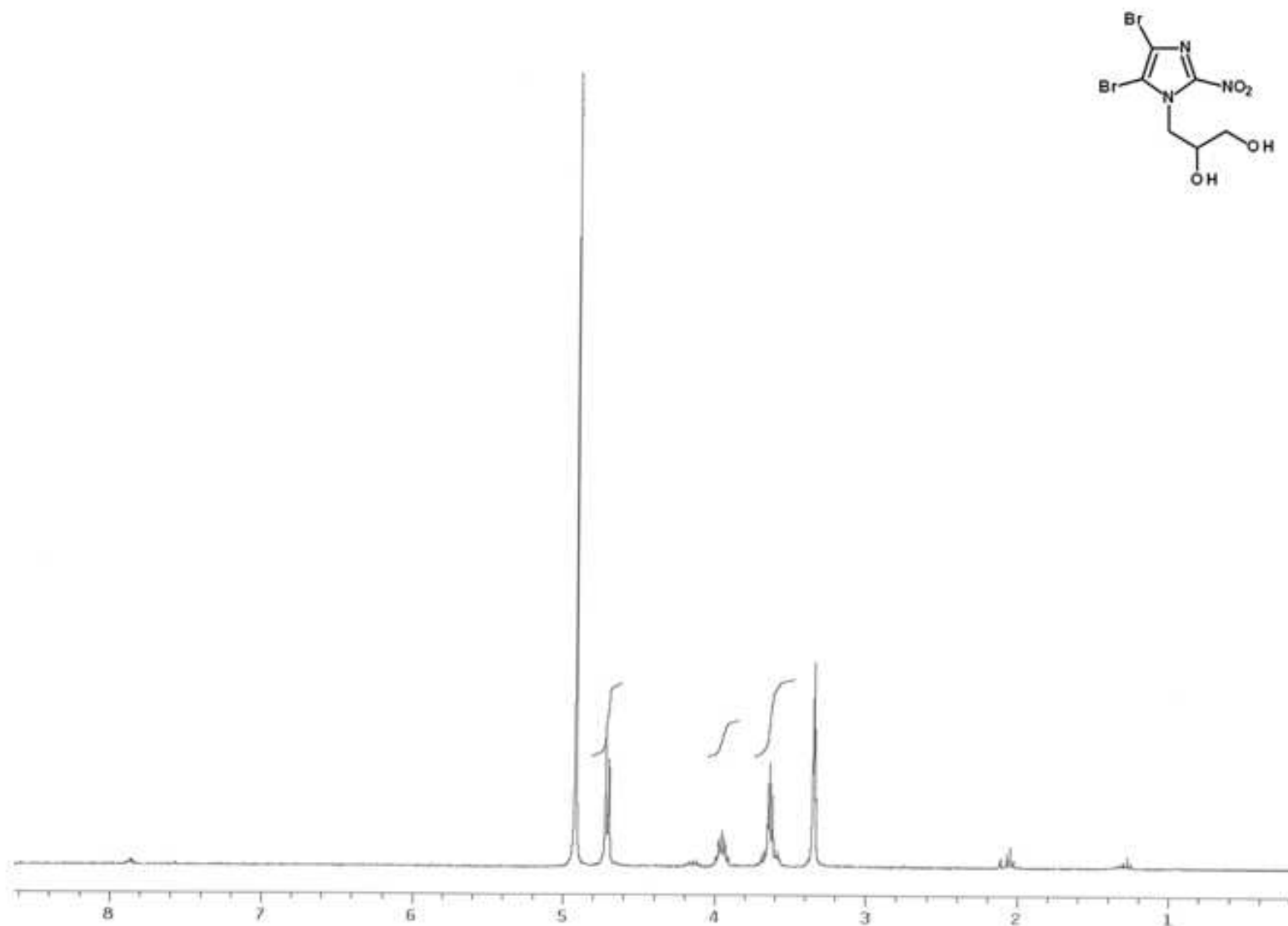
^{13}C -RMN (125 MHz, CD_3OD) compound **21**



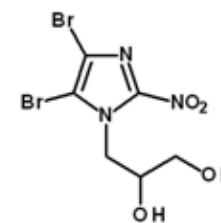
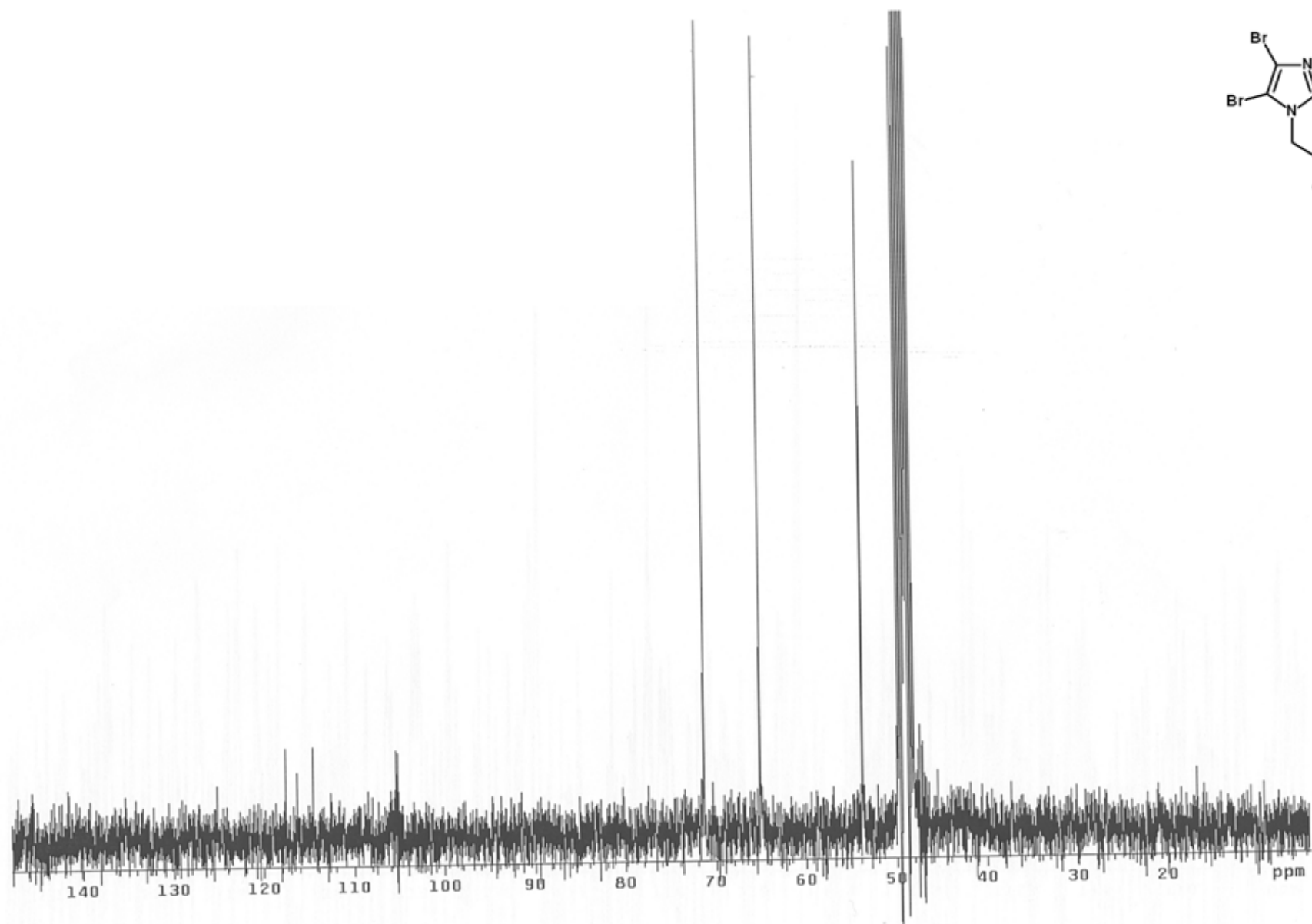
IR (KBr) compound **21**

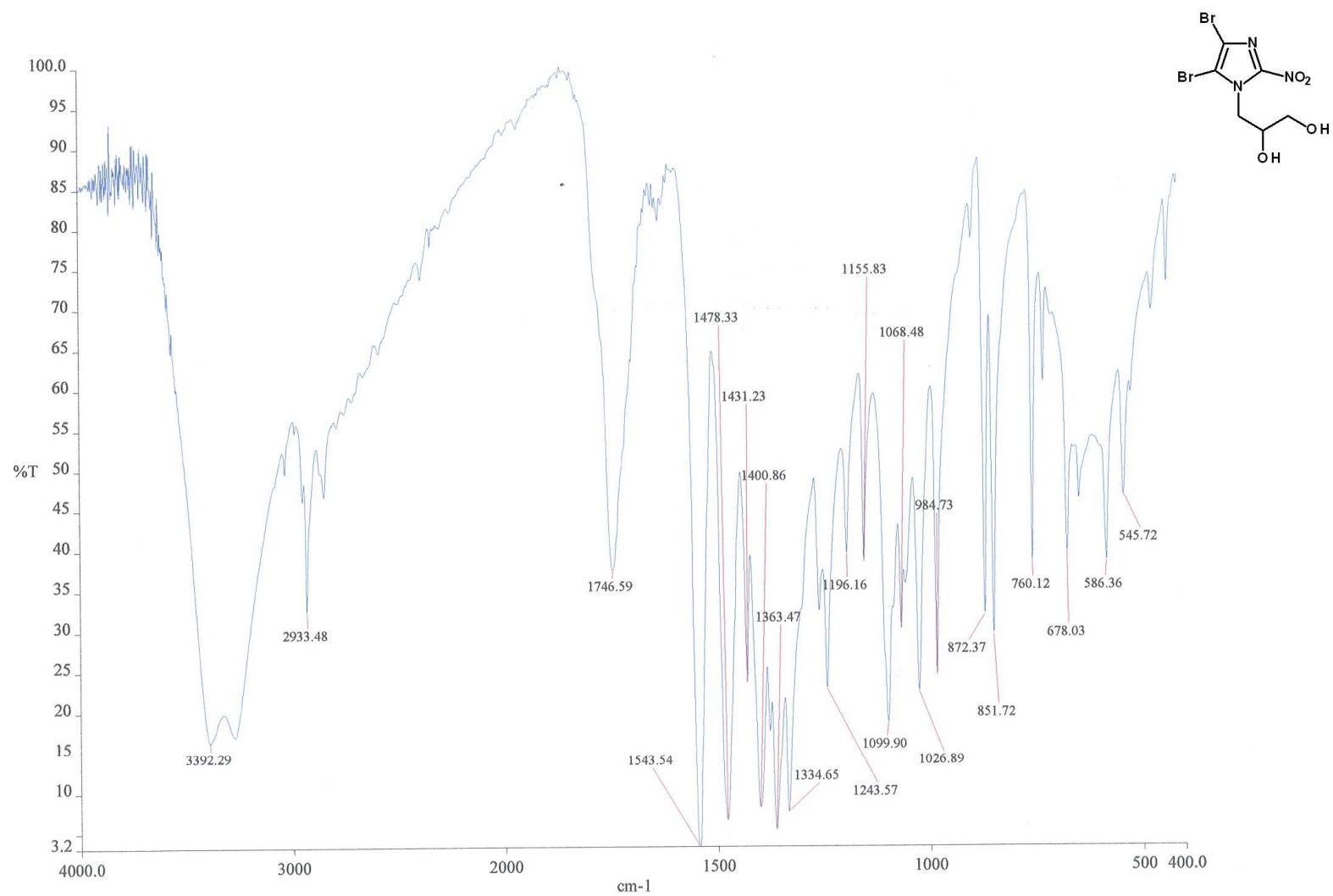
HRMS (TOF-APCI-POS) compound **21**

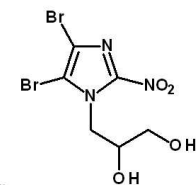
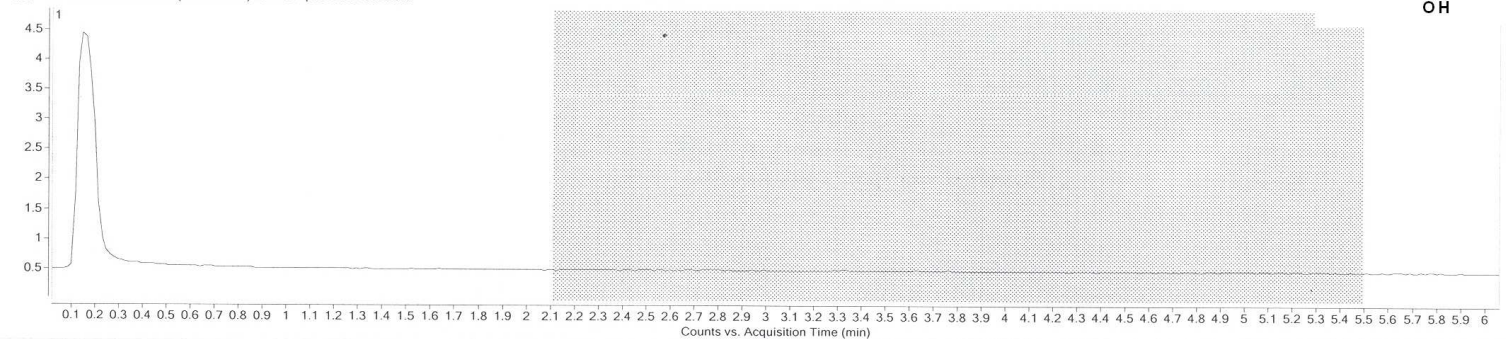
^1H -RMN (300 MHz, CD_3OD) compound **14**



^{13}C -RMN (125 MHz, CDCl_3) compound **14**

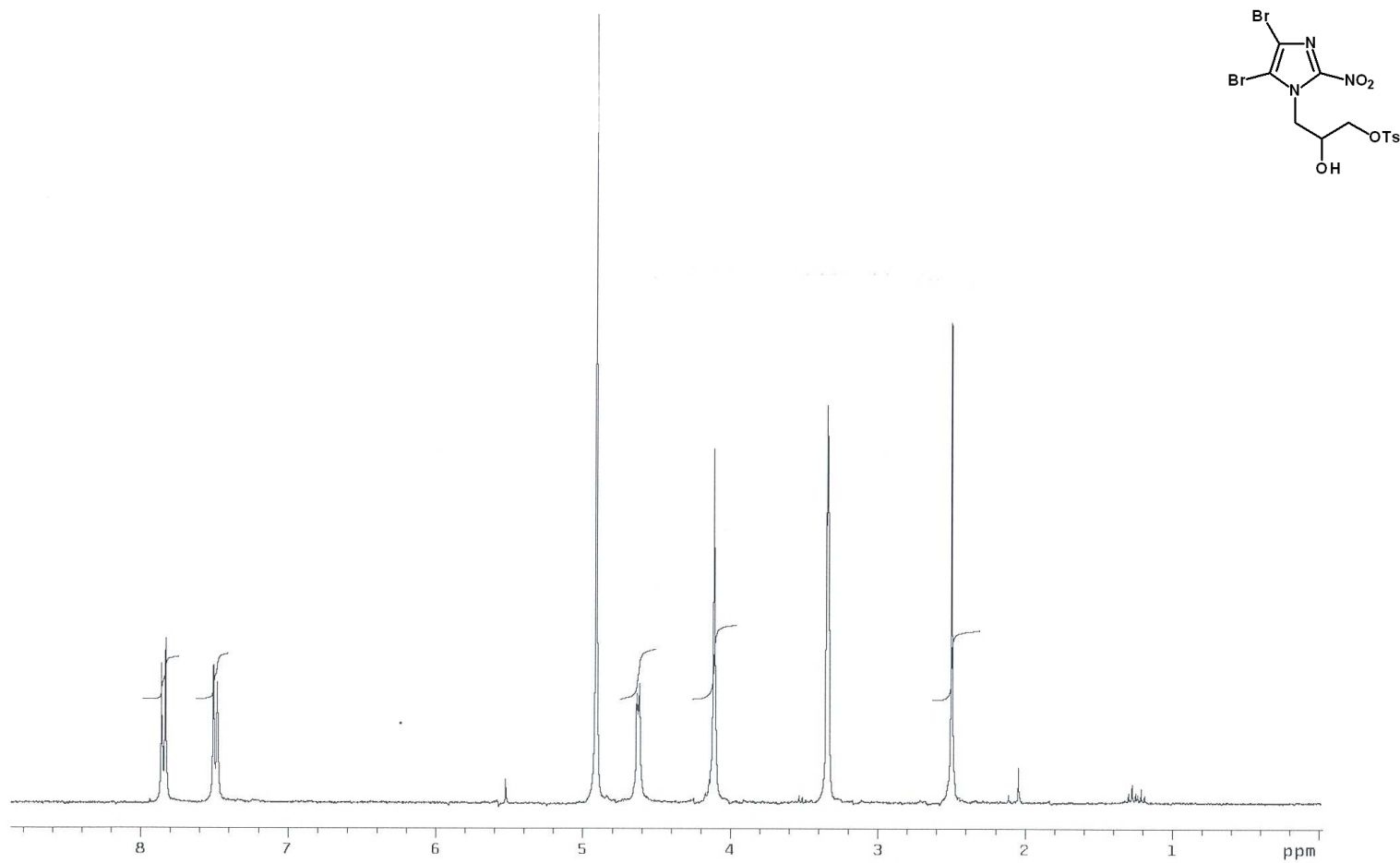


IR (KBr) compound **14**

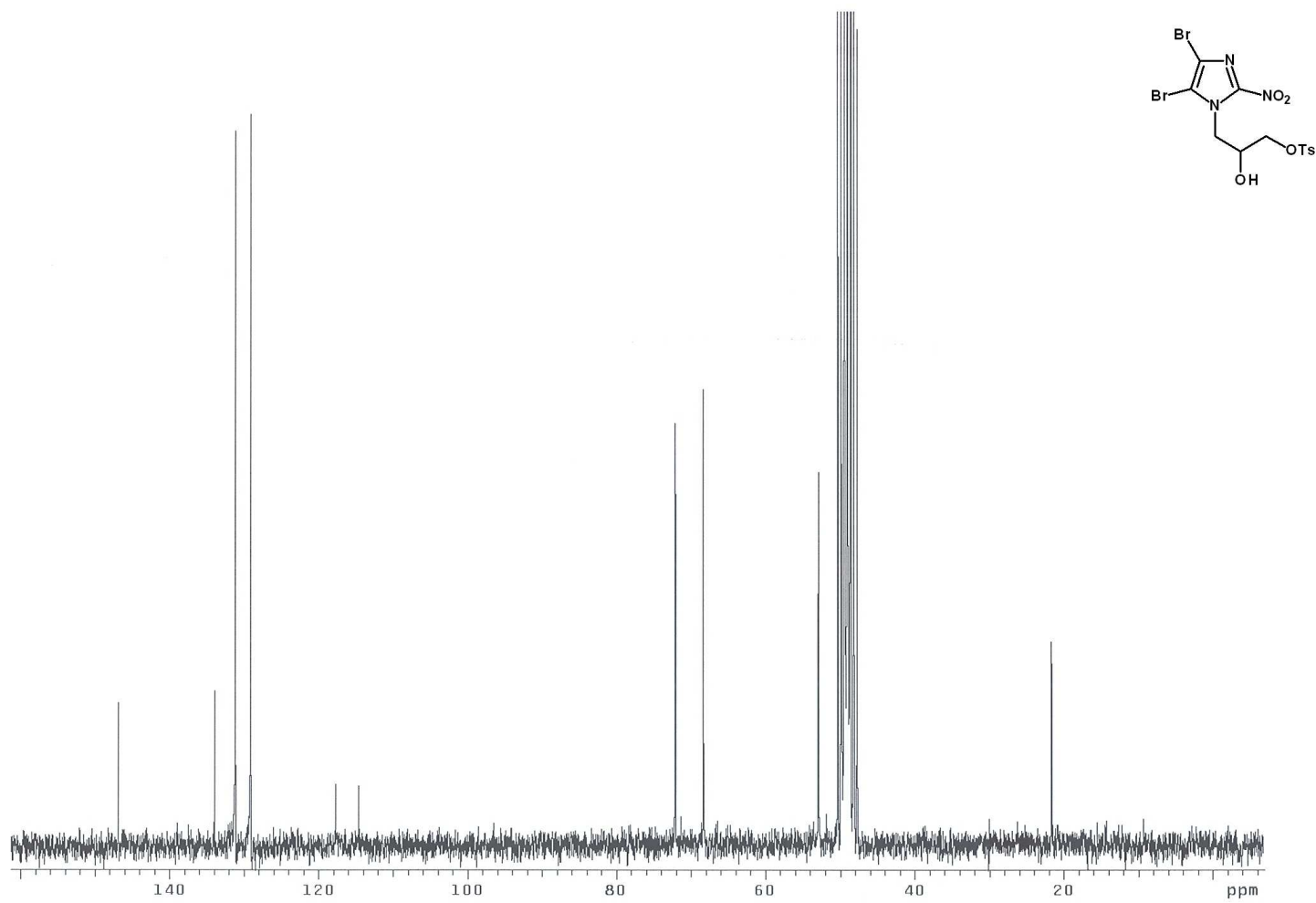
HRMS (TOF-ESI-POS) compound **14**x10⁶ + TIC Scan ENA-722-(28-05-2012)ESI-TOF-pos masa exacta.d

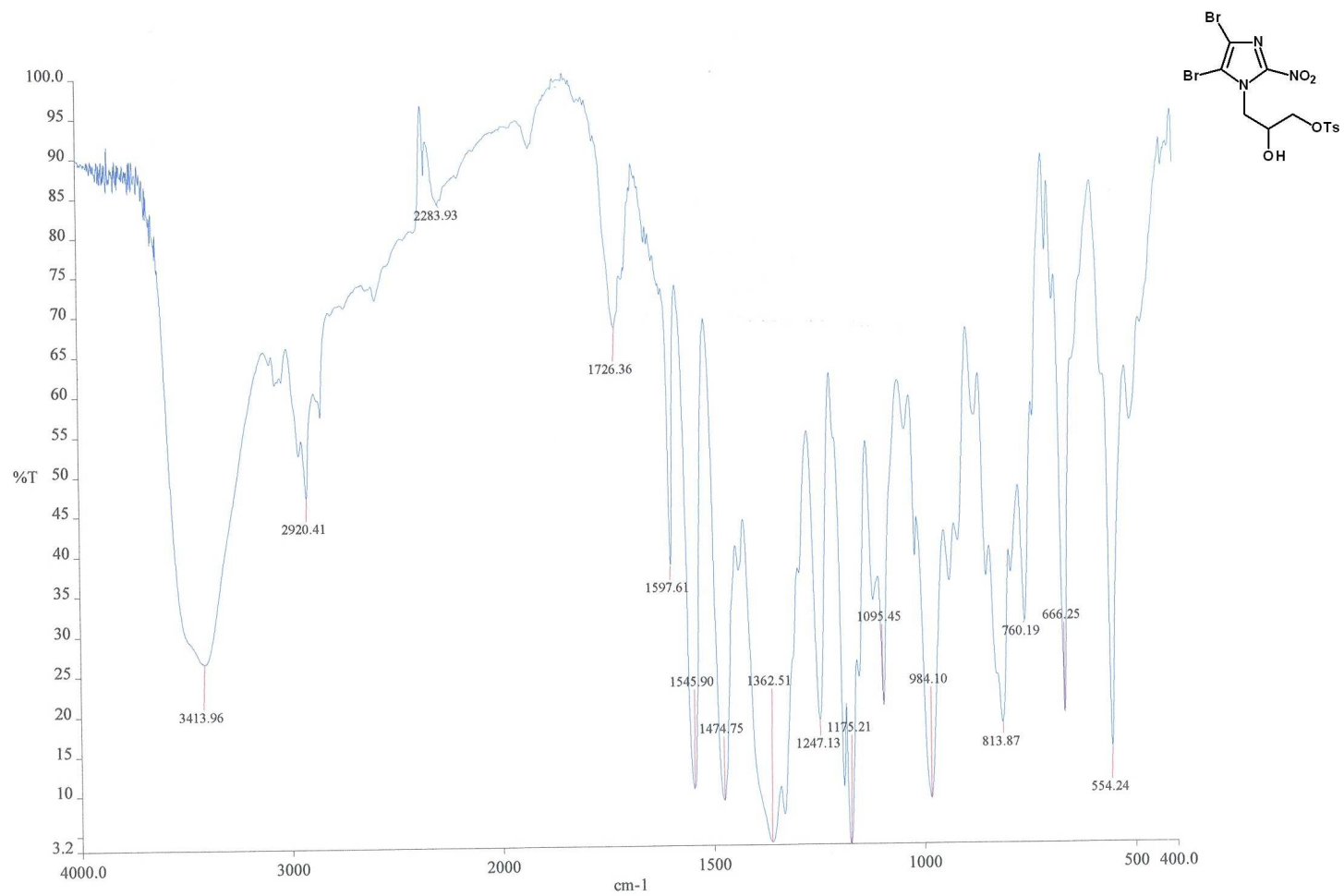
Best	Name	Formula	Score	Mass	Mass [Tgt]	Mass [DB]	Mass [MFG]	Diff [ppm]	Diff [abs. ppm]	Diff [mDa]
		C ₆ H ₇ Br ₂ N ₃ O ₄	91.62	342.079			342.8803	3.74	3.74	1.28
Ion Formula	m/z	Height	Score (MFG)	Score (MFG, MS)	Score (MFG, MS/M)	Score (MFG, mass)	Score (MFG, abund)	Score (MFG, iso. spa)		
C ₆ H ₈ Br ₂ N ₃ O ₄	345.8856	1193.4	91.62	91.62		99.77	73.9	96.59		
m/z (Calc)	m/z	Diff [ppm]	Diff [mDa]	Height [Calc]	Height Sum % [Calc]	Height % [Calc]	Height	Height %	Height Sum %	
343.8876	343.8847	8.38	2.9	727	23.6	51.1	770.9	61.8	25	
344.8901	344.8929	-8.11	-2.8	56.9	1.8	4	74.5	6	2.4	
345.8856	345.8845	3.1	1.1	1422.4	46.1	100	1248.4	100	40.5	
346.8881	346.8853	8.03	2.8	111.3	3.6	7.8	101.7	8.1	3.3	
347.8837	347.8834	0.67	0.2	703.4	22.8	49.5	668.8	53.6	21.7	
348.8861	348.8853	2.31	0.8	54.9	1.8	3.9	119.6	9.6	3.9	
349.888	349.8946	-18.86	-6.6	7.6	0.2	0.5	99.5	8	3.2	

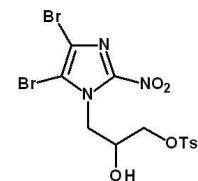
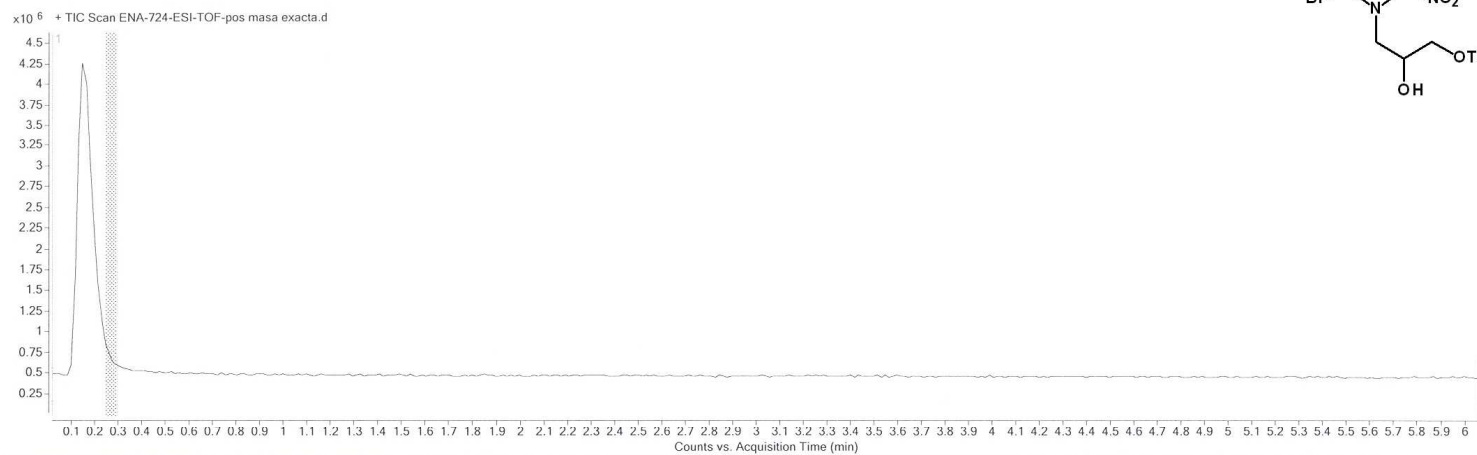
¹H-RMN (300 MHz, CD₃OD) compound **16**



^{13}C -RMN (125 MHz, CDCl_3) compound **16**

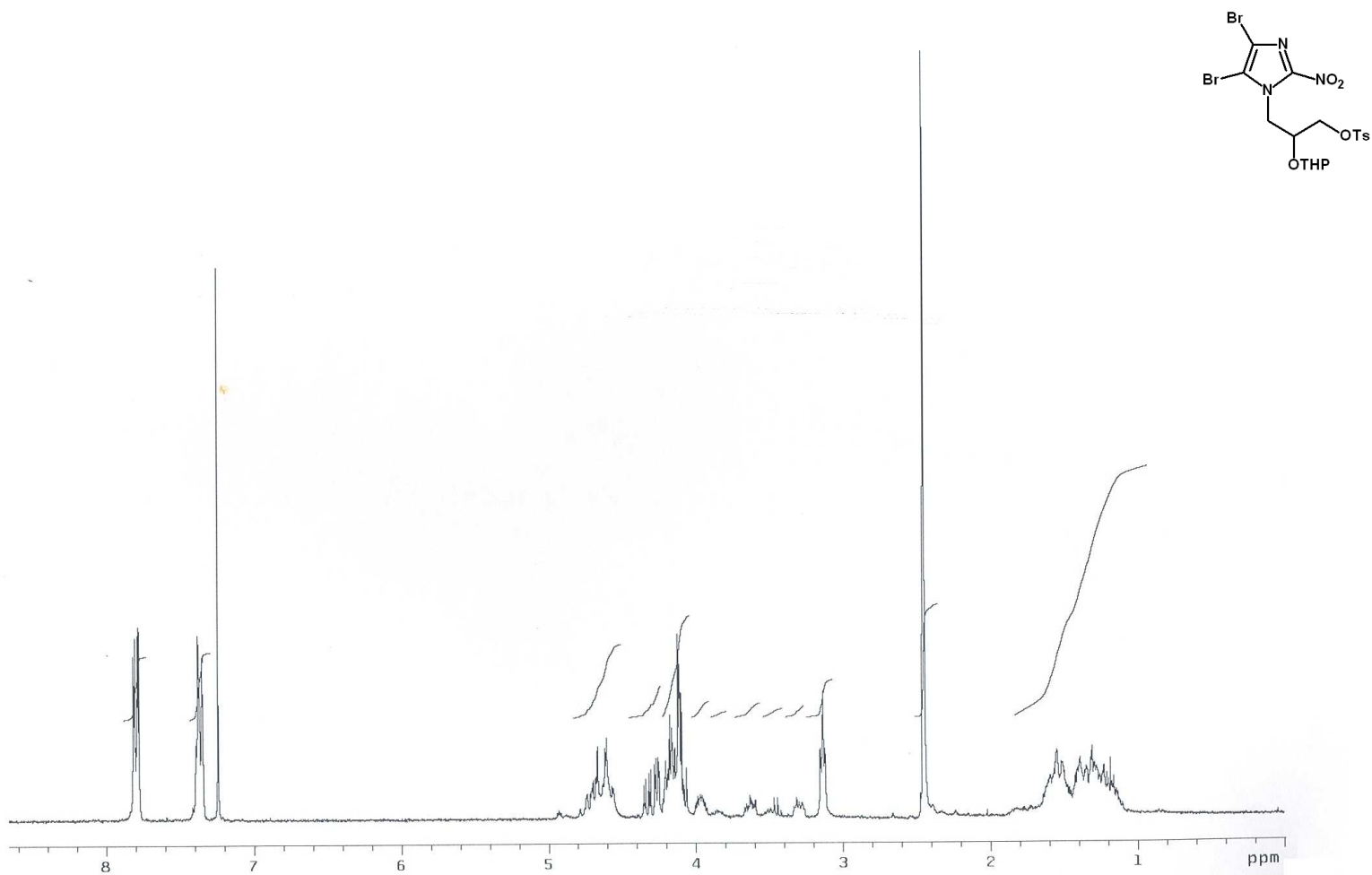


IR (KBr) compound **16**

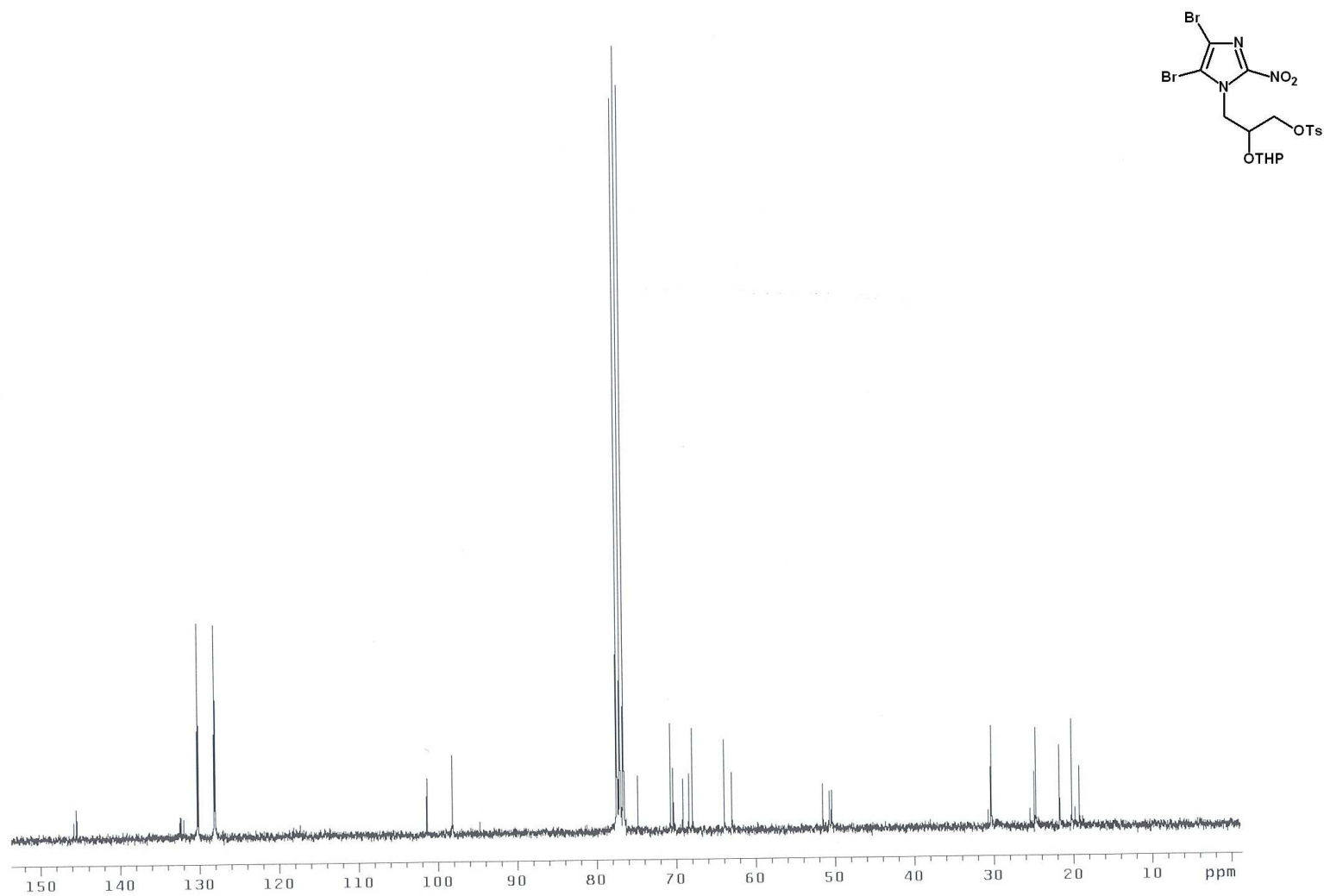
HRMS (TOF-ESI-POS) compound **16**

Best	Name	Formula	Score	Mass	Mass [Tgt]	Mass [DB]	Mass [MFG]	Diff [ppm]	Diff [abs. ppm]	Diff [mDa]
		C ₁₃ H ₁₃ Br ₂ N ₃ O ₆ S	99.1	496.891			496.8892	-3.62	3.62	-1.6
Ion Formula		m/z	Height	Score [MFG]	Score [MFG, MS]	Score [MFG, MS/M]	Score [MFG, mass]	Score [MFG, abund]	Score [MFG, iso. spa]	
C ₁₃ H ₁₄ Br ₂ N ₃ O ₆ S		499.8944	13303.6	99.1	99.1	99.58	97.61	99.94		
m/z [Calc]	m/z	Diff [ppm]	Diff [mDa]	Height [Calc]	Height Sum% [Calc]	Height % [Calc]	Height	Height %	Height Sum %	
497.8965	497.8991	-5.4	-2.7	6246.6	20.7	49.6	6079.5	45.4	20.1	
498.8992	498.9016	-4.65	-2.3	1020.4	3.4	8.1	889.5	6.6	2.9	
499.8944	499.8961	-3.39	-1.7	12587.9	41.6	100	13386.9	100	44.3	
500.8972	500.8988	-3.28	-1.6	2045	6.8	16.2	1848.4	13.8	6.1	
501.8925	501.8945	-3.93	-2	6765.8	22.4	53.7	6581	49.2	21.8	
502.8952	502.8976	-4.84	-2.4	1082.8	3.6	8.6	1014.3	7.6	3.4	
503.8916	503.8945	-5.74	-2.9	428.5	1.4	3.4	371.6	2.8	1.2	
504.8936	504.9008	-14.19	-7.2	58.3	0.2	0.5	64.1	0.5	0.2	

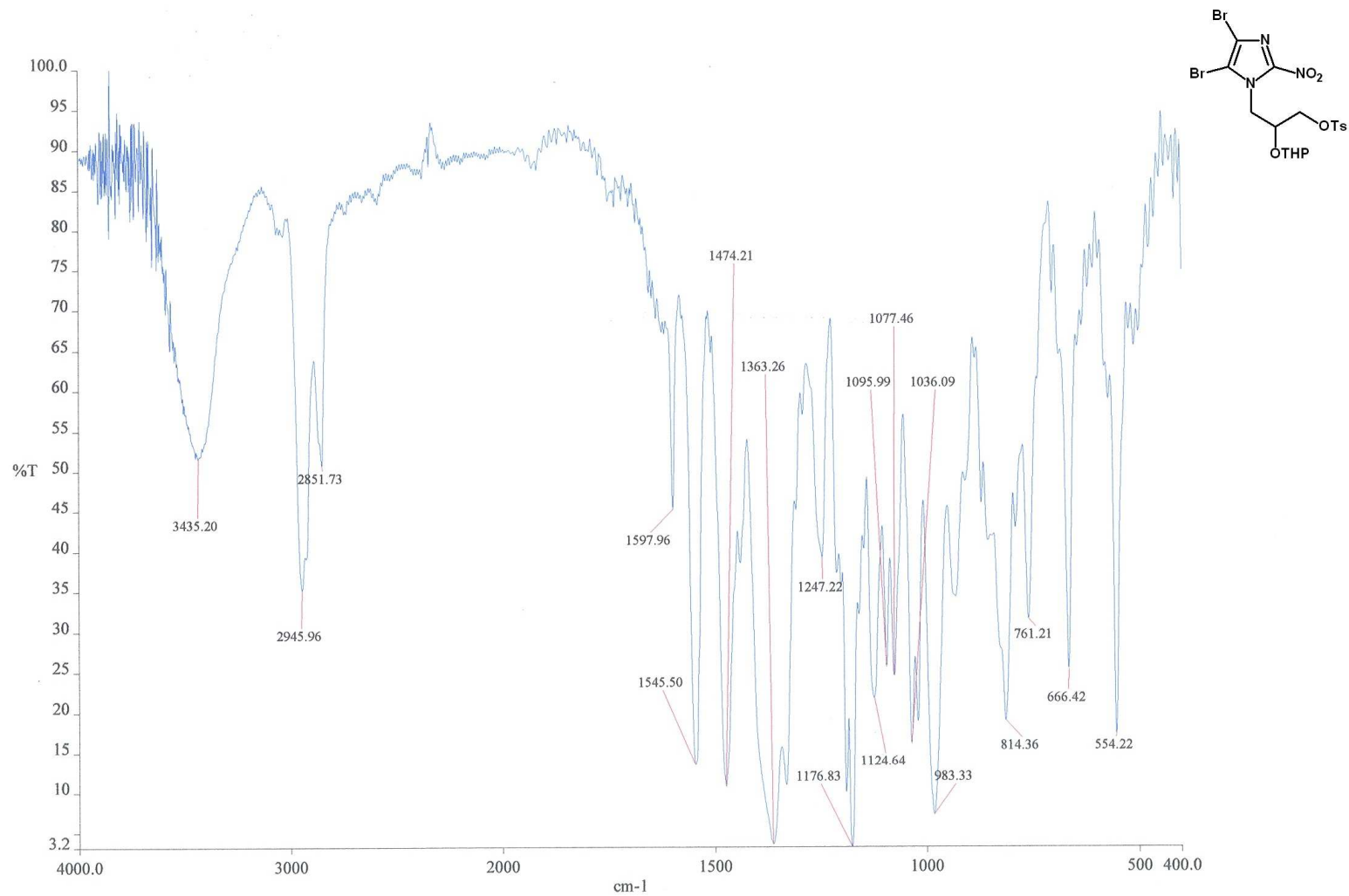
¹H-RMN (300 MHz, CD₃OD) compound **18**



^{13}C -RMN (125 MHz, CDCl_3) compound **18**

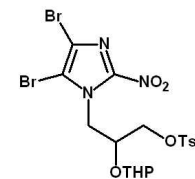


IR (KBr) compound 18

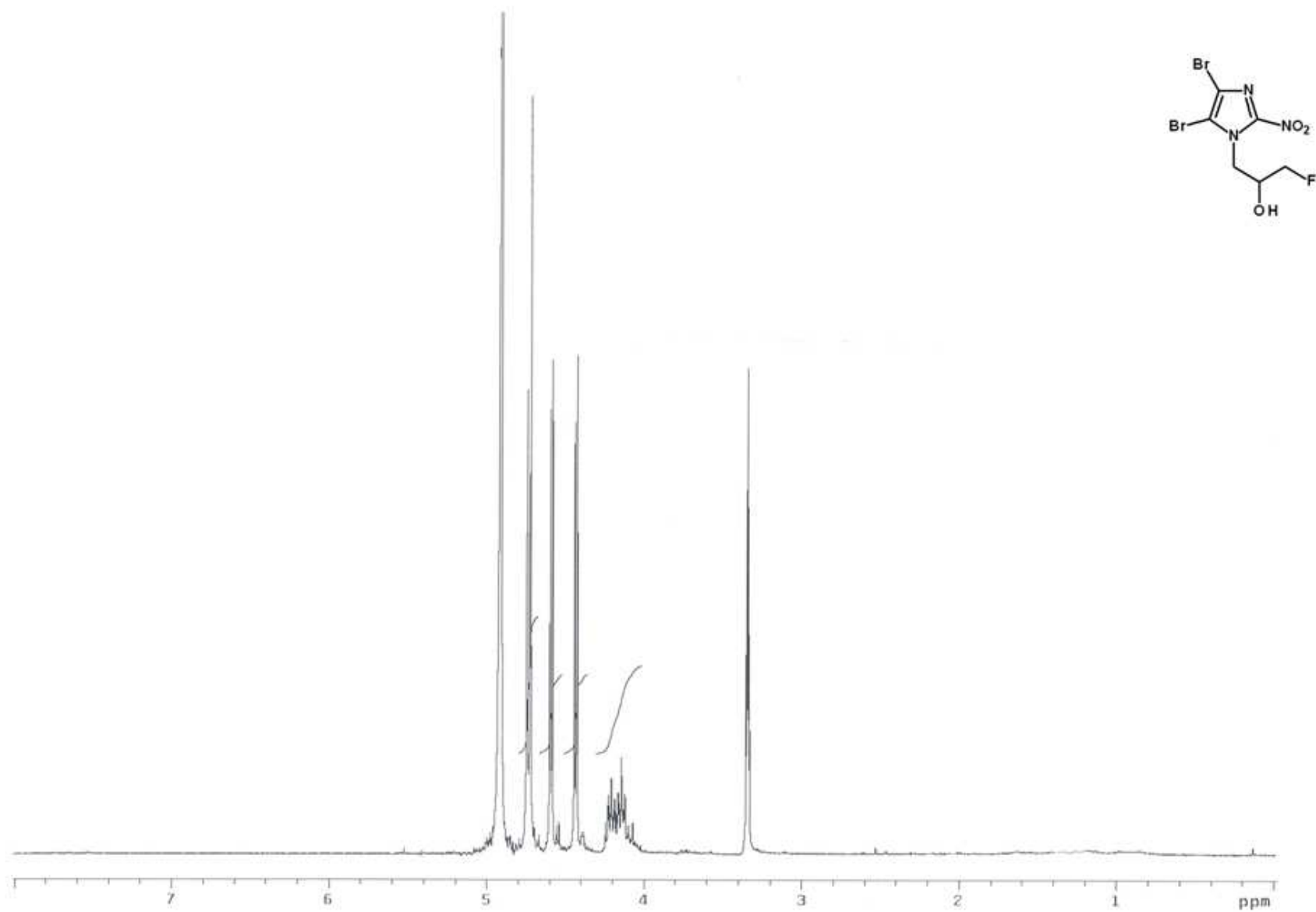


HRMS (TOF-ESI-POS) compound 18

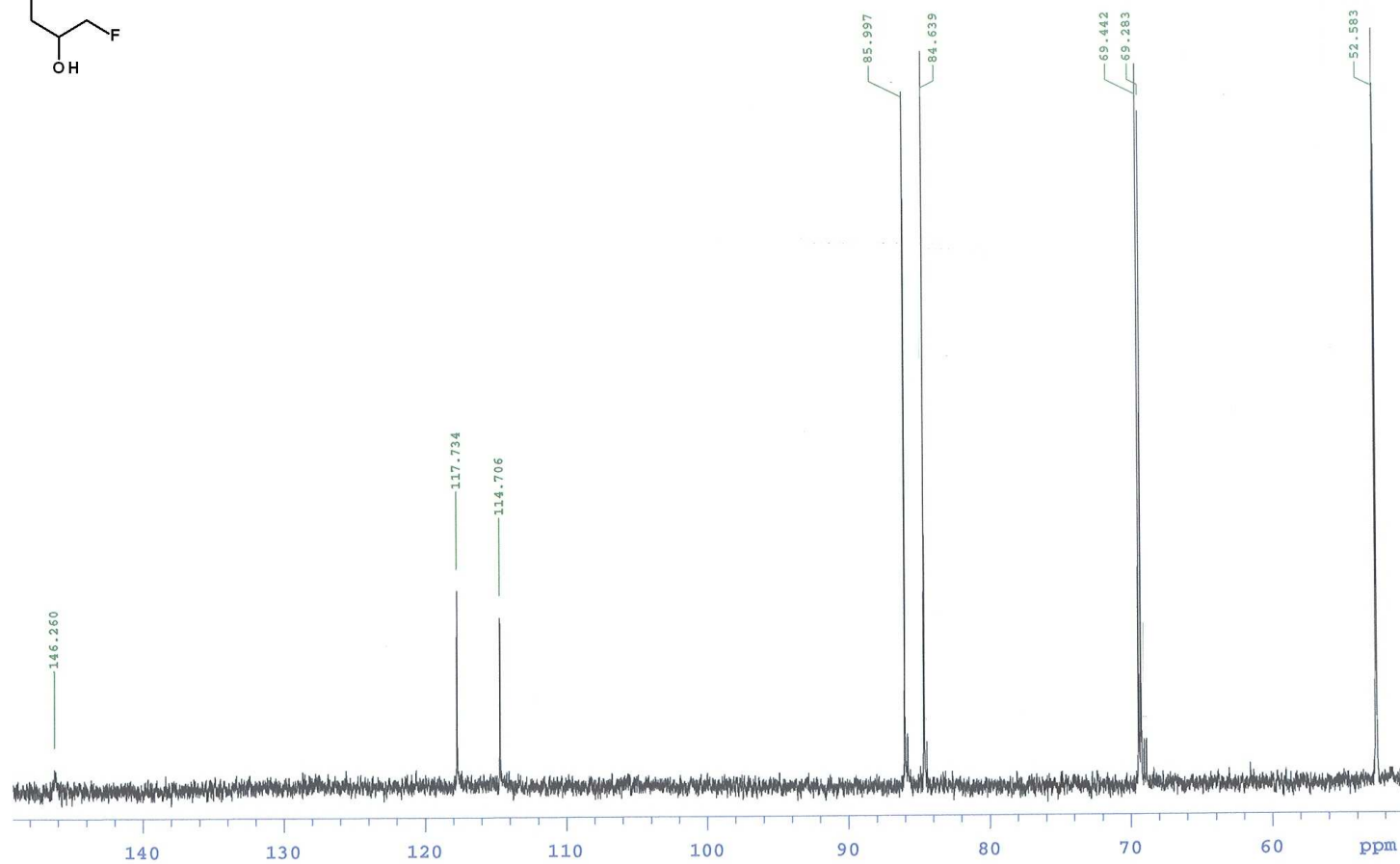
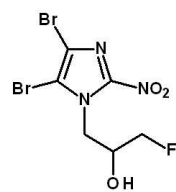
Show/Hide	Formula	Diff (Tgt, ppm)	File	Mass	Base Peak	m/z	Polarity	Area	Width	Abund	Score
<input checked="" type="checkbox"/>	C18H21Br2N3O7S	-0.63	ENA-725-ESI+10F-pos.mssa	580.9463	452.8946	623.9144	Positive	457410	0.254	7901	95.98
Diff (abs. ppm)	Best	Name	Diff (mDa)	Formula	Mass	Score	Diff (ppm)	RT	Mass (Tgt)	Score (Tgt)	
0.69			0.4	C18H21Br2N3...	580.9463	95.96	0.69	0.166	580.9	95.96	
Height	Species	m/z									
912.2	(M+H) ⁺	583.952									
m/z (Calc)	Diff (ppm)	m/z	Height	Height %	Height Sum %	Diff (mDa)					
581.954	-0.89	581.9545	471.1	49.9	19.3	-0.5					
582.9569	-4.78	582.9597	145.9	15.5	6	-2.8					
583.952	0.09	583.952	943.2	100	38.7	0.1					
584.9549	-1.13	584.9556	231.4	24.5	9.5	-0.7					
585.9502	-0.1	585.9503	509.6	54	20.9	-0.1					
586.9523	1.04	586.9523	86.7	9.2	3.6	0.6					
587.9502	-7.03	587.9543	50.7	5.4	2.1	-4.1					
Height	Species	m/z									
154	(M+K) ⁺	621.9079									
m/z (Calc)	Diff (ppm)	m/z	Height	Height %	Height Sum %	Diff (mDa)					
621.9079	-5.49	621.9113	154.9	98.7	40.9	-3.4					
622.9108	-1.99	622.912	66.5	42.3	17.6	-1.2					
623.9061	-13.42	623.9144	157	100	41.5	-8.4					
Height	Species	m/z									
7901.3	(M+Na) ⁺	605.934									
m/z (Calc)	Diff (ppm)	m/z	Height	Height %	Height Sum %	Diff (mDa)					
603.9359	-0.52	603.9362	3677.9	46.3	18.1	-0.3					
604.9389	-0.69	604.9393	775.8	9.8	3.8	-0.4					
605.934	0.72	605.9335	7951.6	100	39.1	0.4					
606.9368	-0.23	606.937	1599.4	20.1	7.9	-0.1					
607.9321	1.03	607.9315	4631.8	58.2	22.8	0.6					
608.9349	-2.16	608.9362	928.5	11.7	4.6	-1.3					
609.9322	-2.31	609.9336	750.7	9.4	3.7	-1.4					



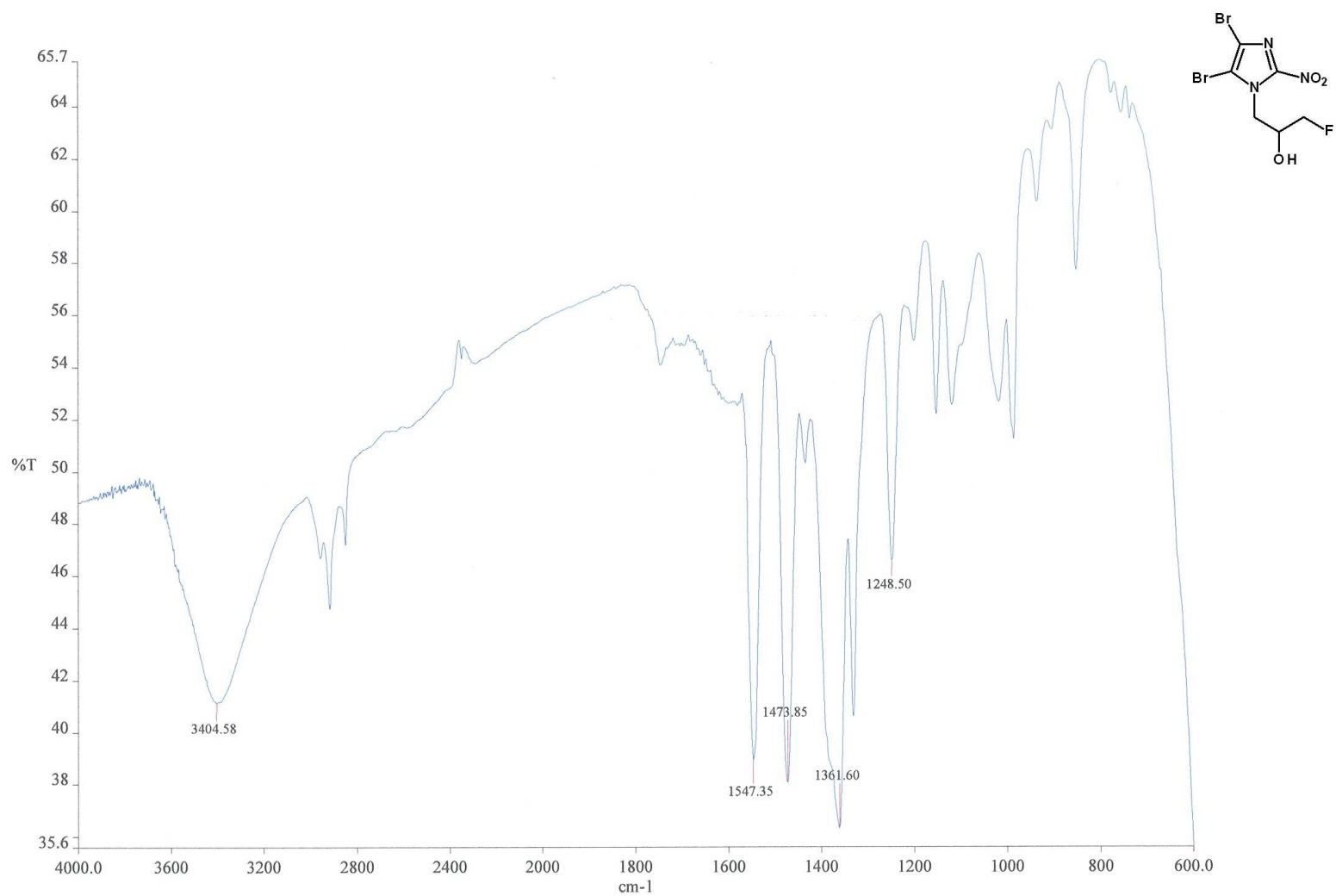
^1H -RMN (300 MHz, CD_3OD) compound **22**



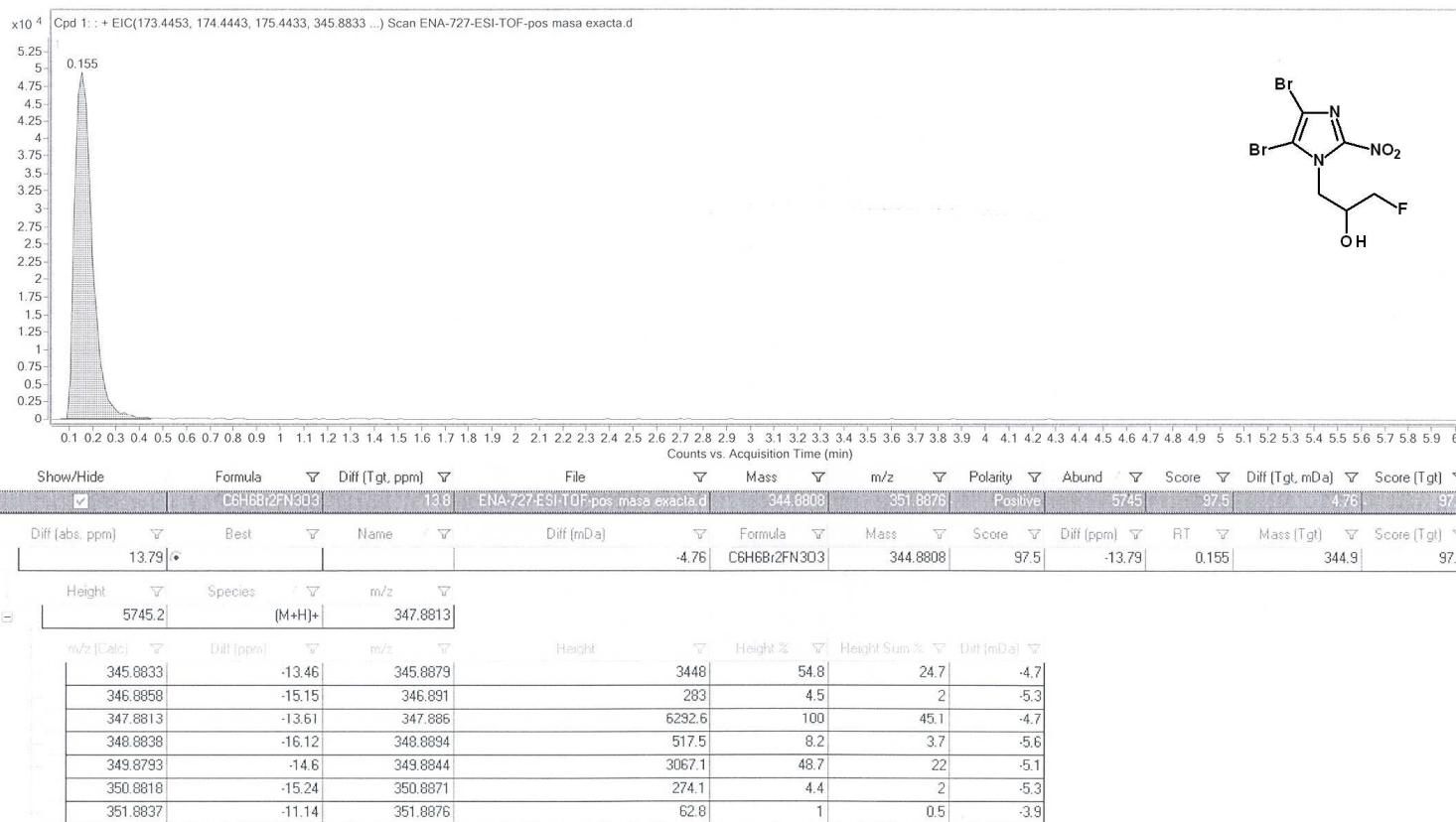
^{13}C -RMN (125 MHz, CDCl_3) compound **22**



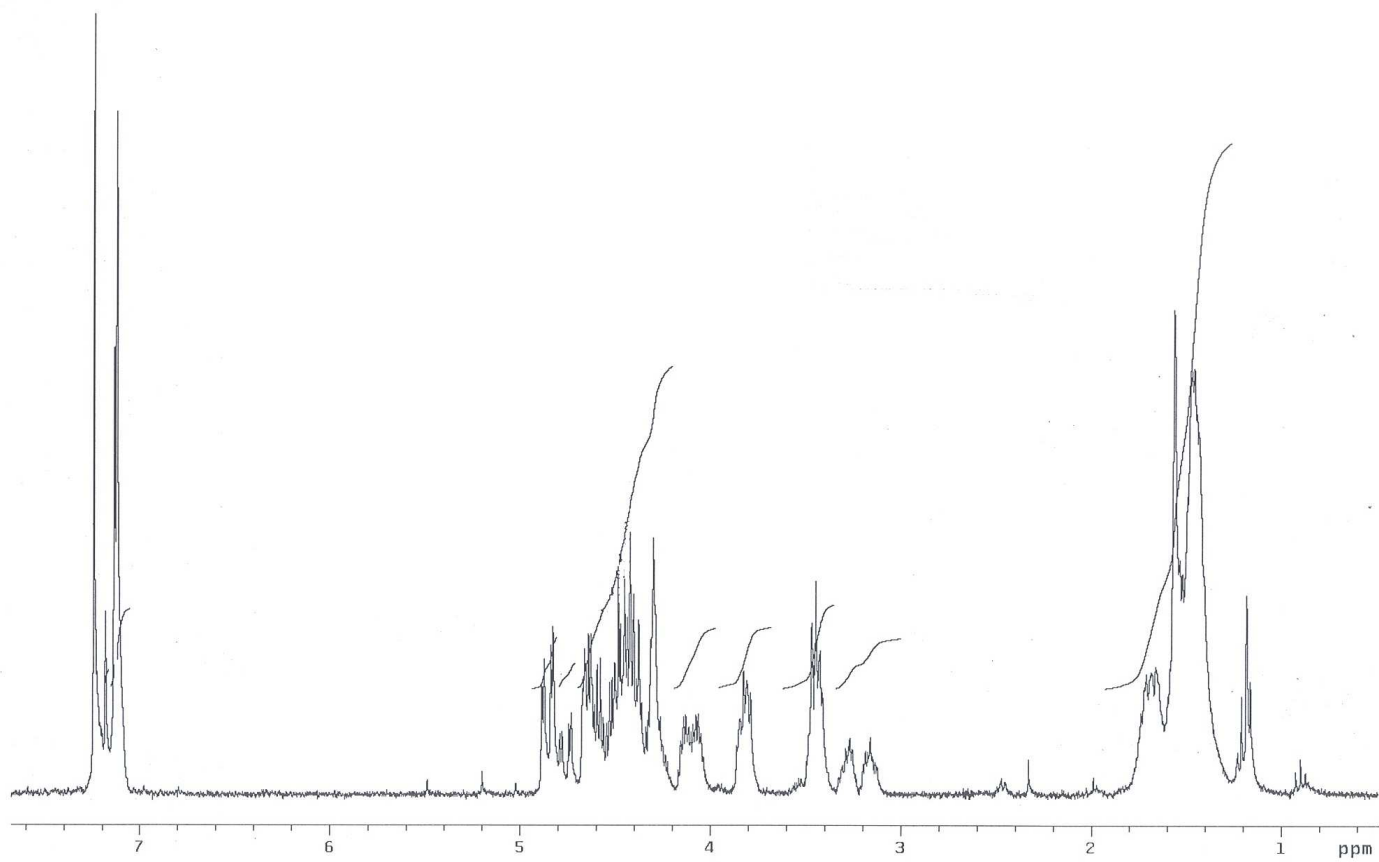
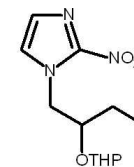
IR (KBr) compound 22



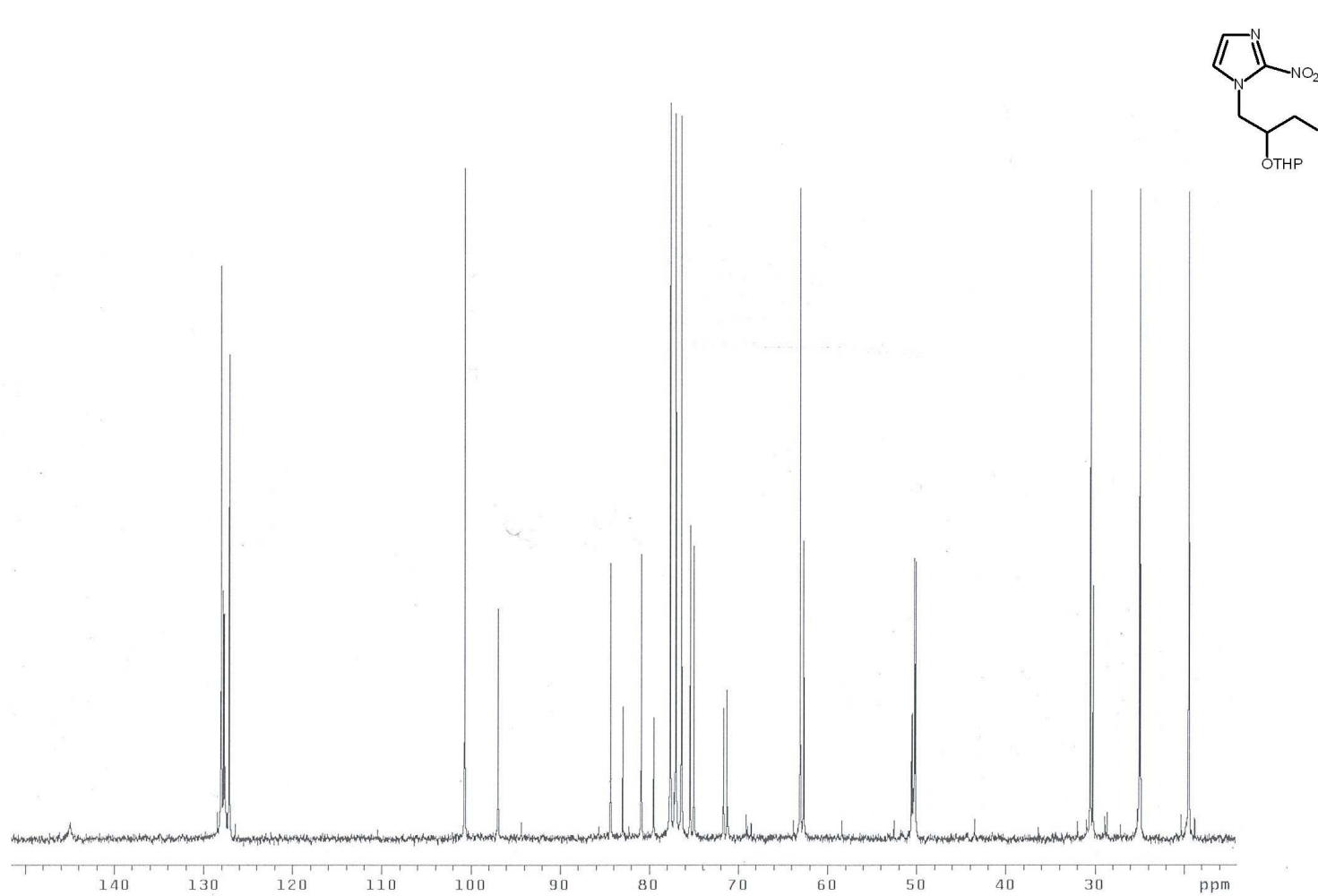
HRMS (TOF-ESI-POS) compound 22



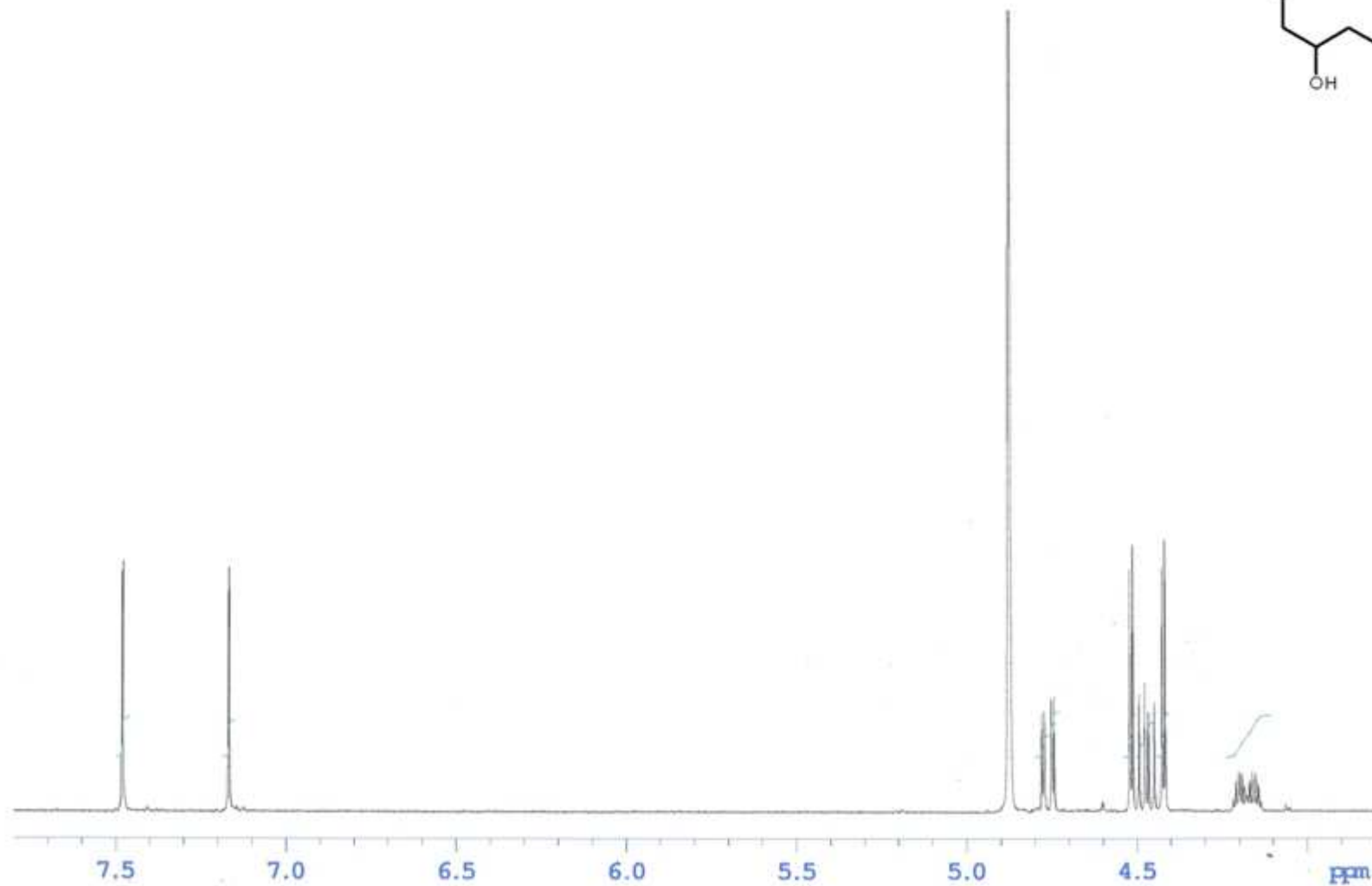
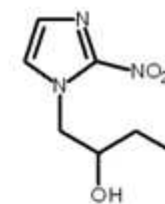
^1H -RMN (300 MHz, CD_3OD) compound **23**



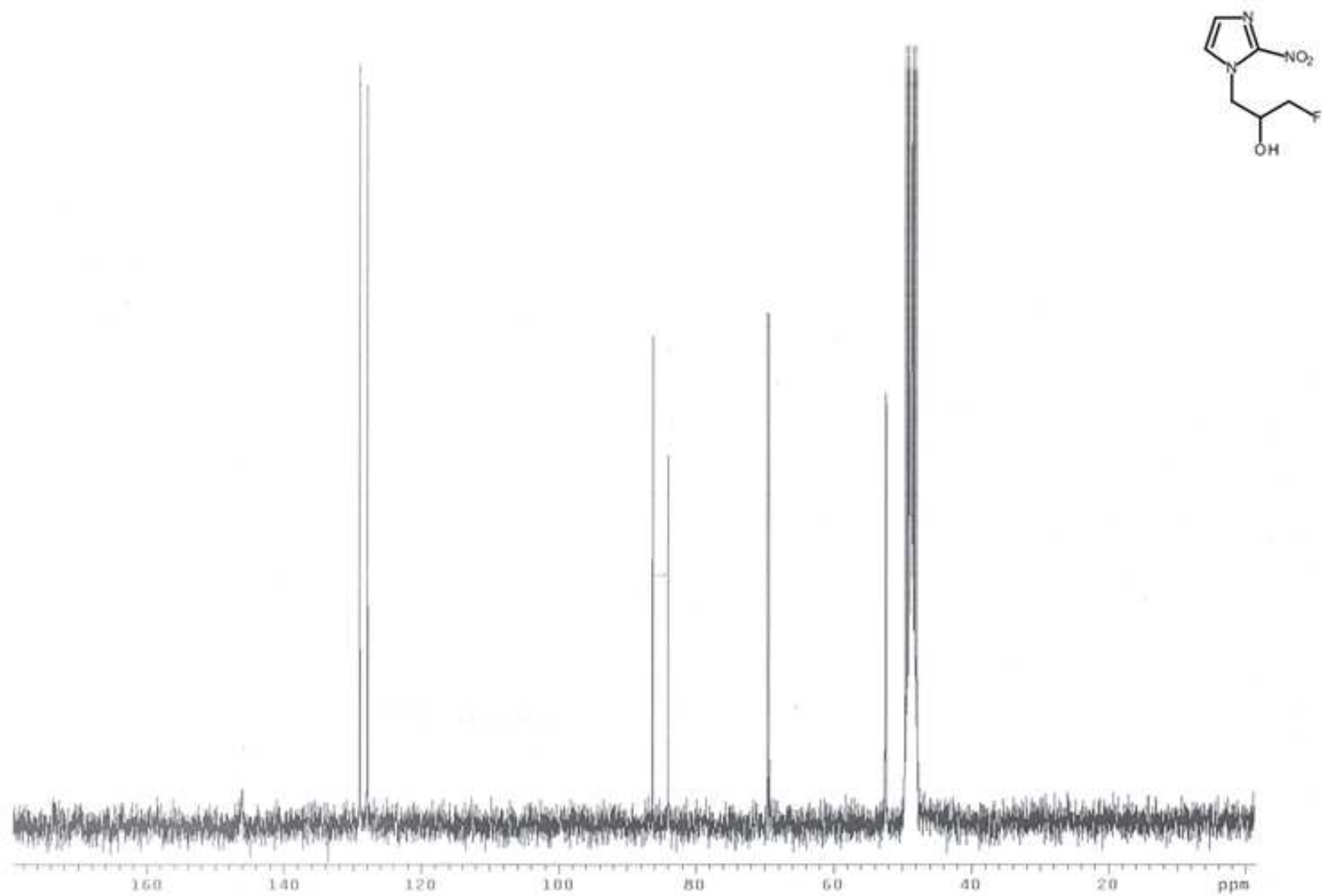
^{13}C -RMN (125 MHz, CDCl_3) compound **23**



¹H-RMN (300 MHz, CD₃OD) compound **1**



^{13}C -RMN (125 MHz, CDCl_3) compound **1**



IR (KBr) compound 1

